

Electronic Thesis and Dissertation Repository

August 2012

Synthesis and Characterization of Graphene-Polymer Nanocomposites via Reversible Addition-Fragmentation Chain-Transfer Polymerization

Renpeng Gu
The University of Western Ontario

Supervisor
Paul Charpentier
The University of Western Ontario

Graduate Program in Chemical and Biochemical Engineering
A thesis submitted in partial fulfillment of the requirements for the degree in Master of Engineering Science
© Renpeng Gu 2012

Follow this and additional works at: <https://ir.lib.uwo.ca/etd>

 Part of the [Polymer Science Commons](#)

Recommended Citation

Gu, Renpeng, "Synthesis and Characterization of Graphene-Polymer Nanocomposites via Reversible Addition-Fragmentation Chain-Transfer Polymerization" (2012). *Electronic Thesis and Dissertation Repository*. 651.

<https://ir.lib.uwo.ca/etd/651>

This Dissertation/Thesis is brought to you for free and open access by Scholarship@Western. It has been accepted for inclusion in Electronic Thesis and Dissertation Repository by an authorized administrator of Scholarship@Western. For more information, please contact wlsadmin@uwo.ca.

**SYNTHESIS AND CHARACTERIZATION OF GRAPHENE-POLYMER
NANOCOMPOSITES VIA REVERSIBLE ADDITION-FRAGMENTATION
CHAIN-TRANSFER POLYMERIZATION**

(Spine title: Synthesis of graphene nanocomposites via RAFT)

(Thesis format: Monograph)

by

Renpeng Gu

Graduate Program in Chemical and Biochemical Engineering

A thesis submitted in partial fulfillment
of the requirements for the degree of
Master of Engineering Science

The School of Graduate and Postdoctoral Studies
The University of Western Ontario
London, Ontario, Canada

© Renpeng Gu 2012

THE UNIVERSITY OF WESTERN ONTARIO
School of Graduate and Postdoctoral Studies

CERTIFICATE OF EXAMINATION

Supervisor

Examiners

Dr. Paul Charpentier

Dr. James Wisner

Supervisory Committee

Dr. Jin Zhang

Dr. Elizabeth Gillies

Dr. Elizabeth Gillies

The thesis by

Renpeng Gu

entitled:

**Synthesis and Characterization of Graphene-Polymer Nanocomposites via
Reversible Addition-Fragmentation Chain-Transfer Polymerization**

is accepted in partial fulfillment of the
requirements for the degree of
Master of Engineering Science

Date

Chair of the Thesis Examination Board

Abstract

Graphene has emerged as a subject of tremendous scientific interest due to its exceptional electrical, mechanical and thermal properties. When incorporated into a polymer matrix, these thin carbon sheets can significantly improve the properties of the host polymer at low loading levels. However, the dispersion of pure graphene throughout a polymer matrix is not homogeneous, due to the strong van der Waals interactions between graphene sheets and the difference in surface compatibilities. To prevent agglomeration of these graphene sheets, surface functionalization is required to weaken the π - π stacking. Living free radical polymerization is a powerful tool for the surface functionalization of nanomaterials such as graphene via the “grafting from” approach. Especially, reversible addition-fragmentation chain transfer (RAFT) polymerization has several attractive advantages as a living technique, such as good compatibility with a wide range of monomers, tolerance to solvents and acidic/basic monomers, and simple implementation for controlling nanocomposite structure.

The goal of this thesis was to develop a facile approach for growing polymer chains from the surface of graphene sheets. Graphene oxide was synthesized by Hummers method by reacting graphite with a mixture of potassium permanganate (KMnO_4) and concentrated sulfuric acid (H_2SO_4). The oxidation and exfoliation of graphite was investigated using FTIR, TEM, and AFM studies. For the methodology of growing polymers from graphene surfaces, polydopamine was coated on graphene oxide as a platform for subsequent “grafting from” RAFT polymerization. This was possible as polydopamine has available hydroxyl groups that can react with carboxylic groups of the RAFT agent via ester linkages. During the formation of polydopamine coating on graphene oxide, graphene oxide can be simultaneously reduced by the released electrons generated by self-polymerization of dopamine. The reduction of graphene oxide was determined by FTIR, UV/Vis, and XPS analysis.

For growing the polymer chains from the graphene surface, the living radical polymerization methodology, RAFT polymerization, was investigated. The RAFT agent, S-dodecyl-S'-(α,α' -dimethyl- α'' -acetic acid)trithiocarbonate, having an available

carboxyl group, was chosen to anchor onto the polydopamine coating and then grow chains of PS, PMMA, PNIPAM, and PtBA from this modified surface. The functionalization of polydopamine/reduced graphene oxide (PDA/RGO) was determined by FTIR and TGA studies. The livingness of the polymerization was verified by GPC characterization of cleaved polymer chains. The additional free RAFT agents in the reaction system could not only enhance the control of the polymerization on PDA/RGO surface and in solution, but also narrow the gap between grafted polymer and free polymer produced in solution as measured by GPC. The polymer grafted PDA/RGO nanocomposites showed excellent dispersibility in several organic solvents. The final polymer matrix dispersed of functionalized reduced graphene oxide showed higher maximum decomposition temperature measured by TGA, indicating better thermal stability.

Key Words:

RAFT polymerization, reduced graphene oxide, polydopamine, grafting from, polystyrene, nanocomposites.

To my dad and mom

For their full love, support, and encouragement

From the other side of the earth

To all my best friends in Canada and China

For the happiness and courage you bring to me

Acknowledgments

I would like to extend my heartfelt gratitude to my advisor, Dr. Paul A. Charpentier, for his supervision, insight, advice, and guidance throughout all stages of this research. He provided me enthusiastic support and encouragement in various ways, and he is such a nice supervisor that I am very proud to have had the opportunity to work with him.

Many thanks to Prof. Elizabeth Gillies, Prof. Jin Zhang, and Prof. James Wisner, members of the advisory and examiners committee, for their important guidance and suggestions.

I would like to express my sincere gratitude to Qasem Alsharari for Raman analysis and to Jenna Allan and Golam Moula for the AFM analysis. Many thanks go to Ross Davidson, Mark Biesinger, and Heather Bloomfield for XPS and EDX elemental analysis and to Hossein Kazemian for XRD analysis. I thank Jeffrey Gribbon for TGA analysis and Richard Gardiner for TEM analysis. I am thankful to Aneta Borecki for GPC measurement. I am also very grateful to Yixing Tang and Qasem Alsharari for their help and suggestions during my research.

In addition, I wish to thank the University of Western Ontario and Department of Chemical and Biochemical Engineering.

At last, I want to thank all my friends and colleagues for their continuous support, and advices.

Table of contents

CERTIFICATE OF EXAMINATION	ii
Abstract	iii
Acknowledgments.....	vi
Table of contents.....	vii
List of Tables	xi
List of Figures	xii
List of Appendices	xvi
List of abbreviations	xvii
Chapter 1	1
Introduction.....	1
1.1 Graphene-Polymer Nanocomposites.....	2
1.2 Living Free Radical Polymerization	4
1.3 RAFT Polymerization	4
1.3.1 Mechanism of RAFT Polymerization	6
1.3.2 Choice of RAFT Agents.....	7
1.4 Graphene	9
1.4.1 Polymer Grafting of Graphene via Living/Controlled Free-Radical Polymerization.....	10
1.4.1.1 The Covalent “Grafting To” Approach.....	10
1.4.1.2 The Covalent “Grafting From” Approach	12
1.4.1.2.1 Atom Transfer Radical Polymerization.....	13
1.4.1.2.2 Reversible Addition Fragmentation Chain-Transfer Polymerization .	14
1.4.1.2.3 The One-pot Approach.....	15

1.4.1.3 Non-Covalent Functionalization.....	16
Chapter 2.....	19
Objectives	19
Chapter 3.....	21
Functionalization of Reduced Graphene Oxide via Surface “Graft from” RAFT Polymerization	21
3.1 Introduction	23
3.2 Experimental	26
3.2.1 Materials.....	26
3.2.2 Experimental Setup	26
3.2.3 Preparation of Graphene Oxide Sheets (GO).....	28
3.2.4 Reduction of Graphene Oxide via Self-polymerization of dopamine.....	29
3.2.5 Synthesis of RAFT agent-bonded graphene sheets	29
3.2.6 Surface RAFT Polymerization of Styrene on RGO/PDA	29
3.3 Characterization	30
3.4 Results and Discussion.....	31
3.4.1 Graphene Oxide.....	31
3.4.2 Dopamine-Induced Reduction of Graphene Oxide	34
3.4.2.1 Effect of Temperature on Reduction of Graphene Oxide.....	37
3.4.2.2 Effect of Weight Ratio between reactants	40
3.4.3. Evidence of Immobilization of RAFT agent.....	41
3.4.5 Evidence of Grafted Polymer and Cleavage of Grafted Polymer	43
3.4.6 Evidence of Grafted Polymer (PMMA, PNIPAM, PtBA) on PDA/RGO.....	44
3.4.7 Dispersibility of Polymer grafted PDA/RGO.....	46

3.5 Conclusion.....	49
Chapter 4.....	51
Livingness and Kinetic Study of Surface “Grafting from” RAFT Polymerization on PDA/RGO.....	51
4.1 Introduction.....	53
4.2 Experimental.....	54
4.2.1 Materials.....	54
4.2.2 Surface RAFT Polymerization of Styrene on RGO/PDA without Free RAFT agent.....	55
4.2.3 Surface RAFT Polymerization of Styrene on RGO/PDA with Free RAFT agent.....	55
4.2.4 Preparation of PS Composite Containing Graphene.....	56
4.2.5 Cleaving Grafted Polymer from RGO/PDA ⁸⁸	56
4.2.6 RAFT Polymerization of Styrene.....	57
4.2.7 Free Radical Polymerization of Styrene.....	57
4.3 Characterization.....	57
4.4 Results and Discussions.....	58
4.4.1 Kinetics of Solution and Surface RAFT Polymerization of Styrene.....	58
4.4.2 Conventional Free Radical and RAFT Polymerization.....	59
4.4.3 Livingness Study of Surface “Grafting from” RAFT Polymerization.....	63
4.4.4 Kinetic Study of Surface “Grafting from” RAFT Polymerization.....	69
4.4.5 Improvement of dispersibility of PS-PDA/RGO nanocomposites.....	72
4.4.6 Improvement of thermal stability of PS-PDA/RGO nanocomposites.....	74
4.5 Conclusion.....	75
Chapter 5.....	77

Conclusions and Recommendations	77
Bibliography	81
Appendices.....	90
Curriculum Vitae	94

List of Tables

Table 3.1. The RAFT agent with its suitability for various monomer types	25
Table 3.2. Reaction conditions of dopamine induced reduction of graphene oxide.....	38
Table 3.3. Reaction conditions of synthesis of RAFT agent bonded PDA/RGO	41
Table 3.4. Atomic percentage (carbon, oxygen, sulfur) of RAFT agent grafted PDA/RGO	42
Table 4.1. Synthesis of PS by conventional free radical polymerization and RAFT polymerization.	60
Table 4.2. Synthesis of PDA/RGO grafted with PS by RAFT polymerization without free RAFT agent in solution. (g): graft polystyrene, (f): free polystyrene.....	63
Table 4.3. Synthesis of PDA/RGO grafted with PS by RAFT polymerization with free RAFT agent in solution (g: graft, f: free).....	66

List of Figures

Figure 1.1. Total publications, papers, and patents on RAFT polymerization based on SciFinder search of terms ‘RAFT Polymerization’, The term ‘papers’ includes journal, letters and reviews but does not include conference abstracts.....	5
Figure 1.2. Mechanism of RAFT Polymerization.	7
Figure 1.3. Structural features of thiocarbonylthio RAFT agent and the intermediate formed on radical addition.	7
Figure 1.4. Four classes of RAFT agents: A) Dithiobenzoates, B) Trithiocarbonates, C) Dithiocarbamates, and D) Xanthates.	8
Figure 1.5. Guidelines for selection of RAFT agents (Z-C(=S)S-R) for various polymerizations. For ‘Z’, addition rates and transfer constants decrease and fragmentation rates increase from left to right. For ‘R’, fragmentation rates decrease from left to right. A dashed line indicates limited control (e.g., retardation, high dispersity likely).	9
Figure 1.6. Schematic representation of the “Grafting To” approach to graphene functionalization with polymers.	11
Figure 1.7. Synthesis of GO-TDI, DDAT-PVK, and GO-PVK.	11
Figure 1.8. Strategy for “clicking” monodispersed PS onto graphene sheets.	12
Figure 1.9. Schematic representation of the “Grafting From” approach to graphene functionalization with polymers.	13
Figure 1.10. Synthesis of surface-functionalized graphene oxide via attachment of and ATRP initiator (α -bromoisobutyryl bromide) followed by polymerization of styrene, butyl acrylate, or methyl methacrylate.....	13
Figure 1.11. Outline for the preparation of PNIPAM/RGO nanocomposites based on click chemistry and RAFT polymerization.....	15
Figure 1.12. Synthesis of homopolymers and diblock copolymers grafted GO by MPTT (a) and TBPT (b) mediated RAFT process and coupling reaction.	16
Figure 1.13. Preparation of graphene/polymer nanocomposites via π - π stacking.....	17
Figure 1.14. Synthesis of pH sensitive pyrene-polymer composites via π - π stacking interactions for the self-assembly of functionalized graphene into layered structures.	18
Figure 3.1. GO synthesis lab setup.	27

Figure 3.2. RAFT polymerization setup.	27
Figure 3.3. Synthesis of dopamine induced reduced graphene oxide and RAFT agent grafted PDA/RGO.....	29
Figure 3.4. Left: Suspension of graphene oxide in H ₂ O. Right: Photo of graphene oxide sheet.	32
Figure 3.5. FT-IR spectrum of GO.	32
Figure 3.6. TEM image of GO (the scale is 500 nm).	33
Figure 3.7. (a) A tapping mode AFM image of graphene oxide (GO) sheets on mica surface. Wrinkles were frequently observed for the large sheets deposited from dispersion in water (scale bar: 1 μm), (b) the height profile of the AFM image, the height difference between two lines is 1.1nm.	34
Figure 3.8. Photograph of aqueous GO (left) and PDA/RGO (right) suspension.	34
Figure 3.9. (a) A tapping mode AFM image of graphene oxide (GO) sheets on mica surface, (b) the height profile of the AFM image, the height difference between two lines is about 4 nm.	35
Figure 3.10. FTIR spectra of graphite (top), PDA/RGO (middle), and GO (bottom).....	35
Figure 3.11. XPS characterization of GO and the PDA modified RGO. <i>Left: C1s, Right: Scan</i>	36
Figure 3.12. UV-Vis absorption spectra of graphene oxide and reduced graphene oxide water suspension.	37
Figure 3.13. X-ray powder diffraction patterns of graphite, graphene oxide (GO) and PDA/RGO. (PDA gave no diffraction in the 2θ of 20-25° region ⁸³).	38
Figure 3.14. Left: XRD image of PDA/RGO. Conditions: dopamine : GO = 2 : 1 (weight ratio) in buffer solution (pH = 8.5) at room temperature and 60 °C. Middle & Right: Raman images of PDA/RGO. Conditions: dopamine : GO = 1 : 1 (middle), dopamine : GO = 2 : 1 (right) in buffer solution (pH = 8.5) at room temperature and 60 °C.	39
Figure 3.15. Left: XRD images of PDA/RGO Conditions: dopamine : GO = 1 : 4, 1 : 2, 2 : 1, and 4 : 1 (weight ratio) in buffer solution (pH = 8.5) at 60 °C. Right: Raman images of PDA/RGO Conditions: dopamine : GO = 1 : 4, and 4 : 1 (weight ratio) in buffer solution (pH = 8.5) at 60 °C.....	40
Figure 3.16. TGA curves of PDA/RGO and RAFT agent grafted PDA/RGO under nitrogen. The weight left at 790 °C is (a) 59 %; (b) 52 %, and (c) 49.4 %.....	41

Figure 3.17. EDX images of RAFT agent grafted PDA/RGO. (Left: PDA/RGO-RAFT 1, Right: PDA/RGO-RAFT 2)	42
Figure 3.18. Elemental mapping of sulfur of RAFT agent grafted PDA/RGO. Right: SEM image. Left: Sulfur element distribution on the same area of left image.....	43
Figure 3.19. FTIR spectrum of PS-PDA/RGO nanocomposite.....	44
Figure 3.20. Left: FTIR spectra of PMMA grafted PDA/RGO and RAFT agent grafted PDA/RGO. Right: TGA curve of PMMA grafted PDA/RGO under nitrogen.	44
Figure 3.21. Left: FTIR spectra of PNIPAM grafted PDA/RGO and RAFT agent grafted PDA/RGO. Right: TGA curve of PNIPAM grafted PDA/RGO under nitrogen.	45
Figure 3.22. Left: FTIR spectra of PtBA grafted PDA/RGO and RAFT agent grafted PDA/RGO. Right: TGA curve of PtBA grafted PDA/RGO under nitrogen.	46
Figure 3.23. (a) Photographs of PS-PDA/RGO samples dispersed in various solvents by sonication for 30 min with a concentration of 1.0 mg/mL. Solvents were hexane, toluene, chloroform, methanol, ethanol, acetone, THF, DMF and water (from left to right). (b) PS-PDA/RGO suspension in acetone after overnight settled to the bottom.....	47
Figure 3.24. Photographs of PMMA-g-PDA/RGO and PtBA-g-PDA/RGO samples dispersed in various solvents with a concentration of 1.0 mg/mL. Solvents were hexane, toluene, chloroform, methanol, ethanol, acetone, THF, DMF and water (from left to right).	48
Figure 3.25. Photographs of PNIPAM-g-PDA/RGO samples dispersed in various solvents with a concentration of 1.0 mg/mL. Solvents were hexane, toluene, chloroform, methanol, ethanol, acetone, THF, and DMF (from left to right).	48
Figure 3.26. (a) PNIPAM-PDA/RGO suspension in water after 1 hour sonication under 40 °C. (b) suspension of (a) after placement of 5 min. (c) PNIPAM-PDA/RGO suspension in water after 10 min sonication under 0 °C.....	49
Figure 4.1. Schematic diagram of RAFT polymerization from a trithiocarbonate RAFT agent anchored to the surface of sheets via Z and R groups.	53
Figure 4.2. Left: Styrene conversion vs. time data for solution RAFT polymerization. Right: Molecular weight vs. styrene conversion data for solution RAFT polymerization (circle), free radical polymerization (square) and theoretical M_w of RAFT polymerization (blue line).	61
Figure 4.3. TGA thermograms of PDA/RGO-g-PS taken at different time intervals (a-f) under nitrogen. The weight left at 600 °C is (a) 46 %; (b) 39 %; (c) 22 %; (d) 10 %; (e) 8 %, and (f) 4 %.	62

Figure 4.4. EDX analysis of residual solid after acid treatment of PS-PDA/RGO.	62
Figure 4.5. Left: Dependence of M_n of grafted polymer on conversion. Right: Dependence of M_n of free polymer on conversion. Condition: without free RAFT agents in solution. Blue line: Theoretical M_n (Appendix 3)	64
Figure 4.6. Key processes in RAFT-mediated graft polymerizations.	65
Figure 4.7. Dependence of M_n of grafted polymer (g) and free polymer (f) on conversion. Blue line: Theoretical M_n (Appendix 3). Condition: with free RAFT agents in solution.	67
Figure 4.8. GPC elution profiles of free (dashed line) and grafted (solid line) PS samples obtained by surface RAFT polymerization on RAFT-PDA/RGO.....	68
Figure 4.9. GPC elution profiles for surface RAFT polymerization on RAFT-PDA/RGO of styrene with AIBN as initiator at 60 °C, for 35 h ($M_n = 12,630$ g/mol, PDI = 1.251), 49.5 h ($M_n = 21,890$ g/mol, PDI = 1.255), 66 h ($M_n = 28,240$ g/mol, PDI = 1.495), 80.5 h ($M_n = 33,130$ g/mol, PDI = 1.496).....	69
Figure 4.10. Dependence of conversion of monomer on time. Black dots (Left: without free RAFT agent in solution. Right: with free RAFT agent in solution). Red dots (conventional RAFT polymerization.	70
Figure 4.11. (a) First-order kinetic plots for the graft polymerization of styrene with functionalized PDA/RGO; solution RAFT polymerization, surface RAFT polymerization with and without free RAFT agent. (b) First-order kinetic plots for free radical polymerization.	71
Figure 4.12. PS/PS-PDA/RGO composites (from left to right: 1.5%, 1.0%, and 0.5% RGO); (a) PS-PDA/RGO nanocomposite has 10.1% RGO; (b) PS-PDA/RGO nanocomposite has 39.4% RGO; (c) PS-PDA/RGO nanocomposite has 46.3% RGO....	73
Figure 4.13. Relative weight loss of pure PS and PS/(PS-PDA/RGO) (0.25% RGO) composite under heating. (PS/RGO-1: 46.3% RGO; PS/RGO-2: 39.4% RGO; PS/RGO-3: 21.9% RGO)	74
Figure 4.14. Left: Relative weight loss of pure PS and PS/(PS-PDA/RGO) composites with different contents of RGO. (0.25% - 1.5%) PS-PDA/RGO nanocomposite contains 21.9% RGO. Right: Relative weight loss of polydopamine under heating.	75

List of Appendices

Appendix 1. Synthesis of PMMA, PNIPAM and PtBA grafted PDA/RGO	91
Appendix 2. Calculation of the amount of RAFT agent attached to PDA/RGO	92

List of abbreviations

Abbreviations:

AFM	Atomic force microscopy
AIBN	2,2'-Azobis(2-methylpropionitrile)
ATRP	Atom transfer radical polymerization
CTA	Chain transfer agent
DLS	Dynamic light scattering
DMAP	4-Dimethylaminopyridine
DMF	N,N-Dimethylform amide
EDC·HCl	N-(3-Dimethylaminopropyl)-N'-ethylcarbodiimide hydrochloride
EDX	Energy dispersive X-ray spectroscopy
FG	Functionalized graphene
FTIR	Fourier transform infrared spectroscopy
GO	Graphene oxide
GPC	Gel permeation chromatography (g/mol)
GN	Graphene nanosheet
LCST	Lower critical solution temperature (°C)
MMA	Methyl methacrylate
NIPAM	N-isopropylacrylamide
NMP	Nitroxide mediated polymerization
PDI	Polydispersity index = M_w/M_n
PMMA	Poly (methyl methacrylate)
PDA	Polydopamine
PDA/RGO	Polydopamine/Reduced graphene oxide
PNIPAM	Poly(N-isopropylacrylamide)
PS	Polystyrene
PtBA	Poly(tert-butyl acrylate)
RAFT	Reversible addition-fragmentation chain-transfer
RAFT-PDA/RGO	RAFT agent grafted PDA/RGO
RGO	Reduced graphene oxide
SEM	Scanning electron microscope

SLS	Static light scattering
tBA	Tert-butyl acrylate
TEM	Transmission electron microscopy
THF	Tetrahydrofuran
Tris-Cl	Tris(hydroxymethyl)amino methane
UV/Vis	Ultraviolet/Visible
XPS	X-ray photoelectron spectroscopy
XRD	X-ray diffraction

Chapter 1
Introduction

1.1 Graphene-Polymer Nanocomposites

Recently, the combination of nanomaterials and polymeric materials has led to a new class of multi-functional materials termed polymer nanocomposites¹. Academic and industrial research on polymer nanocomposites is pursued towards providing added value properties to the neat (i.e. virgin) polymer materials without sacrificing polymer processability or adding excessive weight. One of the main reasons to use nanomaterials as fillers is their large surface to volume ratio, which will enhance their intrinsic properties. The resulting large interfacial area and the corresponding interphase between the nano-sized heterogeneities and the polymer matrix potentially can result in exceptional properties not possible with traditional filled polymers. The category of the nanofiller can be generalized on the basis of the dimensions such as one-dimensional (nanowires² and nanotubes³), two-dimensional (nanoclays⁴) or three-dimensional (spherical⁵ and cubic nanoparticles⁶) structures.

Very recently, a new two-dimensional nanomaterial, denoted as graphene, has been under intense interest since 2004 when Geim and co-workers first successfully stripped graphene from graphite flakes by the “scotch-tape” method⁷. This led to the development of graphene-based polymer nanocomposites being a new direction of research. Graphene is a two-dimensional (2-D) sheet composed of sp^2 carbon atoms densely packed in a honeycomb network, and it possesses excellent electronic conductivity⁸, high thermal conductivity⁹, and superior mechanical strength¹⁰. Therefore, graphene is considered as an excellent choice of nanofiller for making advanced polymer nanocomposites. However, the major drawbacks of pristine graphene as a nanofiller are the strong van der Waals interactions between graphene sheets, resulting in poor compatibility with most polymers. The properties of a graphene-based polymeric nanocomposite greatly depend on the dispersion of graphene in the polymeric matrix. The irreversible aggregation of graphene via π - π stacking will greatly hinder its production, storage and processing¹¹. Hence the functionalization and stabilization of graphene via modification is necessary in order to avoid the undesired aggregation to maximize properties for the intended end-use application.

Functionalized graphene (FG) has many natural advantages as an ideal nanofiller for polymer nanocomposites as:¹²

- (1) The FG possesses most physical properties of graphene, although it has a partially damaged carbon structure.
- (2) The functionalities on the surface of graphene can provide benefits by enhancing the dispersion of graphene in polymeric matrices and increasing the interfacial interaction between graphene and polymeric matrices.

It is well-known that the dispersion and interface are two key parameters in the evaluation of polymer nanocomposites. Many efforts have been undertaken in order to enhance the filler-matrix interactions. Although the attachment of discrete, small molecules has resulted in significant progress in the study and application of graphene, the introduction of polymers is also an area of vigorous research. Due to their large size, a single polymer chain should impart a greater influence over the properties of graphene than the corresponding single small molecule. Also, synthetic polymers are advantageous in that they can be highly processible and soluble, and are easily derivatized via a wide array of functional groups.

Recently-developed polymerization methods, especially living free radical polymerization techniques, allow for the preparation of polymers with precise control over composition, architecture, and molecular weight. Therefore, the introduction of well-defined polymers on the surface of graphene sheets allows the preparation of composites that merge the properties of the polymer with the conductivity and strength of graphene. For these reasons, the polymer chemistry of graphene has recently attracted significant interest.

Strategies to modify the surface of the graphene filler with attachment of stabilizing polymer ligands prepared by living radical polymerization techniques have capitalized on the “grafting to”, “grafting from”, or noncovalent methods. The “grafting to” technique involves the attachment of preformed polymer chains to the graphene sheets, while the “grafting from” technique involves growing the polymer chains from the graphene

surface. This latter approach can help minimize aggregation while strengthening the interactions between the nanofillers and the polymer matrix, as examined in this thesis.

1.2 Living Free Radical Polymerization

Conventional free radical polymerization is one of the most popular and powerful techniques for the commercial production of high molecular weight polymers because of its wide ranging applicability, versatility, and low cost. However, free radical polymerization always gives broad polydispersity indexes ($PDI > 1.5$) and the molecular weight of polymer becomes relatively high in the early stages of polymerization, leading to problems in viscosity. In addition, this technique is limited in its ability to synthesize polymers with complex architectures, including nanocomposites.

Therefore, interest in living polymerization, which is a form of addition polymerization where the ability of a growing polymer chain to terminate has been removed, has shown tremendous growth. In an ideal living polymerization, all chains are initiated at the beginning of the process, grow at the same rate, and have no termination step. Thus, living radical polymerization can become possible in the presence of reagents that react with the propagating radicals by reversible deactivation or reversible chain transfer. Based on this principle, three kinds of living free radical polymerization techniques are most investigated: atom transfer radical polymerization (ATRP)¹³, nitroxide-mediated polymerization (NMP)¹⁴ and reversible addition-fragmentation chain transfer (RAFT)¹⁵.

The ATRP and NMP techniques control growth of chains by reversible deactivation, while the RAFT technique controls chain growth through reversible chain transfer. As the dormant species is a stable compound, it can stop and reinitiate the polymerization easily to produce polymers with controlled and potentially complex architectures.

1.3 RAFT Polymerization

RAFT polymerization is a type of controlled radical polymerization technique first developed by Ezio Rizzardo's group at the Commonwealth Scientific and Industrial

Research Organization (CSIRO) in 1998¹⁵. Since invented, it has emerged as a powerful and popular method of living/controlled free radical polymerization, since the method allows synthetic tailoring of polymers with complex architectures, including graft, block, star, and comb structures with controlled molecular weight¹⁶. Figure 1.1 illustrates the increasing importance of RAFT.

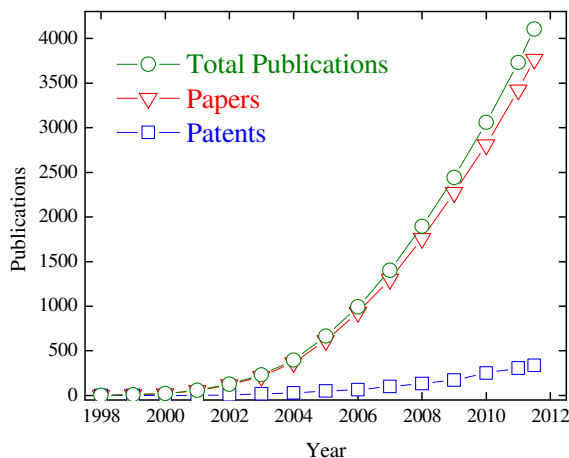


Figure 1.1. Total publications, papers, and patents on RAFT polymerization based on SciFinder search of terms ‘RAFT Polymerization’, The term ‘papers’ includes journal, letters and reviews but does not include conference abstracts.

Compared to ATRP and NMP, the main advantage of RAFT polymerization is its compatibility with a wide range of monomers, including styrenic, (meth)acrylic, (meth)acrylamido¹⁷, isoprene¹⁸, vinylic¹⁹, diallyl²⁰ and charged (anionic²¹, cationic¹⁷ and zwitterionic²²) monomers. The technique is tolerant to unprotected functionalities in the monomer (e.g., OH, NR₂, COOH, CONR₂, SO₃H) and solvent. As well, polymerizations can be carried out in aqueous or protic media.

Another advantage of RAFT polymerization is that it is easy to carry out, similar to a conventional free radical polymerization reaction with introducing a suitable chain transfer agent (CTA), known as the RAFT agent. Also, RAFT can be used in all modes of free radical polymerization: bulk, solution (organic and aqueous²³), suspension, emulsion, mini and micro emulsion polymerizations. As with other living/controlled polymerization techniques, RAFT polymerization has been exploited to build complex molecular

architectures, such as blocks²⁴, combs²⁵, graft²⁵, gradient²⁶, and star²⁷ copolymers. The RAFT-polymers in combination with other nanostructures can generate hybrid multifunctional nanomaterials, including polymer-functionalized graphene²⁸, carbon nanotubes²⁹ and inorganic nanoparticles³⁰.

1.3.1 Mechanism of RAFT Polymerization

RAFT polymerization controls the length of chains via a reversible chain transfer process, which differs from that involved in NMP and ATRP. The addition-fragmentation equilibria shown in Figure 1.2 are the key features of the RAFT mechanism with thiocarbonylthio compounds. There are five main steps in a RAFT polymerization. Initiation and termination (combination or disproportionation) occur as in a conventional radical polymerization, although the termination step should be small during the polymerization. In the early stages, the initiating radicals from a traditional initiator (*e.g.* 2,2'-Azobis(2-methylpropionitrile) (AIBN)) react with the RAFT agent (1). Then, the fragmentation of the intermediate radical can provide a polymeric thiocarbonylthio compound (3) and a reinitiating radical ($R\cdot$), which is able to react with other monomers to start another active polymer chain ($P_m\cdot$). Chain equilibration/propagation is the most significant part in the RAFT process, in which polymer chains rapidly exchange between existing radicals and thiocarbonylthio group capped species. This step allows for approximately the same rate of growth of all chains, leading to polymers with narrow polydispersities. Usually, the thiocarbonylthio groups are retained at the end of the polymer chains.

For the R group, it should be a good leaving group, which is able to stabilize a radical such that the right hand side of the reversible chain transfer/propagation step (B) is favored. R[•] needs to be unstable enough that it can efficiently reinitiate monomer as an expelled radical. On the other hand, the Z group primarily affects the stability of the C=S bond and the stability of the adduct radical (polymer-S-C(Z)-S-polymer).^{19a}

A wide range of RAFT agents with different R and Z groups have been synthesized and studied for their effectiveness in controlling the polymerization of vinyl monomers. Different RAFT agents are more suitable for specific classes of monomers. The main classes of RAFT agents are:³¹

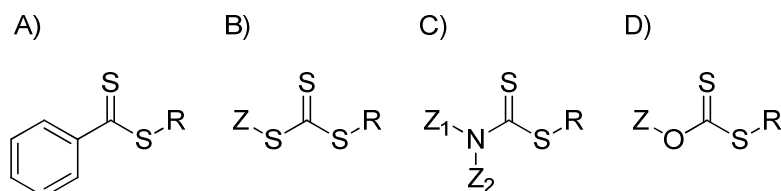


Figure 1.4. Four classes of RAFT agents: A) Dithiobenzoates, B) Trithiocarbonates, C) Dithiocarbamates, and D) Xanthates.

A) Dithiobenzoates

- Very high transfer constants
- Prone to hydrolysis
- May cause polymerization retardation under high concentrations

B) Trithiocarbonates

- High transfer constants
- More hydrolytically stable (than dithiobenzoates)
- Cause less retardation

C) Dithiocarbamates

- Activity determined by substituents on N
- Effective with electron-rich monomers

D) Xanthates

- Lower transfer constants
- More effective with less activated monomers
- Made more active by electron-withdrawing substituents

Figure 1.5 provides guidelines on how to select the appropriate RAFT agent for a particular monomer.

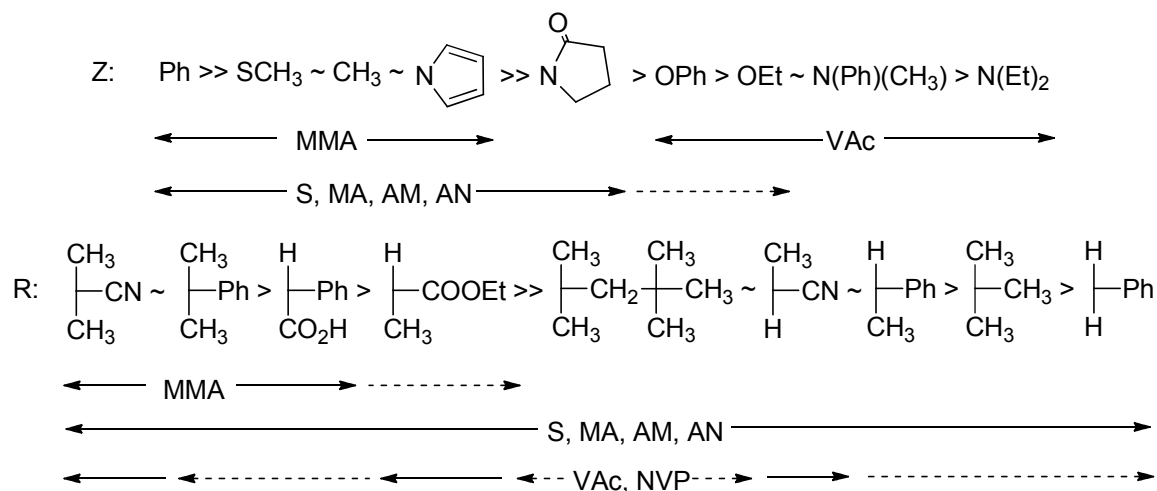


Figure 1.5. Guidelines for selection of RAFT agents (Z-C(=S)S-R) for various polymerizations. For ‘Z’, addition rates and transfer constants decrease and fragmentation rates increase from left to right. For ‘R’, fragmentation rates decrease from left to right. A dashed line indicates limited control (e.g., retardation, high dispersity likely).

1.4 Graphene

The chemistry of graphene has become an area of intense research. The field of research centered on the properties and applications of graphene has experienced fast-paced growth since its discovery. Potential new applications based on graphene and chemically modified graphene have been demonstrated, including electronics³², sensors³³, electromechanics³⁴, solar cells³⁵, memory devices³⁶, hydrogen storage³⁷ and ultracapacitors³⁸. However, the extended π -conjugated framework is also responsible for strong inter-sheet van der Waals interactions, which leads to aggregation of the graphene sheets. The resulting aggregates are completely insoluble in all organic and aqueous

solvents. This lack of solubility poses a significant impediment to their exploitation in many potential commercial applications. Specifically, numerous researchers have focused on improving the solubility of graphene through chemical grafting. Until now, significant effort has been devoted to the attachment of polymers to the surface of graphene, as macromolecules can be more effective in modifying graphene solubility properties than small molecules. It is clear that, due to their large size, a single polymer chain should impart a greater influence over the properties of graphene sheets than that from a corresponding single small molecule.

In addition, functional polymers have enabled the preparation of polymer-graphene nanocomposites that demonstrate a variety of interesting properties, for example, responsiveness to environmental stimuli (temperature³⁹ and pH⁴⁰).

1.4.1 Polymer Grafting of Graphene via Living/Controlled Free-Radical Polymerization

Recently-developed polymerization methods, especially living/controlled free radical polymerization techniques, allow for the preparation of polymers with precise control over polymer composition, architecture and molecular weight.

A variety of different techniques have been applied to the functionalization of graphene with polymers, including “grafting to”, “grafting from”, and noncovalent interactions.

1.4.1.1 The Covalent “Grafting To” Approach

In general, the “grafting to” approach involves pre-formed polymer chains reacting with the surface of either pristine or pre-functionalized graphene sheets (Figure 1.6). Graphene oxide itself is a type of pre-functionalized graphene containing carboxyl and hydroxyl groups. Most functionalizations begin with graphene oxide, or with functionalized graphene synthesized through further reduction.

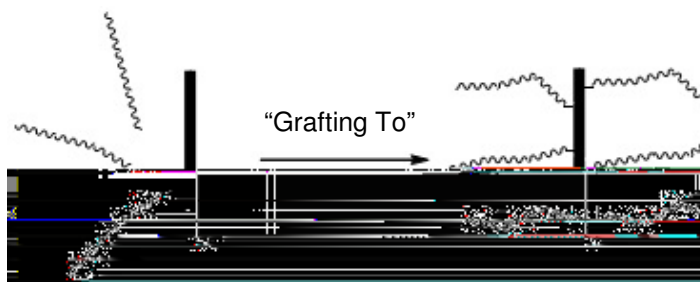


Figure 1.6. Schematic representation of the “Grafting To” approach to graphene functionalization with polymers.

Zhuang *et.al* created anchor sites for grafted polymers on graphene oxide with toluene-2,4-diisocyanate (TDI)⁴¹ (Figure 1.7), since isocyanates can react with carboxyl and hydroxyl groups. The group prepared a donor-acceptor type poly (N-vinylcarbazole)-covalently functionalized GO. Poly (N-vinylcarbazole) (PVK) was synthesized by RAFT polymerization with S-Dodecyl-S’-(α,α' -dimethyl- α' -acetic acid) trithiocarbonate) (DDAT), which has a terminal carboxyl group⁴² (Figure 1.7).

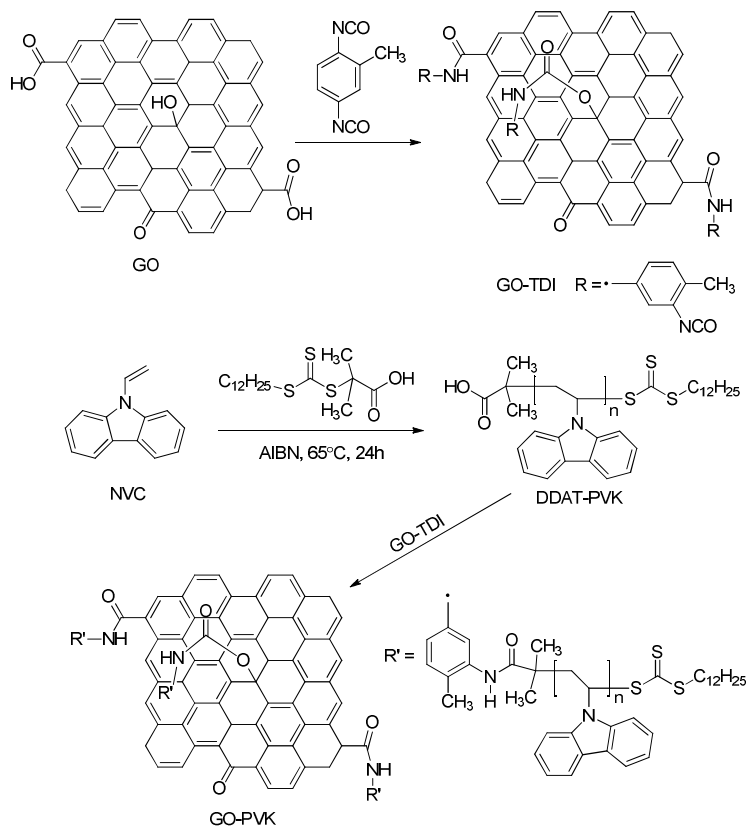


Figure 1.7. Synthesis of GO-TDI, DDAT-PVK, and GO-PVK.

Also recently, Wu and co-workers utilized click chemistry to introduce azide-terminated polystyrene chains onto alkyne-functionalized GO⁴³. The alkyne functionalized GO was accomplished via an acylation reaction with propargyl alcohol, while the azido-terminated monodispersed polystyrene was prepared by ATRP (Figure 1.8). The resulting PS-grafted graphene sheets were well dispersed in DMF, THF, CH₂Cl₂ and toluene, which are all good solvents for PS, but poorly dispersed in water, methanol and hexane, which are poor solvents for PS.

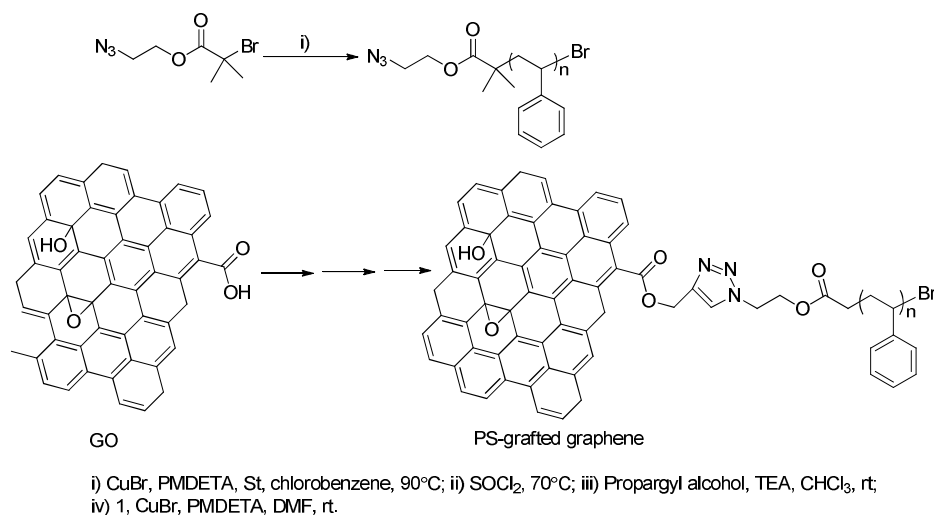


Figure 1.8. Strategy for “clicking” monodispersed PS onto graphene sheets.

1.4.1.2 The Covalent “Grafting From” Approach

The “grafting from” approach involves the polymerization of monomers from surface-derived initiators on GO. (Figure 1.9) These initiators are covalently attached using the various functionalization reactions developed for small molecules. For the “grafting to” strategy, beyond a certain degree of functionalization, diffusion of additional molecules to the surface becomes impeded, establishing an upper limit to reactivity. In contrast, the advantage of surface-initiated polymerization (SIP) is that the polymer growth is not limited by steric hindrance, allowing higher molecular weight polymers to be grown. To demonstrate this approach, ATRP and RAFT techniques have been employed most frequently because of their tolerance to a wide range of monomers.



Figure 1.9. Schematic representation of the “Grafting From” approach to graphene functionalization with polymers.

1.4.1.2.1 Atom Transfer Radical Polymerization

ATRP has been shown to be one of the most successful controlled “living” radical polymerization methods since its discovery in 1995¹³. Ruoff and coworkers recently published a report describing the grafting of polystyrene, poly(methyl methacrylate) and poly(butyl acrylate) from GO by ATRP⁴⁴ (Figure 1.10). The GO-bound initiator groups were introduced by treating GO with excess isobutyryl bromide. The attached polymers exhibited relative low PDIs (typically less than 1.5), which suggests that the aforementioned SIPs proceeded in a controlled manner, despite the fact that the polymerizations were initiated and conducted from a surface.

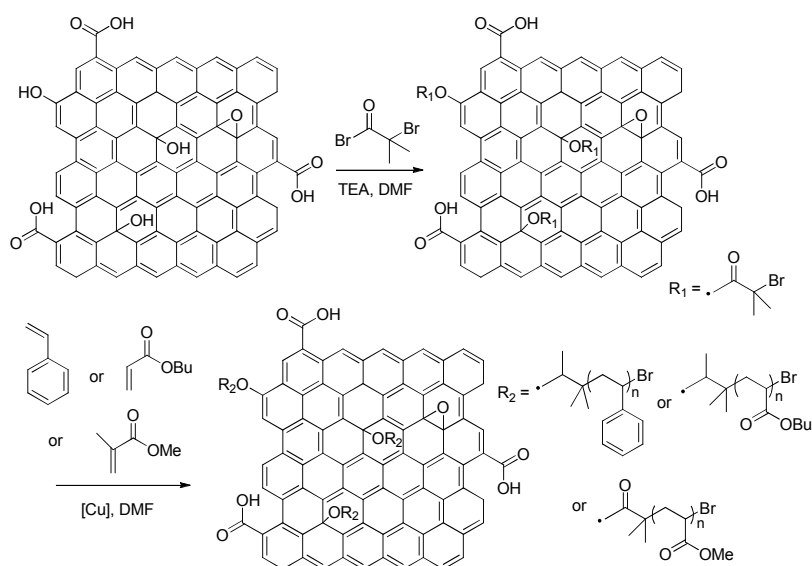


Figure 1.10. Synthesis of surface-functionalized graphene oxide via attachment of and ATRP initiator (α -bromoisobutyryl bromide) followed by polymerization of styrene, butyl acrylate, or methyl methacrylate.

Subsequently, for developing high performance graphene-based nanocomposites, Lu's group reported the attachment of initiator molecules covalently bonded to graphene nanosheets' surface via a diazonium addition⁴⁵. The prominent confinement effect arising from the nanosheets resulted in a 15°C increase in the glass transition temperature (T_g) of PS-GNs loaded polystyrene nanocomposites compared to the pure polymer. The nanocomposites also revealed increases in tensile strength and Young's modulus.

Later, Lu published the first effort to systematically tune the interface structure of single-layer GNs with covalently grafted polystyrene chains⁴⁶. The grafting density of PS was effectively controlled by diazonium addition and ATRP was utilized to tailor the chain length of the grafted PS. Furthermore, Lu demonstrated that modified graphene filled PS composites revealed improvements in thermal conductivity. In this case, the low grafting density composites exhibited higher thermal conductivities than those of the high grafting density samples. The reason for this effect might be that the covalent bonding diminishes the aromaticity of GNs, thus impairing the efficiency of heat transfer.

1.4.1.2.2 Reversible Addition Fragmentation Chain-Transfer Polymerization

Besides ATRP, the RAFT polymerization technique has also been utilized to grow polymer chains on the surface of GO. Chen et al. reported an approach using a RAFT agent attached to GO for growing poly (N-vinylcarbazole) directly from the surface of GO²⁸. The RAFT agent was immobilized on the GO surface by means of an esterification reaction. Also, Etmimi and coworkers prepared the same GO-RAFT agent and dispersed it in monomer to form miniemulsions in the presence of a surfactant and a hydrophobe⁴⁷. The miniemulsion was polymerized to synthesize PS-GO nanocomposite latex particles with core-shell morphology. The mechanical properties (e.g. storage and loss modulus) of the nanocomposites improved significantly as the amount of modified GO increased.

In addition to immobilizing RAFT agents on GO surfaces via an esterification reaction, Zhao et al. developed a new approach to grow polymer brushes (PNIPAM)) on the surface of reduced GO (RGO) sheets based on click chemistry and RAFT

polymerization⁴⁸. As shown in Figure 1.11, alkyne groups were introduced onto the RGO surface through a reaction of RGO sheets with aryldiazonium salts containing alkyne groups. Azide-terminated RAFT agent was synthesized by reaction of S-Dodecyl-S'-(α,α' -dimethyl- α'' -acetic acid)trithiocarbonate and 3-azido-1-propanol. Then the modified RAFT agent was grafted to the surface of RGO by facile click chemistry, and NIPAM was grown on the RGO sheets via RAFT polymerization.

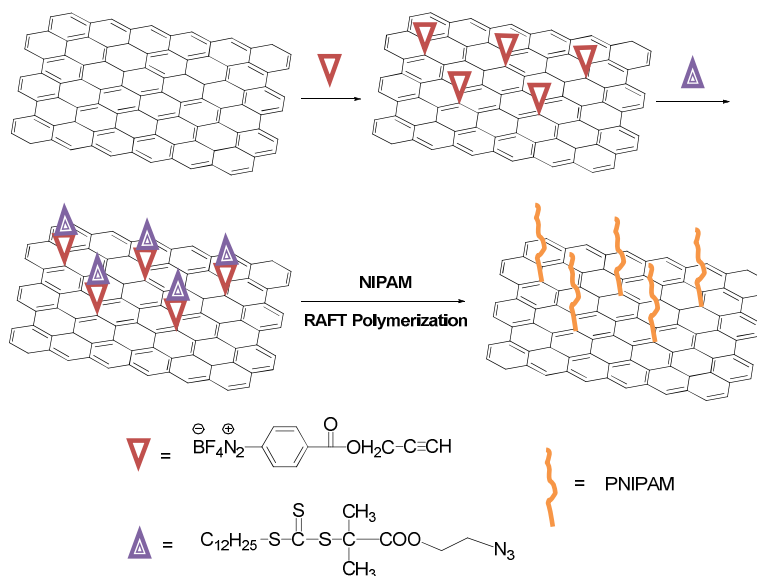


Figure 1.11. Outline for the preparation of PNIPAM/RGO nanocomposites based on click chemistry and RAFT polymerization.

1.4.1.2.3 The One-pot Approach

Zhao and coworkers demonstrated a strategy to synthesize homopolymer and block copolymer grafted graphene oxide by a simultaneous coupling reaction and RAFT process⁴⁹. As shown in Figure 1.12, two couplable RAFT agents (Z or R-alkoxysilane-functionalized chain transfer agents) were used to prepare the polymer grafted nanocomposites. The resultant composites gave enhanced solubility and dispersibility in a wide range of solvents including hexane and water. This surface modification technique offers the opportunity to alter GO morphologies. Some surface morphologies involving nanosheets, nanoparticles and nanorods were observed when the nanocomposites were originally dispersed in different solvents.

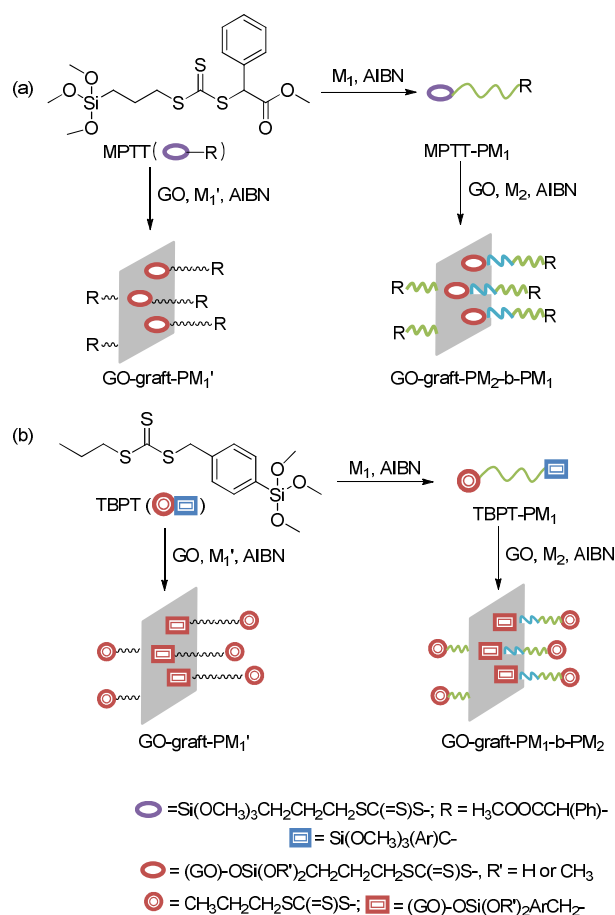


Figure 1.12. Synthesis of homopolymers and diblock copolymers grafted GO by MPTT (a) and TBPT (b) mediated RAFT process and coupling reaction.

1.4.1.3 Non-Covalent Functionalization

In addition to covalent polymer-grafting chemistry, the non-covalent methods appear versatile and promising. The interactions resulting from non-covalent modifications are relatively weak compared with covalent ones, but are easy to achieve over the entire graphene surface and reversible in some cases. There are a few non-covalent methods to modify graphene, amongst which, π - π stacking is one of the most popular ones.

π - π stacking interaction, which is a kind of strong non-covalent bonding, usually occurs between two relatively large non-polar aromatic rings having overlapping π orbitals. Moreover, π - π stacking modification does not disrupt the conjugation of the graphene sheets, and therefore preserves the electronic properties of graphene. Pyrene is a π -

orbital-rich group that is able to form strong π - π stacking interactions with other polyaromatic materials. In order to modify graphene with polymer via π - π stacking, one strategy is to synthesize polymer with pyrene moieties as the terminus of the polymer chains. RAFT polymerization can be a useful tool to reach this target. Polymers with pyrene-end-groups have been made using this technique in several recent literatures⁵⁰.

In recent studies, Davis and coworkers have investigated thermal sensitive graphene/polymer nanocomposites.⁵¹ They first synthesized a well-defined thermoresponsive pyrene-terminated PNIPAM using RAFT polymerization. When the pyrene-functional polymers were attached onto the basal plane of graphene sheets via π - π stacking interactions, the aqueous solutions of the resultant graphene-polymer composites exhibited a lower critical solution temperature (LCST) of 24°C.

As an extension of this work, thermal sensitive random copolymers of oligoethylene glycol acrylate (OEG-A) and diethylene glycol ethyl ether acrylate (DEG-A) with controllable LCST were synthesized using the same RAFT mechanism as shown in Figure 1.13. These thermo-sensitive copolymers were further used to functionalize graphene via π - π stacking to afford graphene/polymer composites with controllable LCSTs from 22 to 72°C.⁵²

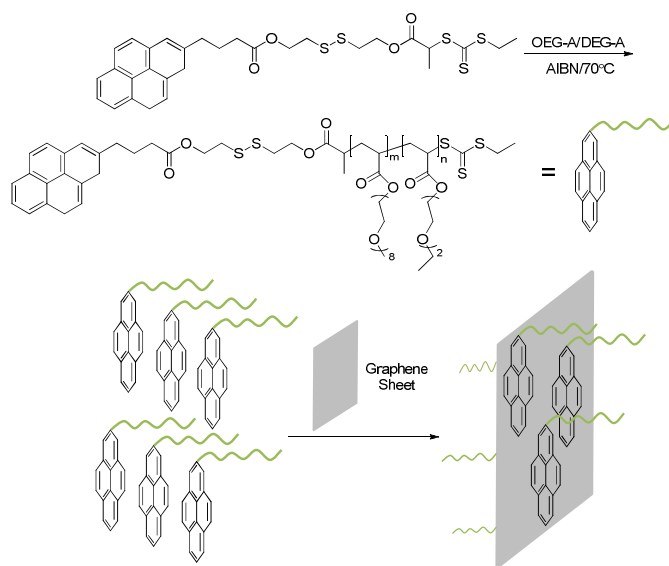


Figure 1.13. Preparation of graphene/polymer nanocomposites via π - π stacking.

By using π - π stacking interactions, Davis's group also applied a similar synthesis method to prepare pH sensitive graphene/polymer composites by the modification of graphene basal planes with pyrene-terminated poly(2-N,N'-(dimethyl amino ethyl acrylate) (PDMAEA) and poly(acrylic acid) (PAA) (Figure. 1.14).⁴⁰ The graphene-polymer composites demonstrated phase transfer behavior between aqueous and organic media at different pH values. The two graphene-polymer composites with opposite charges were self-assembled into layer-by-layer (LBL) structures as evidenced by high-resolution SEM and quartz crystal microbalance measurements.

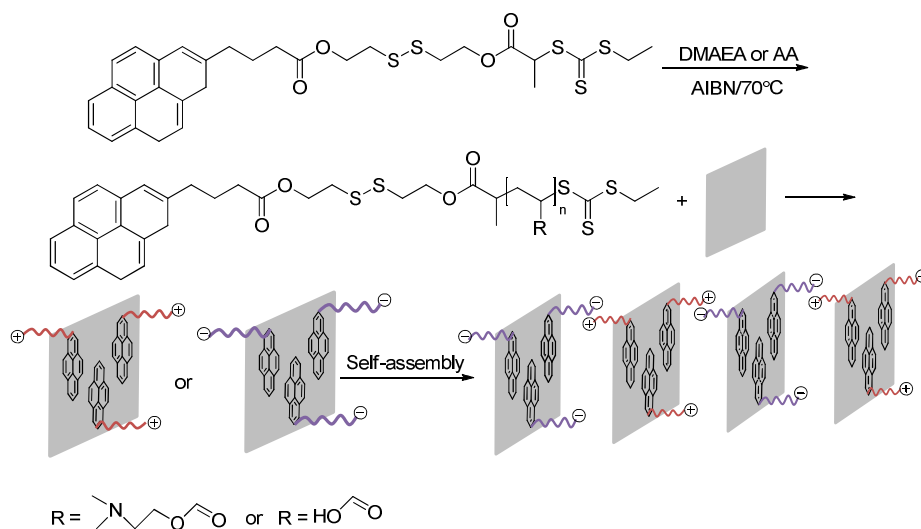


Figure 1.14. Synthesis of pH sensitive pyrene-polymer composites via π - π stacking interactions for the self-assembly of functionalized graphene into layered structures.

In addition to the RAFT mechanism, Kang et al also utilized ATRP to synthesize perylene bisimide-containing poly(glyceryl acrylate) (PBIPGA) for modification of reduced graphene oxide via π - π stacking interactions, which gave water-soluble and fluorescent graphene composites.⁵³

Chapter 2

Objectives

The objectives of this thesis are as follows:

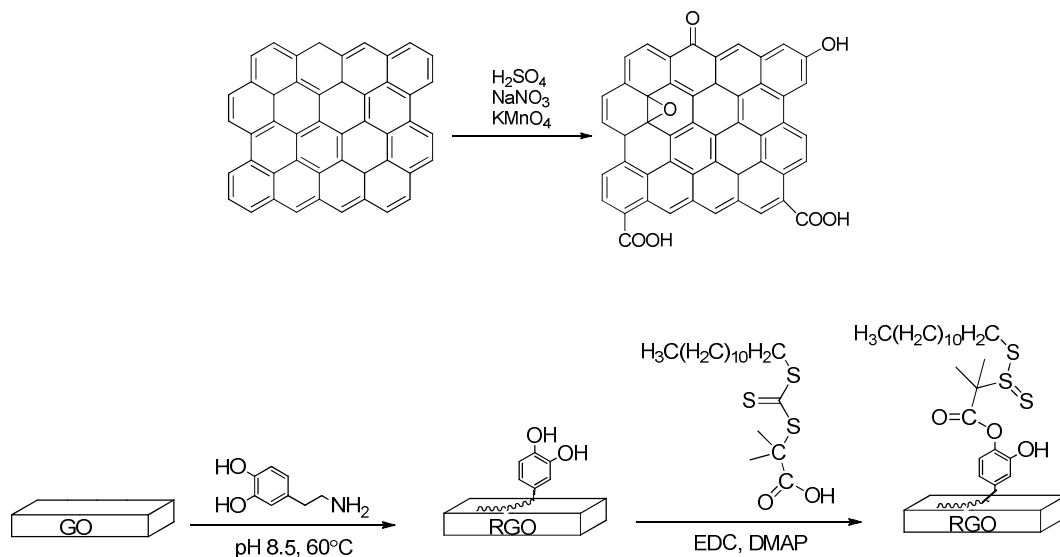
1. Reduce graphene oxide via self-polymerization of dopamine. Use polydopamine coating as a platform to graft RAFT agent.
2. Develop a new approach to grow polymers graphene via surface “graft from” RAFT polymerization without causing unrecoverable defects based on the polydopamine coating.
3. Study the livingness and kinetics of the surface “graft from” RAFT polymerization.

Chapter 3

Functionalization of Reduced Graphene Oxide via Surface “Graft from” RAFT Polymerization

Graphene sheets, as a kind of nanofiller, have a strong aggregation tendency in polymeric matrices due to strong van der Waals interactions of π - π stacking between them. In order to enhance the interactions between nanofiller and polymer substrate, this study focused on living polymerization that was initialized from the surface of polydopamine/reduced graphene oxide (PDA/RGO). A new “grafting from” RAFT polymerization method for synthesizing polymer functionalized graphene nanocomposites was found with a good dispersion of the nanocomposites by using the RAFT agent, S-Dodecyl-S’-(α,α' -dimethyl- α'' -acetic acid)trithiocarbonate.

The graphene oxide (GO), which was obtained by Hummers method⁵⁴, was reduced by self-polymerization of dopamine. The RAFT agent used has an available carboxyl group to anchor onto the polydopamine/reduced graphene oxide (PDA/RGO) surface, and a -S=C(SC₁₂H₂₅) moiety for subsequent RAFT polymerization of four different monomer (styrene, MMA, NIPAM, tBA) to form polymer-PDA/RGO nanocomposites by the RAFT polymerization process. The synthesis of GO and reduction of GO was determined by FTIR, TEM, AFM, UV, and XPS. The grafted polymers were characterized by FTIR and TGA.



3.1 Introduction

The development of various methods for producing graphene has stimulated a vast amount of research in recent years, since the discovery of graphene by Andre Geim and Konstantin Novoselov which resulted in a Nobel Prize in 2010⁷. The remarkable properties of graphene include large theoretical specific surface areas ($2630 \text{ m}^2\text{g}^{-1}$)³⁸, high values of charge carrier mobility ($200,000 \text{ cm}^2\text{V}^{-1}\text{s}^{-1}$)⁵⁵, thermal conductivity ($\sim 5000 \text{ Wm}^{-1}\text{K}^{-1}$)⁵⁶, Young's modulus ($\sim 1,100 \text{ GPa}$)¹⁰ and fracture strength (125 GPa)¹⁰. During the last half decade, many potential applications based on graphene and chemically modified graphene have been studied, such as energy-related materials⁵⁷, 'paper-like' materials⁵⁸, polymer composites⁵⁹, and field-effect transistors⁷.

Presently, the primary methods to produce graphene include chemical vapour deposition (CVD) growth on epitaxially matched metal surfaces⁶⁰, micromechanical exfoliation of graphite⁷, exfoliation of graphene in solvents⁶¹, gas-phase synthesis of graphene platelets under microwave plasma⁶², and graphite oxide reduction⁶³. Oxidative exfoliation of natural graphite by acid treatment and subsequent reduction by hydrazine or sodium borohydride has been evaluated as one of the most efficient methods for low-cost, large-scale production of graphene⁶⁴.

In general, GO is synthesized by Brodie⁶⁵, Staudenmaier⁶⁶, or Hummers method⁵⁴, or some variation of these methods. All three methods involve the oxidation of graphite. Hummers method involves treatment of graphite with potassium permanganate (KMnO_4) and sulfuric acid (H_2SO_4), while Brodie and Staudenmaier used a combination of potassium chlorate (KClO_3) with nitric acid (HNO_3) to oxidize graphite.

Graphene can be obtained via thermal treatment⁶⁷ or chemical reduction of the graphene oxide colloidal dispersion with several reducing agents, such as hydrazine^{63a, 68}, dimethylhydrazine⁵⁹, hydroquinone⁶⁹, sodium borohydride (NaBH_4)⁷⁰, and ascorbic acid⁷¹.

Dopamine is a biomolecule, mimicking the adhesive proteins, that contains catechol and amine functional groups. Inspired by the composition of adhesive proteins in mussels,

Messersmith's group developed a simple and versatile strategy for surface modification of multiple classes of materials via simultaneous self-polymerization of dopamine and coating of polydopamine on substrate⁷². The polydopamine coating is able to form on virtually all types of surfaces, including noble metals (Au, Ag, Pt, and Pd), metals with native oxide surfaces (Cu, stainless steel, and NiTi shape-memory alloy), oxides (TiO₂, SiO₂, and Al₂O₃), semiconductors (GaAs and Si₃N₄), ceramics (glass and hydroxyapatite), and synthetic polymers⁷³.

The polydopamine coating was found to be an extremely versatile platform for secondary reactions, including:

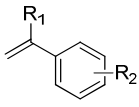
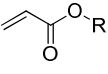
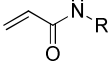
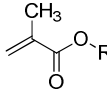
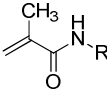
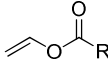
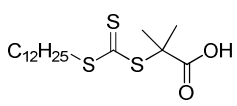
1. Depositing adherent and uniform metal coatings onto substrates by electroless metallization.
2. Creation of functional organic layers (alkanethiol monolayer, synthetic polymer, and biopolymer coatings) by Michael addition or Schiff base reactions via thiol- or amine-catechol adduct formation.⁷⁴
3. Surface-induced polymerization, such as ATRP, from polydopamine coatings to grow polymer brushes.⁷⁵

The exact polymerization mechanism is not yet clearly known, but according to the literature⁷⁶, it may involve the spontaneous oxidation of catechol in dopamine accompanying intra/intermolecular cross-linking reactions. As, the polymerization is an electron release process, thus the released electrons can be utilized for the reduction of the substrate, such as graphene oxide⁷⁷, during the self-polymerization of dopamine and coating on materials. Therefore, dopamine and its derivatives can be potential candidates for reduction of graphene oxide and further functionalization⁷⁸.

In this research, the hydroxyl groups of polydopamine were reacted with a RAFT agent (S-Dodecyl-S'-(α,α' -dimethyl- α'' -acetic acid)trithiocarbonate) with an available carboxylic group via an esterification reaction. This allows the grafted RAFT agent on the PDA/RGO surface to be utilized for subsequent RAFT polymerization functionalization.

One of the main advantages of RAFT polymerization is its tolerance towards polymerizing a wide range of vinyl monomer functionalities. The compatibility with monomers is based on the chosen RAFT agent. The RAFT agent (S-Dodecyl-S'-(α,α' -dimethyl- α'' -acetic acid)trithiocarbonate) used in this study is suitable for several other vinyl monomers, including styrenes, acrylates, acrylamides, methacrylates and methacrylamides (Table 3.1). To demonstrate the utility of this functionalization approach with different monomers, four common additional types of polymer polystyrene (PS), poly(methyl methacrylate) (PMMA), poly(N-isopropylacrylamide) (PNIPAM), poly(tert-butyl acrylate) (PtBA)) were chosen to be grown from the surface of the RAFT agent grafted PDA/RGO. The successful growth of these polymers can prove this new approach to be a versatile technique. Also if different types of RAFT agents are attached on polydopamine coating, the compatibility of this technique can cover a wide range of vinyl monomers suitable for conventional RAFT polymerization.

Table 3.1. The RAFT agent with its suitability for various monomer types

						
	styrenes	acrylates	acrylamides	methacrylates	methacrylamides	vinyl esters
	+++	+++	+++	+	+	—

+++ : very good, + : good, — : not suitable.

FTIR and TGA analysis confirmed the presence of grafted polymers from the PDA/RGO surface, with these polymer functionalized PDA/RGO species showing good dispersibility in several solvents.

3.2 Experimental

3.2.1 Materials

Graphite flake (99%, median 7-10 micron) was purchased from Alfa Aesar. Phosphorus pentoxide (P_2O_5), sodium nitrate ($NaNO_3$), hydrogen peroxide solution (H_2O_2 , contains inhibitor, 30 wt.% in H_2O), S-Dodecyl-S'-(α,α' -dimethyl- α'' -acetic acid)trithiocarbonate, tris(hydroxymethyl)aminomethane, dopamine hydrochloride, 4-(Dimethylamino)pyridine (DMAP), and N-(3-Dimethylaminopropyl)-N'-ethylcarbodiimide hydrochloride (EDC·HCl) were purchased from Sigma-Aldrich without further purification. Nylon 66 filter membrane was purchased from Sigma-Aldrich. Styrene ($\geq 99\%$, Sigma-Aldrich, contains 4-*tert*-butylcatechol as stabilizer), Methyl methacrylate (MMA), N-isopropylacrylamide (NIPAM), and *tert*-butyl acrylate (tBA) were purified by passing through a basic alumina column before use and stored at 4 °C, 2,2'-Azobis(2-methylpropionitrile) (AIBN, Dupont) was recrystallized twice from methanol before use and stored at 4 °C. Potassium persulphate ($K_2S_2O_8$), potassium permanganate ($KMnO_4$), sulphuric acid (H_2SO_4), hydrochloric acid (HCl), and N,N-Dimethylformamide (DMF), toluene, methanol, and tetrahydrofuran (THF) were purchased from Caledon Laboratories Ltd, and used as received. Dialysis tubing (Regenerated Cellulose, MWCO 12,000 to 14,000) was purchased from VWR.

3.2.2 Experimental Setup

The GO synthesis experimental setup is shown in Figure 3.4. A two-neck, round bottom flask was equipped with a magnetic stirrer, an ice bath, and a thermometer, which were used to mix the solvent and reactants, while controlling and monitoring temperature of the mixture.

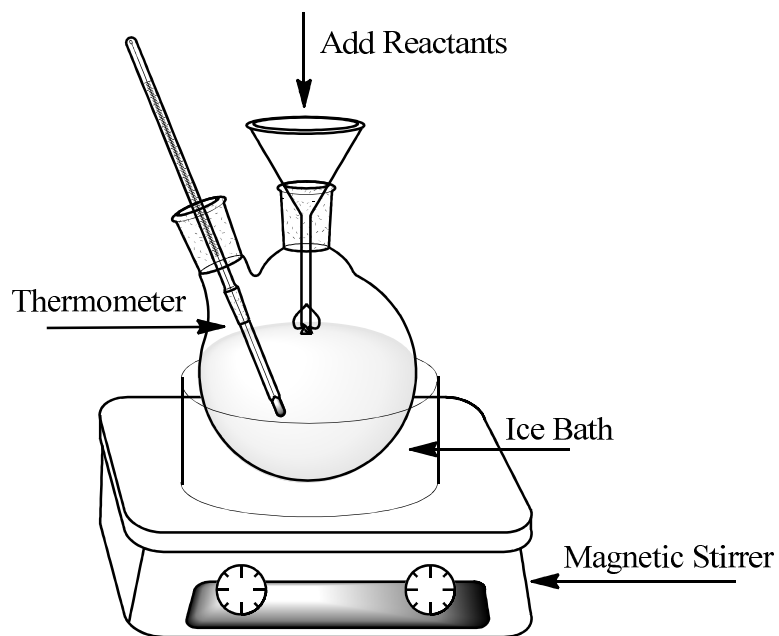


Figure 3.1. GO synthesis lab setup.

The RAFT polymerization experimental setup is shown in Figure 3.2. A schlenk tube flask was equipped with a magnetic stirrer, an oil bath, a bubbler and a needle. The bubbler and needle, connected with nitrogen/argon line manifold, are for the N₂ bubbling. After bubbling, the needle and bubbler were removed from the reaction tube, and the flask was immersed in an oil bath at 60 °C.

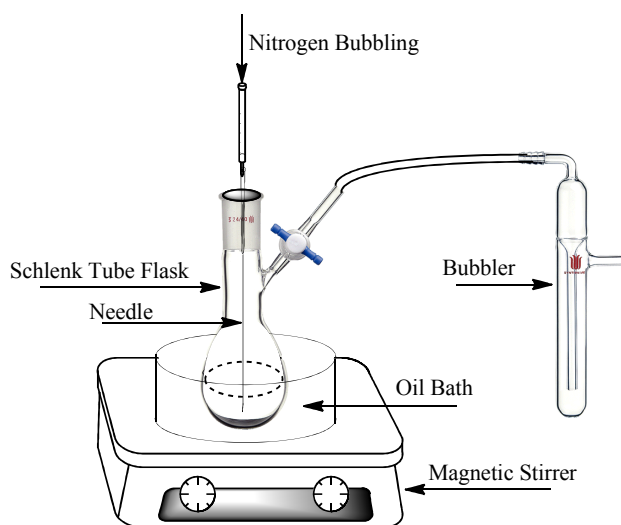


Figure 3.2. RAFT polymerization setup.

3.2.3 Preparation of Graphene Oxide Sheets (GO)

Graphene oxide was synthesized from graphite flake by a modified Hummers method, in which pre-oxidation of graphite was followed by oxidation using Hummers method⁷⁹.

In the pre-oxidation step, $K_2S_2O_8$ (5 g) and P_2O_5 (5 g) were completely dissolved in concentrated H_2SO_4 (50 mL) at 90 °C using an oil bath. After dissolution in a round bottom flask, the solution was then cooled to 80 °C, and graphite (5 g) was added with stirring. The mixture was kept at 80°C for 4.5 h after which the mixture was cooled to room temperature and diluted with 500 ml of deionized water. After stirring overnight, the product was filtered with a Nylon 66 Filter Membrane (0.2 μ m) and washed with 1.5 L deionized water until the pH of the filtrate became neutral. The pre-oxidized graphite was dried in air at ambient temperature overnight.

Using Hummers method, pre-oxidized graphite (2 g) and $NaNO_3$ (2 g) were dispersed by stirring into chilled H_2SO_4 (98 mL) in a round bottom flask in an ice bath and kept stirring for 2 h. $KMnO_4$ (12.5 g) was added slowly with stirring to keep the temperature of the reaction mixture below 20°C. The resulting thick, dark green paste was allowed to react at 35°C for 2 h followed by gradual addition of deionized water (200 mL) to give a dark brown solution. To avoid rapid temperature rise with foaming by water addition, the flask was chilled in an ice bath with close monitoring of temperature (kept below 70°C). After stirring for 2 h, the solution was poured into more deionized water (500 mL) after which H_2O_2 (30%, 15 mL) was added and the color of the mixture turned to a bright yellow. The mixture was allowed to settle overnight without disturbance and the supernatant was decanted. The remaining product was dispersed in 3 wt% HCl aqueous solution. The dispersion was centrifuged at 10,000 rpm for 10 min to remove supernatant fluid. The washing process was repeated twice more to remove ions of the oxidant and other inorganic impurities. Then the product was washed with deionized water to remove acid via disperse-centrifuge-removal of the supernatant-redisperse cycle until the pH of the supernatant was higher than 2. Finally, the mixture was transferred to dialysis bags and dialyzed against deionized water to remove the acid completely for a week. To obtain the graphene oxide powder, the mixture was dried under vacuum at 40°C.

3.2.4 Reduction of Graphene Oxide via Self-polymerization of dopamine

Graphene oxide (60 mg) and dopamine (120 mg) were added to 10 mM Tris-Cl buffer solution (120 mL, pH = 8.5) and dispersed in a one-neck, round bottom flask by sonication for 30 min in an ice bath. The reaction mixture was stirred at 60°C or room temperature for 24 h. After the reduction reaction, the polydopamine-coated reduced graphene oxide (PDA/RGO) was filtered with a 0.2 μm nylon membrane filter, washed with deionized water and DMF several times, and stored in DMF suspension (Figure 3.3)

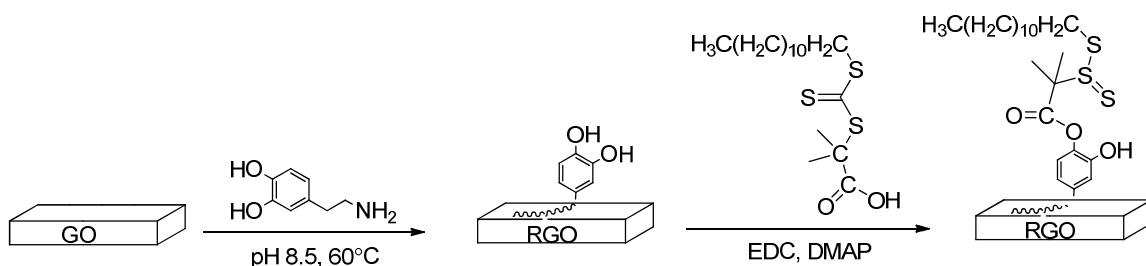


Figure 3.3. Synthesis of dopamine induced reduced graphene oxide and RAFT agent grafted PDA/RGO.

3.2.5 Synthesis of RAFT agent-bonded graphene sheets

PDA/RGO (0.2 g) was sonicated in DMF (30 mL) for 15 min. RAFT agent (0.3 g) was added and the resultant mixture was transferred into a one-neck round bottom flask, then stirred for 10 min at room temperature. EDC·HCl (0.3 g) and DMAP (60 mg) were dissolved in DMF (10 ml) and then added to the mixture in the flask. The mixture was stirred at room temperature for 48 h, then vacuum-filtered through a nylon filter membrane (0.45 μm). The collected product was washed with DMF four times to remove the unattached RAFT agents. The resultant product was then stored in DMF solvent (Figure 3.3)

3.2.6 Surface RAFT Polymerization of Styrene on RGO/PDA

RAFT-PDA/RGO (31.5 mg, 0.01 mmol RAFT agent (Appendix 2)) was suspended in a mixture of styrene monomer (5 mL), DMF (2 mL), and AIBN (0.01 mmol) by sonication.

A sealed 10 mL dried Schlenk tube was degassed and refilled with nitrogen three times. The mixture was added into the tube via a syringe, and the solution was bubbled with nitrogen for 30 min. The reaction tube was placed in a thermostated oil bath at 60 °C. After 36 hours, the tube was immersed into an ice bath to stop the polymerization. The suspension was then dropped slowly in methanol with stirring. The solid was obtained via filtration through a 0.2 µm nylon membrane, which was then washed with toluene three times to remove free polystyrene and dried under vacuum at 40 °C.

The syntheses of PMMA-PDA/RGO, PNIPAM-PDA/RGO and PtBA-PDA/RGO nanocomposites were similar. (see Appendix 1)

3.3 Characterization

Fourier transform infrared (FTIR) spectra were recorded from KBr pellets using a Nicolet 6700 FTIR, connected to a computer, supported by Thermo Scientific OMNIC software in the range of 400-4000 cm^{-1} with a resolution of 2 cm^{-1} and 32 scans for each sample.

The thermal properties of the products were measured by thermogravimetric analysis (TGA). The samples were heated from room temperature to 800 °C at a heating rate of 10 °C/min under nitrogen atmosphere on a TA Instruments SDT Q600.

Transmission electron microscope (TEM) observations were carried out on a Philips CM-10 transmission electron microscope equipped with a Tungsten filament and a 35 mm photo camera. TEM specimens were prepared by depositing the dilute colloids on copper grids (carbon coated) and drying the grids in air.

Atomic force microscopy (AFM) imaging was performed on a Nanoscope IIIA atomic force microscope (Veeco Metrology Group) equipped with a “J” scanner in tapping mode under ambient conditions. Commercial silicon tips with force constants of 60 N/m and resonance frequencies of 260-420 kHz were used as probes. AFM samples were prepared by depositing the sufficiently diluted colloids on freshly cleaved micas and then dried naturally at room temperature for at least 24 h.

The X-ray photoelectron spectroscopy (XPS) spectra were recorded on a Kratos AXIS Ultra spectrometer. All XPS spectra were recorded using an aperture slot of 400 ×700 microns. Survey spectrum was recorded with pass energy of 160 eV, and high-resolution spectra were recorded with pass energy of 40 eV.

UV/vis absorption spectral measurements were carried out using a Shimadzu UV-3600 spectrophotometer equipped with two lamps (halogen and deuterium) and three detectors (photomultiplier tube, InGaAs and PbS) in the wavelength range of 200-500 nm at room temperature.

Energy-dispersive X-ray (EDX) elemental analysis was performed using a Quartz Xone EDX scattering device attached to Hitachi S-4500 field emission scanning electron microscope (SEM).

3.4 Results and Discussion

3.4.1 Graphene Oxide

As mentioned in the experimental section, a modified Hummers method was employed to oxidize and exfoliate graphite by treatment of KMnO_4 and concentrated H_2SO_4 into GO. The GO has a brown color and could be easily dispersed in H_2O (Figure 3.6 left) with the help of oxidized functional groups. The GO film could be made by passing GO dispersion through a filter membrane, followed by removing the layer of GO from the membrane. As shown in Figure 3.4 right, GO film is quite flexible.

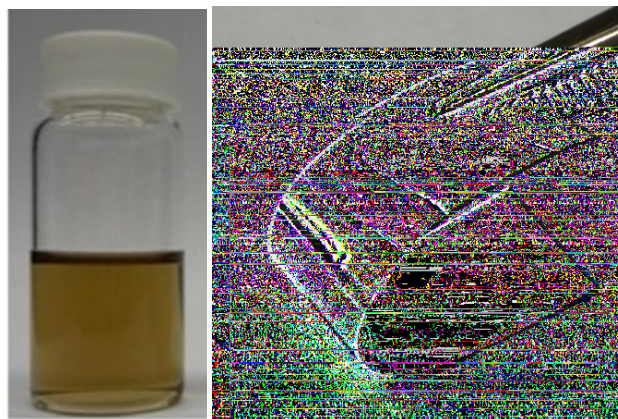


Figure 3.4. Left: Suspension of graphene oxide in H₂O. Right: Photo of graphene oxide sheet.

The GO was characterized by FTIR in transmittance mode. The amount of sample added to the KBr had to be strictly controlled, because the dark product can absorb most of the infrared rays if a too high a concentration is used.

The FTIR spectrum shown in Figure 3.5 provides evidence of the typical functional groups found in graphene oxide. The main characteristic absorption bands are located at 1728 cm⁻¹ (C=O carbonyl stretching), 1377 cm⁻¹ (C-OH deformation vibration), 1279 cm⁻¹ (C-O-C stretching) and 1071 cm⁻¹ (C-O stretching). The resonance at 1625 cm⁻¹ can be assigned to the skeletal vibrations of unoxidized graphitic domains (eg. C=C).

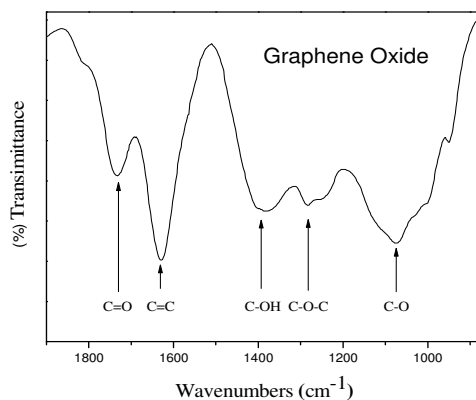


Figure 3.5. FT-IR spectrum of GO.

The morphology of GO was revealed by TEM images as shown in Figure 3.6. GO was dispersed in H₂O under sonication, with the TEM specimens prepared by dropping a drop of solution on carbon coated copper grid and drying in air. The transparent GO sheet showed a wrinkled silk shape, which is typical and characteristic of single GO sheets. The production of individual GO sheets is very significant since the attractive properties of GO are based on its existence as a single layer.

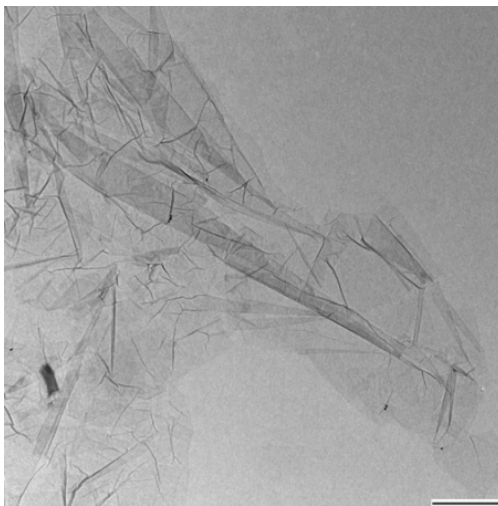


Figure 3.6. TEM image of GO (the scale is 500 nm).

To confirm the number of layers of graphene oxide, the thickness of graphene oxide sheets was measured by AFM. The sample for AFM imaging was prepared by drop-casting the dispersions onto freshly cleaved mica substrates, which were then allowed to dry under vacuum at room temperature. The AFM image (Figure 3.7) shows that the GO sheet is flat and smooth, with the GO having a thickness of 1.1 nm, which is similar to that reported in the literature^{63b, 80}, indicating the successful formation of mono-layer GO sheets.

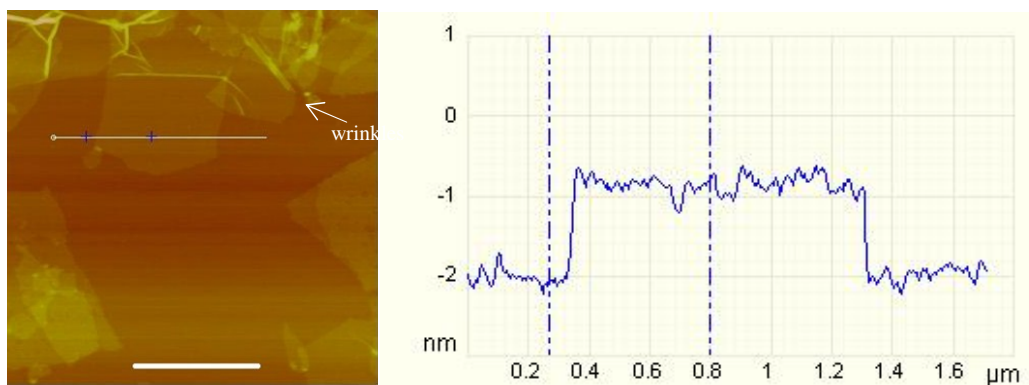


Figure 3.7. (a) A tapping mode AFM image of graphene oxide (GO) sheets on mica surface. Wrinkles were frequently observed for the large sheets deposited from dispersion in water (scale bar: 1 μm), (b) the height profile of the AFM image, the height difference between two lines is 1.1nm.

3.4.2 Dopamine-Induced Reduction of Graphene Oxide

The graphene oxide was reduced via the self-polymerization of dopamine process. The released electrons created by the process may facilitate reduction of the oxygen-containing functional groups on GO. Clearly, after the treatment, the color of the aqueous suspension change from brown (GO) to black (PDA/RGO), as shown in Figure 3.8.

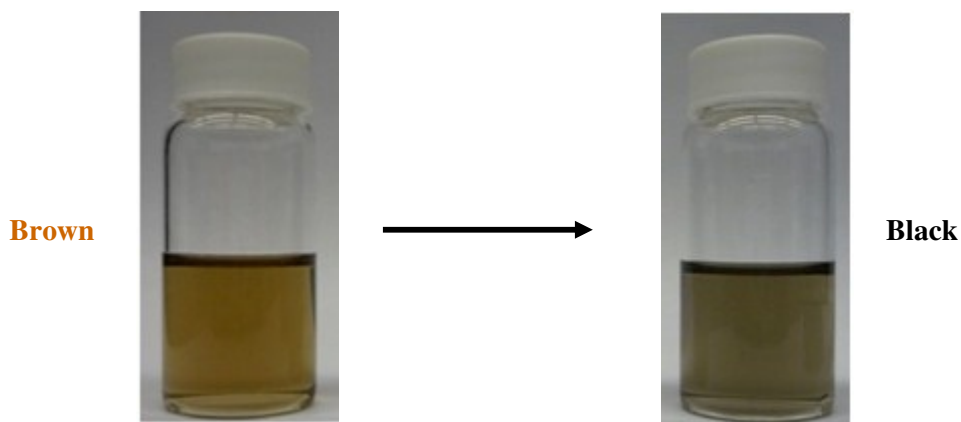


Figure 3.8. Photograph of aqueous GO (left) and PDA/RGO (right) suspension.

The morphology of PDA/RGO nanosheets was revealed by AFM images as shown in Figure 3.9. Since PDA has a tendency to form free PDA particles at high dopamine concentration and temperature, the PDA/RGO was filtered and washed with water and

DMF. Attributed to these treatments and the high affinity of PDA, no free particles were observed in the AFM images. The thickness of PDA/RGO nanosheets increased to about 4 nm, which confirmed the coating of PDA.

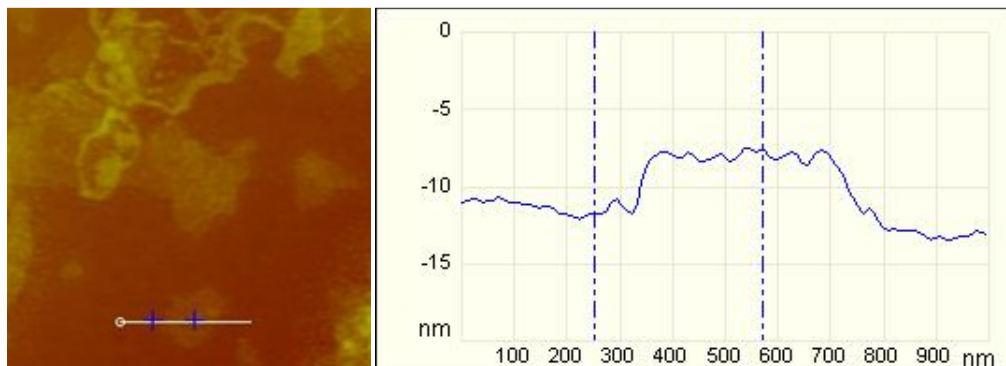


Figure 3.9. (a) A tapping mode AFM image of graphene oxide (GO) sheets on mica surface, (b) the height profile of the AFM image, the height difference between two lines is about 4 nm.

Further characterization by FTIR spectroscopy was performed to evaluate the simultaneous reduction of GO and surface coating by PDA. The IR peak at 1560 cm^{-1} (ring stretching from a benzene ring) confirmed the presence of the coated PDA layer on RGO (Figure 3.10). Also, the decreased peak intensity at 1726 cm^{-1} is a strong indication of graphene oxide reduction.

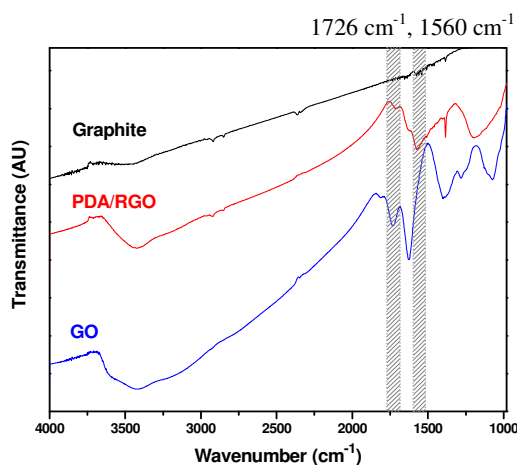


Figure 3.10. FTIR spectra of graphite (top), PDA/RGO (middle), and GO (bottom).

The oxidation of graphite and reduction of graphene oxide was also characterized by X-ray photoelectron spectroscopy (XPS). XPS is a surface analytical technique, which can provide detailed information on the nature of the functional groups. The strong degree of oxidation of graphene oxide was demonstrated by XPS survey spectrum of graphene oxide, which yielded a C/O atomic ratio of 2.54. A significant decrease of XPS signals at 286-290 eV which corresponds to C-O and C=O groups, indicated that the PDA-functionalized graphene oxide was chemically reduced. The N (1s) peak of XPS spectroscopy (Figure 3.11 right) revealed the coating of polydopamine.

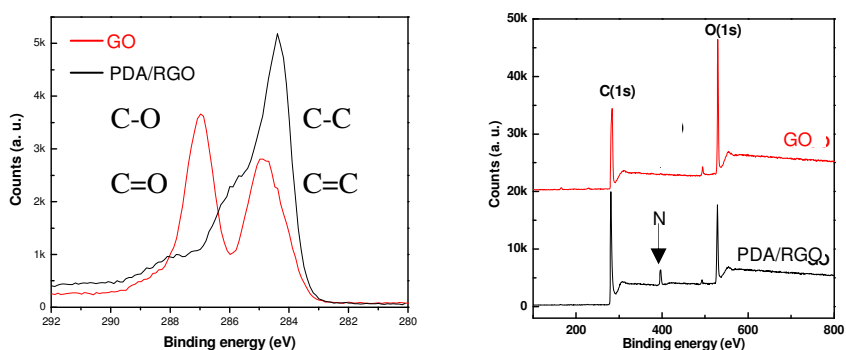


Figure 3.11. XPS characterization of GO and the PDA modified RGO. *Left: C1s, Right: Scan.*

The UV-vis spectra (Figure 3.12) also demonstrated the reduction of GO. The spectrum of the GO dispersion showed two characteristic features that can be used as a means of identification: the strong absorption peak at 228 nm corresponds to the $\pi \rightarrow \pi^*$ transitions of aromatic C-C bonds, and the shoulder at ~ 300 nm is attributed to $n \rightarrow \pi^*$ transitions of C=O bonds; both are bathochromically shifted by conjugation. After treatment with self-polymerization of dopamine in buffer solution (pH=8.5) and removal of PDA from the RGO surface by alkaline treatment (1 M NaOH), the absorption peak at 228 nm was red-shifted to 270 nm, suggesting that the electronic conjugation within the reduced graphene sheets was revived upon the dopamine-induced reduction.

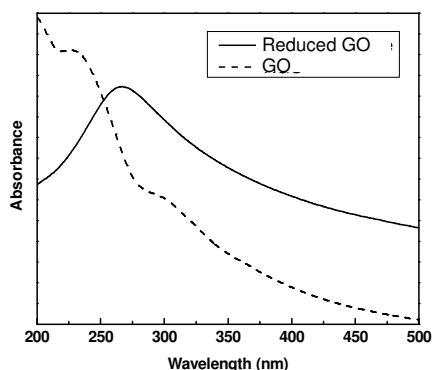


Figure 3.12. UV-Vis absorption spectra of graphene oxide and reduced graphene oxide water suspension.

3.4.2.1 Effect of Temperature on Reduction of Graphene Oxide

Recently, two research groups presented a method involving simultaneous reduction and pH-induced aqueous functionalization of graphene oxide by the catecholamine polymers (polydopamine and poly(norepinephrine)). However, the reaction conditions of the functionalization in these two literatures are very different⁷⁹⁻⁸⁰. These results inspired us to investigate the effects of different reaction conditions (temperature and ratio of reactants) on the reduction of graphene oxide. X-ray diffraction (XRD) and Raman spectroscopy were used to measure the degree of reduction and recovery of the graphene structure.

XRD is an effective method to investigate the interlayer changes and the crystalline properties of the synthesized material. Figure 3.13 shows the XRD patterns of pristine graphite, GO and PDA/RGO. The distance between the two layers is an important parameter to give the structural information of the as-prepared graphene. The strong peak in the XRD pattern of graphite appears at $2\theta=26.6^\circ$, corresponding to the interlayer spacing of 0.335 nm. The GO pattern shows a characteristic peak at $2\theta=11.05^\circ$, corresponding to interlayer spacing around 0.8 nm, indicating the presence of oxygen-containing functional groups formed during oxidation. These groups cause the GO sheets to stack more loosely.

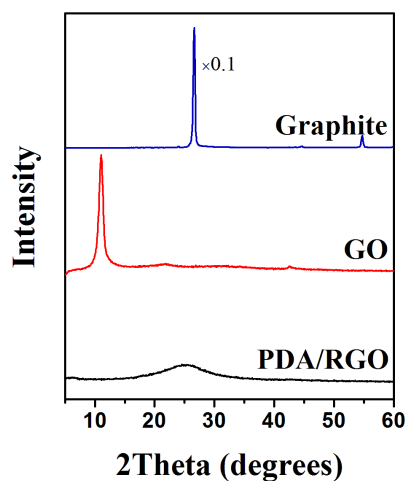


Figure 3.13. X-ray powder diffraction patterns of graphite, graphene oxide (GO) and PDA/RGO. (PDA gave no diffraction in the 2θ of $20\text{-}25^\circ$ region⁸³).

Whereas the sharp diffraction peak in GO (at $2\theta=11.05^\circ$) has decreased dramatically after reduction, a new broad diffraction peak (at $2\theta=24.5^\circ$) has appeared in the PDA/RGO. This diffraction peak is closer to the typical diffraction peak of graphite (at $2\theta=26.6^\circ$). Since PDA gave no diffraction in the 2θ of $20\text{-}25^\circ$ region⁸³, the change of peaks might indicate the successful reduction of GO.

Table 3.2. Reaction conditions of dopamine induced reduction of graphene oxide.

Experiment	Graphene Oxide	Dopamine	Temperature
1	60 mg	15 mg	60°C
2	60 mg	30 mg	60°C
3	60 mg	60 mg	60°C
4	60 mg	120 mg	60°C
5	60 mg	240 mg	60°C
6	60 mg	60 mg	25°C
7	60 mg	120 mg	25°C

As mentioned previously, the peak at $2\theta=11.05^\circ$ indicates the oxygen-containing functional groups and the peak at $2\theta=24.5^\circ$ is indicative of reduced graphene oxide.

Therefore, the ratio between these two peaks could be an indicator of the degree of reduction. The results of controlled trials (Table 3.2 (4, 7)) were studied by XRD (Figure 3.14 Left.). The ratio (1.33) between the peaks ($24.5^\circ/11.05^\circ$) of experiment 7 is much less than that (1.95) in experiment 4, indicating that reduction under heating is more effective.

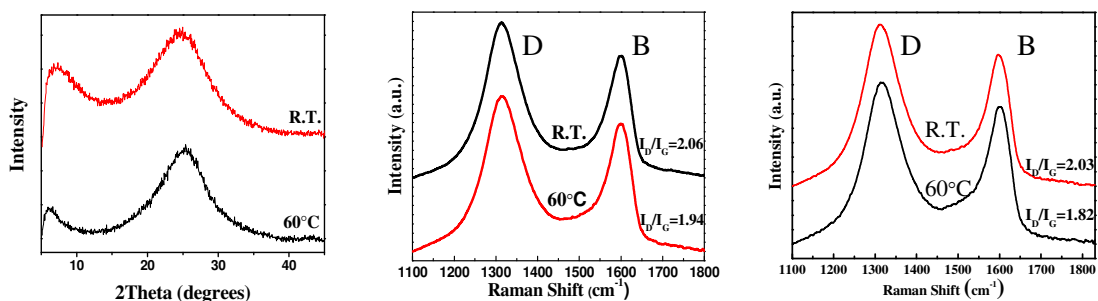


Figure 3.14. Left: XRD image of PDA/RGO. Conditions: dopamine : GO = 2 : 1 (weight ratio) in buffer solution (pH = 8.5) at room temperature and 60 °C. Middle & Right: Raman images of PDA/RGO. Conditions: dopamine : GO = 1 : 1 (middle), dopamine : GO = 2 : 1 (right) in buffer solution (pH = 8.5) at room temperature and 60 °C.

Raman spectroscopy is a powerful probe for characterizing sp^3 and sp^2 hybridized carbon atoms. D means diamond, and G means graphite. It is noted that the area ratio of the integrated Raman peak area between the D and G bands, I_D/I_G , has been shown to be related to the degree of recovery for sp^2 C=C bonds in graphitic structures. At the higher reaction temperature (Figure 3.15), I_D/I_G is smaller (dopamine:GO = 1:1, 1.94 (60 °C) < 2.06 (R.T.); dopamine:GO = 2:1, 1.82 (60 °C) < 2.03 (R.T.)), indicating that more sp^2 C=C structure has been recovered during the reduction. These Raman results show the same effects of temperature on reduction of graphene oxide.

3.4.2.2 Effect of Weight Ratio between reactants

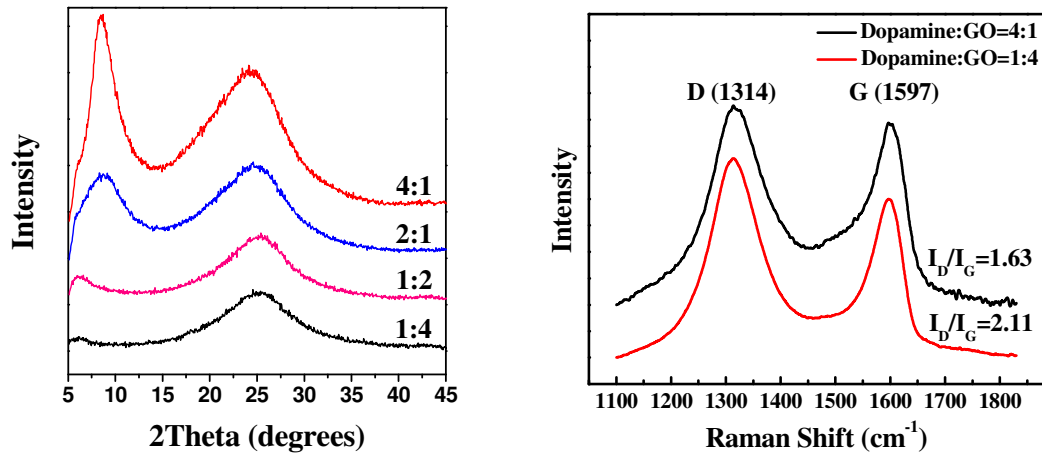


Figure 3.15. Left: XRD images of PDA/RGO Conditions: dopamine : GO = 1 : 4, 1 : 2, 2 : 1, and 4 : 1 (weight ratio) in buffer solution (pH = 8.5) at 60 °C. Right: Raman images of PDA/RGO Conditions: dopamine : GO = 1 : 4, and 4 : 1 (weight ratio) in buffer solution (pH = 8.5) at 60 °C.

Also, the influence of the ratio between reactants on the reduction was demonstrated by XRD (Figure 3.15 Left). The weight ratio between graphene oxide and dopamine ranges from 4:1 to 1:4 (all reactions were conducted at 60°C). Clearly, the peak on the left decreases when more dopamine was added into the reaction system (the ratio of right peak/left peak: 0.748, 1.11, 1.95, and 2.25). Thus, if more dopamine participated in the reaction, the reduction was more effective and complete. The Raman measurement also demonstrates the same result (Figure 3.15 Right). The I_D/I_G ratio decreases along with the increase of addition of dopamine to the reaction system.

However, the XRD and Raman results are not strong evidence of the reduction of graphene oxide. In the XRD analysis, the meaning of the broad peak of PDA/RGO is not very clear, since the position and the shape of the peak is still different from the typical peak of graphite. Also, the coating of polydopamine has both of sp^3 and sp^2 carbon atoms. These carbons could affect the Raman analysis of PDA/RGO. More evident characterization method is required to demonstrate the influence of temperature and ratio of reactants on the effect of reduction of graphene oxide.

3.4.3. Evidence of Immobilization of RAFT agent

The RAFT agent with a free carboxylic group can attach to the polydopamine coating via an esterification reaction. To confirm the attached RAFT agent, the products were characterized using the TGA and EDX techniques. TGA allows us to determine the relative weight loss of organic molecules while EDX helps indicate the presence of sulfur element from the attached RAFT agent. For comparison, the TGA curves (Figure 3.16) include PDA/RGO and two PDA/RGO samples containing different densities of RAFT agent. Since the RAFT agent is a kind of organic molecule, it would be removed by heat under N₂ flow. TGA of the PDA/RGO was found to have 40 wt% weight loss, while the RAFT agent modified PDA/RGO sheets have 46 wt% and 49 wt% weight loss. The higher weight loss of PDA/RGO-RAFT 2 is consistent with attachment of the RAFT agents (a higher weight loss of PDA/RGO-RAFT 2 agent occurred, as more RAFT agent was added into the reaction mixture (Table 3.3))

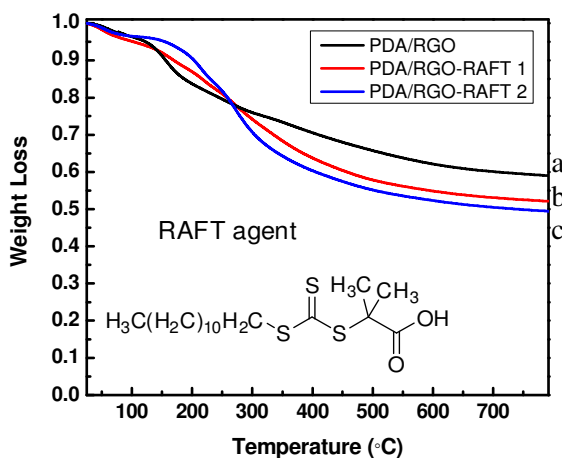


Figure 3.16. TGA curves of PDA/RGO and RAFT agent grafted PDA/RGO under nitrogen. The weight left at 790 °C is (a) 59 %; (b) 52 %, and (c) 49.4 %.

Table 3.3. Reaction conditions of synthesis of RAFT agent bonded PDA/RGO

	PDA/RGO	RAFT agent	DMF	EDC HCl	DMAP
PDA/RGO-RAFT-1	200 mg	300 mg	40 mL	300 mg	60 mg
PDA/RGO-RAFT-2	200 mg	600 mg	40 mL	600 mg	120 mg

In addition to the TGA results, the EDX of RAFT-PDA/RGO also demonstrates the presence of grafted RAFT agent. Figure 3.17 shows that after immobilization of RAFT agent on PDA/RGO, a peak (S), which belongs to the RAFT agent, appears in the EDX images.

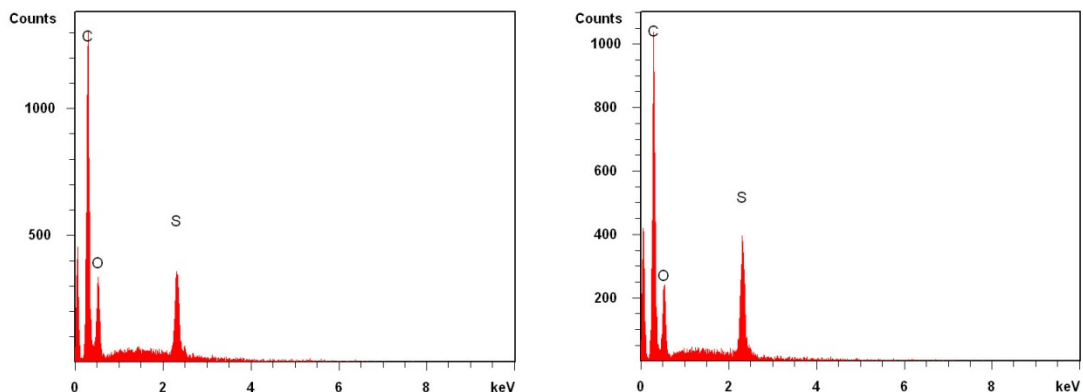


Figure 3.17. EDX images of RAFT agent grafted PDA/RGO. (Left: PDA/RGO-RAFT 1, Right: PDA/RGO-RAFT 2)

When more RAFT agent was added into the reaction system, more RAFT agent was linked to the PDA/RGO sheets. The observed increase in atomic percentage of sulfur, from 2.98 to 3.76 (Table 3.4), helps confirm this. The higher density of linked RAFT agents corresponds to the stronger signal of sulfur, as well as the TGA curves of higher weight loss.

Table 3.4. Atomic percentage (carbon, oxygen, sulfur) of RAFT agent grafted PDA/RGO

PDA/RGO-RAFT agent 1				PDA/RGO-RAFT agent 2			
Atomic %	C	O	S	Atomic %	C	O	S
1	77.19	19.86	2.95	1	78	18.24	3.76
2	77.24	19.95	2.81	2	78.32	17.95	3.73
3	77.87	18.94	3.19	3	78.4	17.82	3.78

Also the elemental mapping of sulfur of PDA/RGO-RAFT agent materials (Figure 3.18) indicates that the RAFT agents are evenly attached on the sheets, as all the yellow dots are equally distributed.

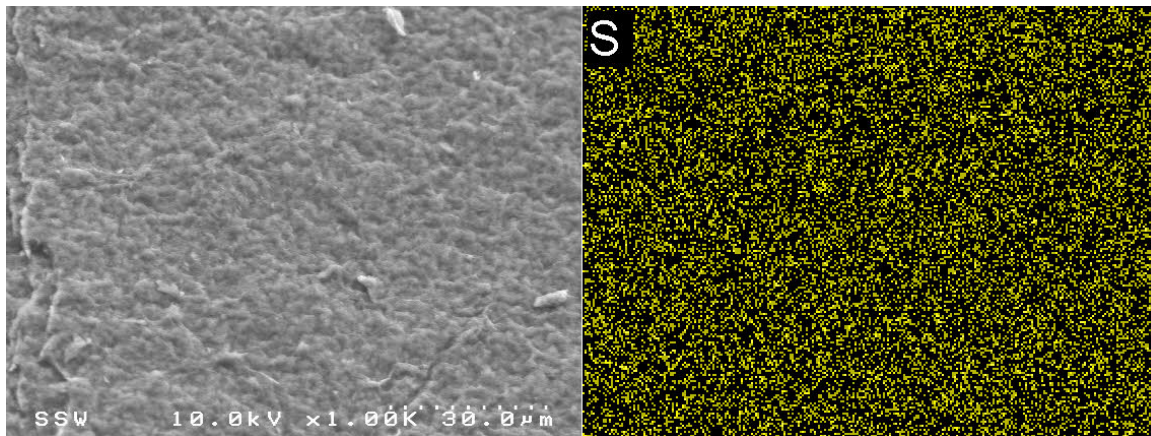


Figure 3.18. Elemental mapping of sulfur of RAFT agent grafted PDA/RGO. Right: SEM image. Left: Sulfur element distribution on the same area of left image.

3.4.5 Evidence of Grafted Polymer and Cleavage of Grafted Polymer

RAFT agent was grafted on the PDA/RGO surface. During the polymerization, polymer free radical propagated from initial free radical would undergo RAFT process with grafted RAFT agent to form grafted polymer chain with RAFT moiety, which could be attacked by other free radicals subsequently. In this way, polymer would grow from the surface. FTIR spectroscopy is one of the most powerful and convenient tools for identifying and investigating the presence of various functional groups in polymers. Figure 3.19 shows the FTIR spectra of the synthesized PS-PDA/RGO nanocomposite. The spectrum shows absorption bands at 3025 and 2921 cm^{-1} corresponding to aromatic and aliphatic C-H stretching, respectively. The peaks at 1600 and 1492 cm^{-1} are assigned to aromatic C=C stretching. The C-H deformation vibration band of benzene ring hydrogen's (5 adjacent hydrogen's) appears at 756 cm^{-1} , while ring deformation vibration is observed at 697 cm^{-1} . These functional groups confirm the grafted PS on PDA/RGO.

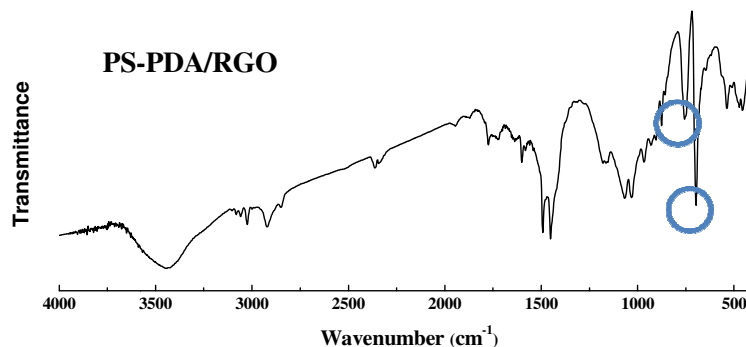


Figure 3.19. FTIR spectrum of PS-PDA/RGO nanocomposite.

3.4.6 Evidence of Grafted Polymer (PMMA, PNIPAM, PtBA) on PDA/RGO

FTIR and TGA measurements are powerful tools to confirm the successful attachment of grafted polymer to various surface species. FTIR investigations provide information on the functional groups of grafted polymer while TGA allows one to estimate the amount of grafted polymer, as organic polymer is removed by heat under inert gas. All of the TGA images of PMMA-PDA/RGO (Figure 3.20), PNIPAM-PDA/RGO (Figure 3.21), and PtBA-PDA/RGO (Figure 3.22) showed sharp increases of weight loss compared with that of RAFT-PDA/RGO (47.7% weight loss caused by removal of PDA).

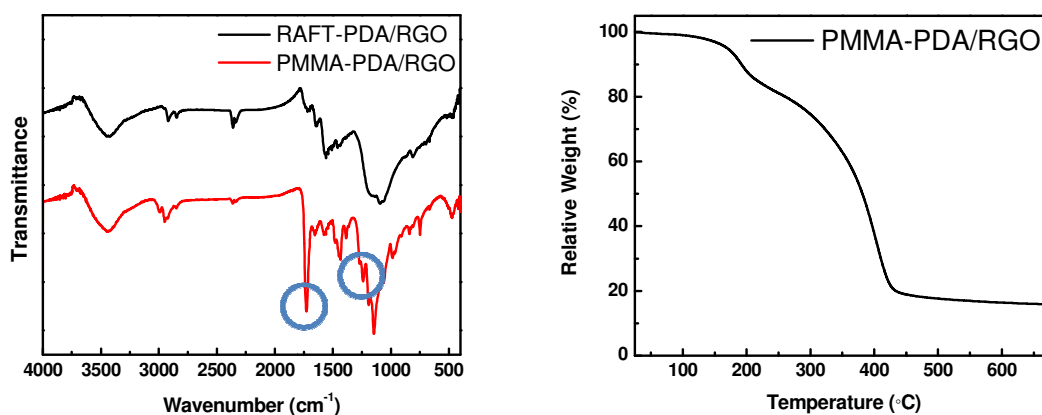


Figure 3.20. Left: FTIR spectra of PMMA grafted PDA/RGO and RAFT agent grafted PDA/RGO. Right: TGA curve of PMMA grafted PDA/RGO under nitrogen.

The IR spectrum of PMMA-PDA/RGO (Figure 3.20) shows absorption bands at 2949 and 1728 cm^{-1} due to $-\text{CH}_3$ asymmetric stretching and $\text{C}=\text{O}$ stretching respectively. The peak at 1728 cm^{-1} increased significantly after polymerization, indicating a higher amount of $\text{C}=\text{O}$ groups (PMMA) in the nanocomposite. The vibrational bands at 1483 and 1449 cm^{-1} are attributed to CH_2 scissoring and the CH_3 asymmetric peak at 1385 cm^{-1} appears due to $\text{O}-\text{CH}_3$ deformation from PMMA. The bands appearing at 1271 and 840 cm^{-1} correspond to $\text{C}-\text{O}$ stretching and $\text{C}-\text{O}-\text{C}$ stretching of PMMA. The absorption bands corresponding to CH_2 twisting wagging and rocking modes of PMMA appear at 1191, 966, and 749 cm^{-1} respectively. The PMMA degradation under nitrogen from TGA shows two steps, which occurred in the temperature range of 100-200 $^\circ\text{C}$ and 200-410 $^\circ\text{C}$, respectively. The two degradation steps of PMMA were described by Grassie and Melville⁸¹ who suggested that the process is initiated at the vinylidene end groups. Once the vinylidene terminated chains have unzipped, further degradation is initiated by random scission that corresponds to the second mass loss step⁸¹.

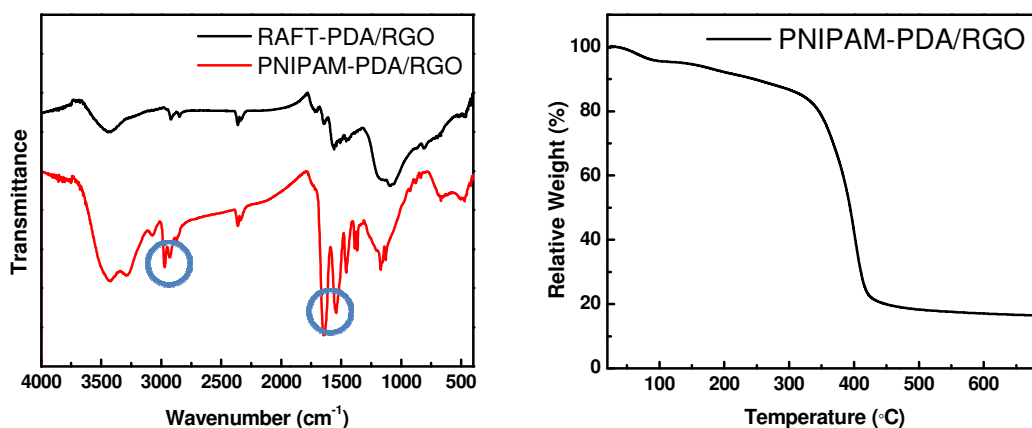


Figure 3.21. Left: FTIR spectra of PNIPAM grafted PDA/RGO and RAFT agent grafted PDA/RGO. Right: TGA curve of PNIPAM grafted PDA/RGO under nitrogen.

The IR spectrum of PNIPAM-PDA/RGO (Figure 3.21) showed absorption bands at 3288 cm^{-1} due to a secondary amide $\text{N}-\text{H}$ stretching and the band appearing at 2970 cm^{-1} corresponds to $-\text{CH}_3$ asymmetric stretching from PNIPAM. The bands at 1647 and 1541 cm^{-1} are attributed to secondary amide $\text{C}=\text{O}$ stretching and secondary amide $\text{N}-\text{H}$

stretching. Deformation bands of two methyl groups at 1386 and 1366 cm^{-1} are attributable to PNIPAM are clearly visible in the spectrum of the PNIPAM-PDA/RGO nanocomposite. According to the TGA curve, the weight loss before 310 $^{\circ}\text{C}$ may be attributed to the decomposition of PDA or other impurities. Then the decomposition of PNIPAM contributed to the increasing weight loss until most chains were broken around 350-400 $^{\circ}\text{C}$.

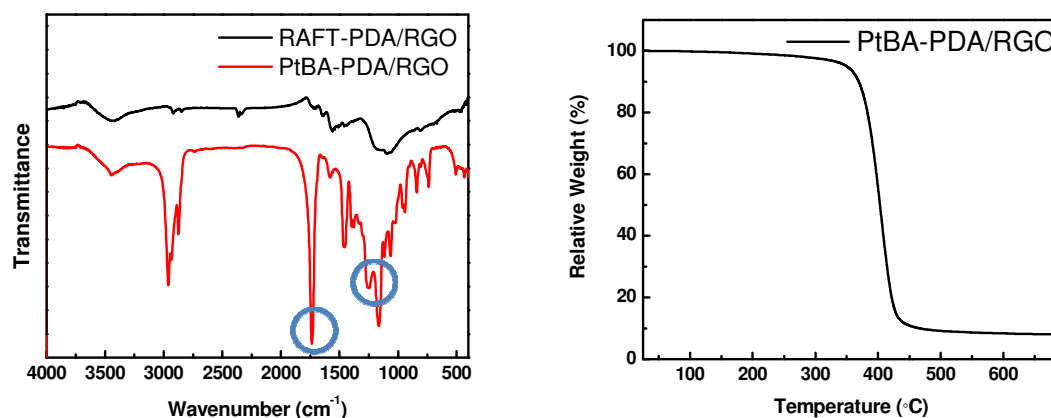


Figure 3.22. Left: FTIR spectra of PtBA grafted PDA/RGO and RAFT agent grafted PDA/RGO. Right: TGA curve of PtBA grafted PDA/RGO under nitrogen.

Figure 3.22 shows the FTIR spectrum of PtBA-PDA/RGO. The sharply increased peak at 1736 cm^{-1} is assigned to the ester group ($-\text{COO}$), the peaks at 1256 and 1164 cm^{-1} are attributed to C-O, and the peak at 2960 cm^{-1} belongs to the asymmetric CH_3 stretching vibration. The characteristic absorption bands of the C-H stretching vibration appeared at 2874 and 2935 cm^{-1} , while the C-H in-plane bending vibration appeared at 1379 and 1458 cm^{-1} , respectively. In the TGA image, the main weight loss occurred in the temperature range of 350-430 $^{\circ}\text{C}$, corresponding to the decomposition of PtBA.

3.4.7 Dispersibility of Polymer grafted PDA/RGO

After grafting polymer chains, the solubility of the polymer-PDA/RGO in various solvents improved significantly.

The resultant PS-PDA/RGO nanocomposites exhibited considerable dispersibility in several solvents. With the aid of sonication treatment, the nanocomposites were efficiently dispersed in toluene, chloroform, DMF and THF, which are good solvents for PS, although could not be dispersed in hexane, methanol, ethanol or water (Figure 3.23 (a)). It was found that PDA/RGO after drying could not be dispersed in these solvents even though after a long sonication time.

The dispersion situation in acetone was slightly different from the other solvents. At the beginning, the nanocomposite was well dispersed under sonication. However, settling overnight, the nanocomposites in acetone precipitated (Figure 3.23 (b)). The reason is that the grafted PS doesn't dissolve, but swells in acetone. So under sonication, the swelled PS helps separate the aggregation of the nanocomposites, but the swelled nanocomposites cannot form stable suspensions without mechanical force. The excellent dispersibility of PS-PDA/RGO nanocomposite in good solvents for PS further confirmed the successful grafted PS.

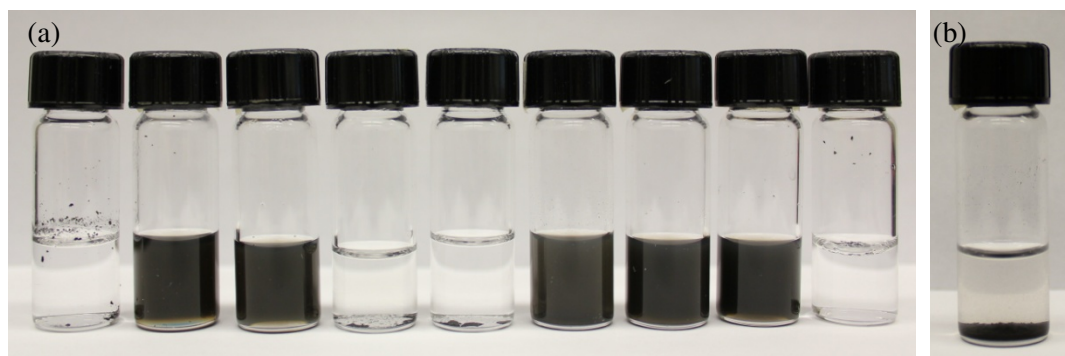


Figure 3.23. (a) Photographs of PS-PDA/RGO samples dispersed in various solvents by sonication for 30 min with a concentration of 1.0 mg/mL. Solvents were hexane, toluene, chloroform, methanol, ethanol, acetone, THF, DMF and water (from left to right). (b) PS-PDA/RGO suspension in acetone after overnight settled to the bottom.

PMMA grafted PDA/RGO was completely dispersed in toluene, chloroform, acetone, THF, and DMF, and partly dispersed in methanol and ethanol. PtBA-PDA/RGO was very well or partly dispersed (hexane and methanol) in all solvents, except water (Figure 3.24)

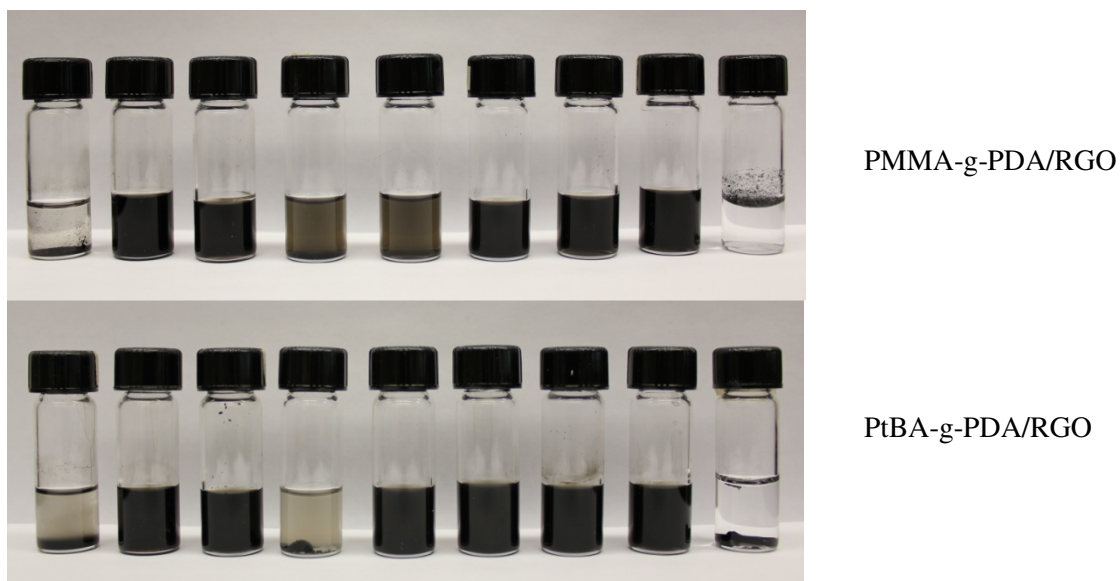


Figure 3.24. Photographs of PMMA-g-PDA/RGO and PtBA-g-PDA/RGO samples dispersed in various solvents with a concentration of 1.0 mg/mL. Solvents were hexane, toluene, chloroform, methanol, ethanol, acetone, THF, DMF and water (from left to right).

As shown in Figure 3.25, the PNIPAM grafted PDA/RGO was completely and homogeneously suspended in chloroform, methanol, ethanol, acetone, THF, and DMF, while partly dispersed in toluene.

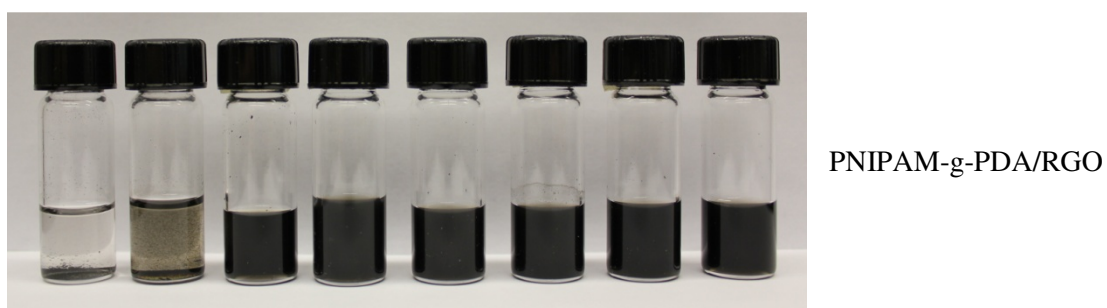


Figure 3.25. Photographs of PNIPAM-g-PDA/RGO samples dispersed in various solvents with a concentration of 1.0 mg/mL. Solvents were hexane, toluene, chloroform, methanol, ethanol, acetone, THF, and DMF (from left to right).

PNIPAM is a type of thermo-sensitive polymer, which when heated in water above 32 °C, undergoes a reversible LCST phase transition from a swollen hydrated state to a shrunken dehydrated state. Visually, the solution of PNIPAM changes from clear to opaque and the particle size increases (not dissolved) above the LCST.

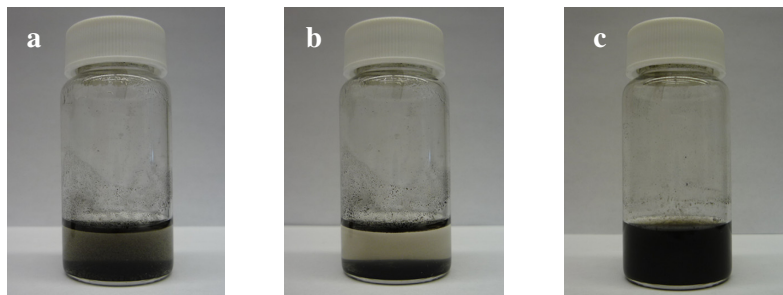


Figure 3.26. (a) PNIPAM-PDA/RGO suspension in water after 1 hour sonication under 40 °C. (b) suspension of (a) after placement of 5 min. (c) PNIPAM-PDA/RGO suspension in water after 10 min sonication under 0 °C

The PNIPAM grafted PDA/RGO should also have this as a similar property. To prove this, the nanocomposite was dispersed in water under sonication at different temperatures. When it was sonicated at 40 °C, which is higher than the LCST of PNIPAM, it could not be completely dispersed and precipitated quickly after sonication (Figure 3.26 (a) (b)). But when sonicated in water in an ice bath, it was very well dispersed in 5 min and the homogeneous suspension was stable for weeks (Figure 3.26 (c)). Since the temperature of an ice bath is lower than the LCST, grafted PNIPAM can be dissolved in water. The extension of grafted PNIPAM chains separated the nanocomposite apart, resulting in homogeneous and stable suspension. On the other hand, when the temperature was higher than the LCST of PNIPAM, grafted PNIPAM was undissolvable and aggregated on the surface of PDA/RGO, leading to precipitation of the nanocomposite.

3.5 Conclusion

Graphite was oxidized and peeled to graphene oxide with sulfuric acid and potassium permanganate by Hummers method. Dopamine was examined to reduce graphene oxide via its self-polymerization in alkaline buffer solution. Simultaneously, reduced graphene

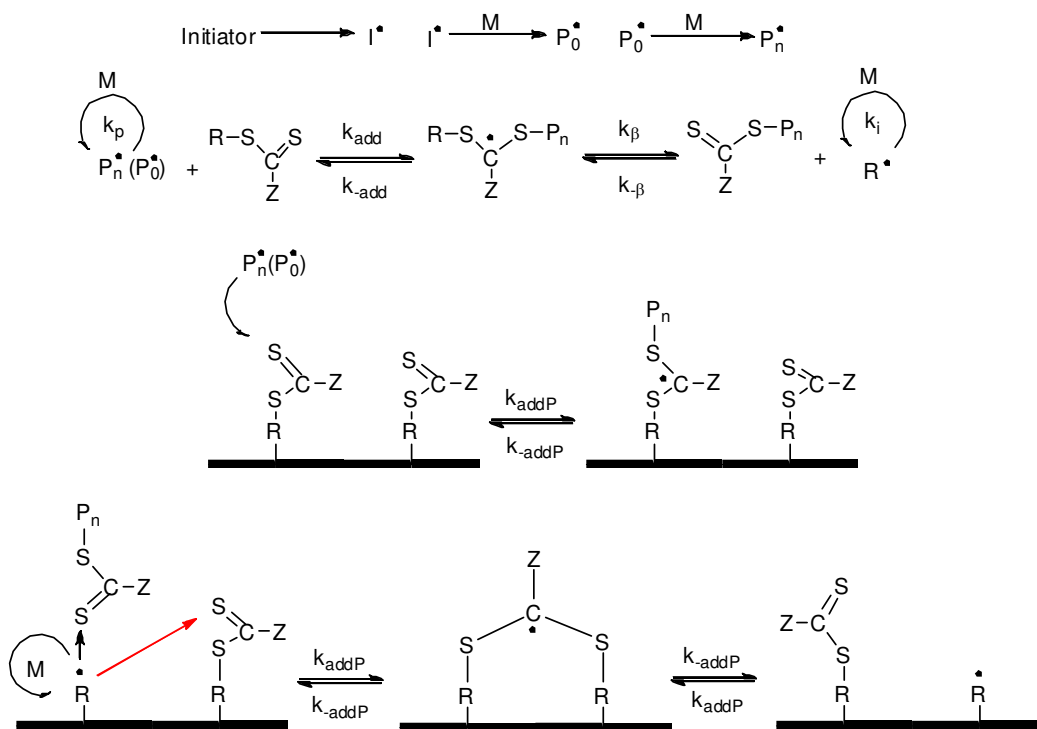
oxide could be coated with polydopamine to form PDA/RGO as a platform for secondary modification. It was demonstrated that the RAFT agent grafted PDA/RGO was synthesized by esterification reaction between hydroxyl groups of polydopamine and carboxylic groups of RAFT agent. The attached RAFT agent, which was evenly distributed, was prepared for subsequent surface “grafting from” RAFT polymerization.

This study demonstrates that our new approach for using RAFT-PDA/RGO as the RAFT agent for growing of polymer from the surface of polydopamine coating is compatible with a wide range of monomers, including styrene, MMA, NIPAM and tBA. The grafted polymer was confirmed by FTIR and TGA with enhanced dispersibility of the polymer grafted nanocomposites in various solvents. Also, the suitability with monomers depends on the grafted RAFT agent. Since different RAFT agents suit polymerization of different monomers, potentially other kinds of RAFT agent with carboxylic group could be synthesized and attached to the PDA coating, allowing this method to be applied to a variety of grafted PDA/RGO nanocomposites. Moreover, this new approach can also be utilized to functionalize other substrates coated by PDA with grafted polymers.

Chapter 4

Livingness and Kinetic Study of Surface “Grafting from” RAFT Polymerization on PDA/RGO

In this chapter, polymer chains of polystyrene were grown from polydopamine/reduced graphene oxide (PDA/RGO) surface by the reversible addition-fragmentation chain transfer polymerization process. The livingness and kinetics of styrene polymerization from “grafting from” PDA/RGO was studied. The livingness of the polymerization of styrene is demonstrated by GPC analysis. Two different conditions (with or without free RAFT agent) of surface RAFT polymerization were compared to analyze the livingness of the polymerization. The monomer conversion and molecular weight kinetics were explored for the living RAFT polymerization in both conditions. The kinetic of surface RAFT polymerization, such as induction and retardation phenomena, was demonstrated and investigated. Also, the dispersion of the nanocomposite filler in the polymer matrix was studied using thermal analysis.

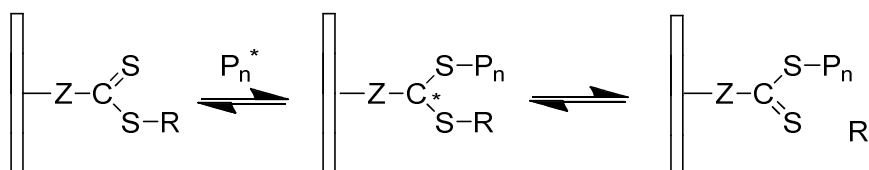


4.1 Introduction

Recent progress in living/controlled radical polymerization such as ATRP or RAFT polymerization has opened new routes for the synthesis of polymers with controlled molecular weights, well-defined functional groups, and narrow polydispersities. These techniques provide the ability to functionalize the surface of nanomaterials, such as silica,^{30a} TiO₂,⁸² carbon nanotube,⁸³ and graphene.⁸⁴ Previously, several groups have demonstrated the surface “grafting from” polymerization on graphene oxide via the RAFT process^{28, 47-48}, in which the RAFT agent was attached to the graphene oxide sheets.

Anchoring of a RAFT agent to a solid surface can be accomplished via either the Z or R group (Figure 4.2). In the Z-group approach, the RAFT agent is attached to the support through the Z-group, while in the R-group approach, the RAFT agent is attached to the support via the R-group. R-designed attachments allow the termination of two macro-radicals on the surface and detachment of the RAFT agent during the polymerization, which may result in the loss of immobilized functionalities.⁸⁵ On the other hand, in the Z-group approach, these side reactions can be prevented,⁸⁶ but suffers from hindrance problems.

Z approach



R approach

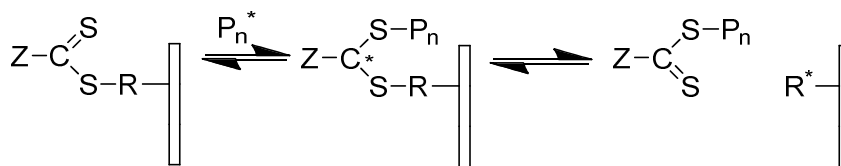


Figure 4.1. Schematic diagram of RAFT polymerization from a trithiocarbonate RAFT agent anchored to the surface of sheets via Z and R groups.

In this study, a RAFT agent (S-Dodecyl-S'-(α,α' -dimethyl- α'' -acetic acid)trithiocarbonate) that has a carboxylic end group in the reinitiating group (R) was used to form a macro chain-transfer agent (RAFT-PDA/RGO) for subsequent RAFT polymerization of styrene. In this R-group approach, low molar mass monomer can easily diffuse to the functionalized surface to start polymerization and grow the polymer chain.

The difference from previous approaches is that the polymer chains were not grown from the graphene oxide surface directly, but grown on polydopamine coating on reduced graphene oxide. Cao and coworkers conducted ATRP on a polydopamine coating before^{75,87}, but no investigations have published the application of RAFT polymerization on this material. Therefore, this is the first study to employ RAFT polymerization on polydopamine coating surface, which have applications in a new generation of melt processible conductive coatings.

4.2 Experimental

4.2.1 Materials

Styrene ($\geq 99\%$, Sigma-Aldrich, contains 4-*tert*-butylcatechol as stabilizer) were purified by passing through a basic alumina column before use and stored at 4 °C, 2,2'-Azobis(2-methylpropionitrile) (AIBN, Dupont) was recrystallized twice from methanol before use and stored at 4 °C, N,N-Dimethylformamide (DMF), toluene, methanol, tetrahydrofuran (THF), 1-butanol, concentrated sulfur acid (H_2SO_4) were purchased from Caledon Laboratories, and were used as received. The PS polymer with a weight average molecular weight (M_w) of 350,000 g/mol and a polydispersity of 2.5 was purchased from Sigma-Adrich, and was used as received.

4.2.2 Surface RAFT Polymerization of Styrene on RGO/PDA without Free RAFT agent

RAFT-PDA/RGO (31.5 mg, 0.01 mmol RAFT agent (Appendix 2)) was suspended in a mixture of styrene monomer (5 mL), DMF (2 mL), and AIBN (0.01 mmol) by sonication. A sealed 10 mL dried Schlenk tube was degassed and refilled with nitrogen three times. The mixture was added into the tube via a syringe, and the solution was bubbled with nitrogen for 30 min. The reaction tube was placed in a thermostated oil bath at 60 °C. After a determined time, the tube was immersed into an ice bath to stop the polymerization. The suspension was then dropped slowly in methanol with stirring. The solid was obtained via filtration through a 0.2 µm nylon membrane, which was then washed with toluene three times to remove free polystyrene and dried under vacuum at 40 °C.

4.2.3 Surface RAFT Polymerization of Styrene on RGO/PDA with Free RAFT agent

RAFT-PDA/RGO (33.5 mg, 0.015 mmol RAFT agent (Appendix 2)) was suspended in a mixture of styrene monomer (5 mL), DMF (2 mL), AIBN (0.01 mmol) and free RAFT agent (0.015 mmol) by sonication. A sealed 10 mL dried Schlenk tube was degassed and refilled with nitrogen three times. The mixture was added into the tube via a syringe, and the solution was bubbled with nitrogen for 30 min. The reaction tube was placed in a thermostated oil bath at 60 °C. After a determined time, the tube was immersed into an ice bath to stop the polymerization. The suspension was then dropped slowly in methanol with stirring. The solid was obtained via filtration through a 0.2 µm nylon membrane, which was then washed with toluene three times to remove free polystyrene and dried under vacuum at 40 °C.

4.2.4 Preparation of PS Composite Containing Graphene

The PS polymer matrix (Sigma-Adrich) and the synthesized PS-PDA/RGO nanocomposites were used to prepare the composite films. In a typical preparation procedure, different mass fractions of PS-PDA/RGO were dispersed in THF by bath sonication at room temperature. The PS matrix was added in the solution, with the mixture sonicated to achieve homogeneous suspensions. Finally, these suspensions were slowly dropped into clean Teflon dishes and dried in vacuum. The resulting films were removed from the Teflon substrate prior to further characterization. The weight ratio between pure PS and PS-PDA/RGO was controlled to make the composites containing 1.5%, 1.0%, 0.5% and 0.25% (weight) reduced graphene oxide.

For example, if 300 mg composites containing 1.0% reduced graphene oxide were to be prepared, the PS-PDA/RGO containing 10% weight (the weight of RGO which could not be removed under nitrogen flow) after burning under nitrogen. Then the weight of PS-PDA/RGO needed equals to $300 \times 1.0\% / 10\%$ mg (30 mg), and the weight of pure PS equals to $300 - 30$ mg (270 mg).

4.2.5 Cleaving Grafted Polymer from RGO/PDA⁸⁸

A 50 mL vial was charged with 20 mg of PS-PDA/RGO, 10 mL of toluene, 4.5 mL of 1-butanol, and 1 mL of concentrated sulfuric acid. The mixture was sonicated for 15 min to form a homogeneous black suspension. Then the mixture was stirred at 70 °C for 10 days, with the suspension then dropped into 300 mL methanol with stirring. The solvent was removed by filtration through a 0.2 μm nylon membrane, and the residual solid was dispersed in toluene. The solvent containing dissolved polymer was collected by filtration, with the solvent removed by vacuum.

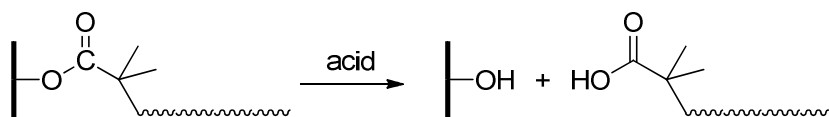


Figure 4.2. Cleavage of grafted polymer by strong acid.

4.2.6 RAFT Polymerization of Styrene

A sealed 10 mL dried Schlenk tube was degassed and refilled with nitrogen three times. The mixture of RAFT agent (0.01mmol), AIBN (0.01 mmol), styrene (5 mL) and DMF (1 mL) was added into the tube via syringe, with the solution then bubbled with nitrogen for 30 min. The reaction tube was placed in a thermostated oil bath at 60 °C. After the desired time, the tube was immersed into an ice bath to stop the polymerization. Polystyrene in the mixture was precipitated in methanol and the product dried under vacuum for 24 h.

4.2.7 Free Radical Polymerization of Styrene

A reaction tube containing styrene (5 mL), AIBN (0.01 mmol), and DMF (1 mL) was placed in a thermostated oil bath at 60 °C with stirring. After a determined time, the tube was placed in an ice bath to stop the polymerization. The product was then precipitated in methanol with the polymer dried under vacuum.

4.3 Characterization

The molecular weight of PS was measured by static light scattering (SLS) with a Zetasizer Nano S or gel permeation chromatography (GPC) with a Viscotek instrument using triple detectors referenced to PS standards (1 mL/min, at 30 °C).

The thermal properties of the products were measured by thermogravimetric analysis (TGA) on a TA Instruments SDT Q600. The samples were heated from room temperature to 800 °C at a heating rate of 10 °C/min under nitrogen atmosphere.

Energy-dispersive X-ray (EDX) elemental analysis was performed using a Quartz Xone EDX scattering device attached to a Hitachi S-4500 field emission scanning electron microscope (SEM).

4.4 Results and Discussions

4.4.1 Kinetics of Solution and Surface RAFT Polymerization of Styrene

Usually, the M_n in RAFT polymerization is determined by the concentration of RAFT agent. However, in the case of traditional RAFT polymerization and surface RAFT polymerization without free RAFT agent, the concentration of initiator is equal to the concentration of RAFT agent. Thus the concentration of free radical would be higher than the concentration of RAFT agent.

Assume the efficiency of initiator is 100%, the number average molecular weight, M_n can be calculated by the concentration of monomer converted to polymer divided by the concentration of polymer chains. It equals to the concentration of active free radical, twice of the concentration of initiator is there is little termination during the polymerization:

$$M_n = \frac{[M]_0 \cdot x\% \cdot M_{n,monomer}}{2[I]_0} \quad (4.1)$$

Where $x\%$ is the monomer conversion and $M_{n,number}$ is the molecular weight of the monomer.

In these polymerizations,

$$M_n = \frac{5ml \cdot 0.91g/ml \cdot x\%}{2 \cdot 0.01mmol} = 2275x \quad (4.2)$$

In the case of surface RAFT polymerization with free RAFT agent, the concentration of total RAFT agent is higher than the twice concentration of initiator. Then the initiator in this situation only determines the concentration of active radicals, not the number of polymer chains, when we assume that all the polymer chains will be initiated by the

liberated R-groups from the RAFT agent to form the start of a polymer chain. Hence, we need to modify Eq. 1 to take this into consideration.

$$M_n = \frac{[M]_0 \cdot x\% \cdot M_{n,monomer}}{[RAFT]_{graft} + [RAFT]_{free}} \quad (4.3)$$

Where $[RAFT]_{graft}$ is the concentration of the grafted RAFT agent, $[RAFT]_{free}$ is the concentration of the free RAFT agent.

In this polymerization,

$$M_n = \frac{5ml \cdot 0.91g/ml \cdot x\%}{0.015mmol + 0.015mmol} = 1516.7x \quad (4.4)$$

4.4.2 Conventional Free Radical and RAFT Polymerization

Before performing the surface “grafting from” RAFT polymerizations on the polydopamine/reduced graphene oxide (PDA/RGO), suitable reaction conditions, such as temperature, ratio of reactants, and time, should be determined to optimize the living/controlled polymerization behavior. Since RAFT polymerization, like other living/controlled polymerizations, is a much slower process than conventional free radical polymerization, the ratio between initiator and RAFT agent is significant. Too few initiator “active sites” result in long reaction times, while a too high initiator concentration can impair the control ability of the RAFT system resulting in a reduced polymer chain length.

In most cases, the mole ratio used in the literature between RAFT agent and initiator ($n_{RAFT}/n_{initiator}$) is 10 to 4^{51, 89}. However, when the ratio is too low, the resulting reaction rate is very low (less than 10% monomer conversion after 10 days). When the mole ratio is high (RAFT agent: AIBN=1:1), the reaction rate is acceptable, however, this ratio should be confirmed on whether control of the molecular weight is still effective in the RAFT process.

In this thesis, conventional RAFT polymerization based on a 1:1 molar ratio between the RAFT agent and initiator was carried out to verify the living/controlled character. A corresponding free radical polymerization without RAFT agent was also conducted as the control experiment. The molecular weight results measured by SLS are shown in Table 4.1, and plotted in Figure 4.3.

Table 4.1. Synthesis of PS by conventional free radical polymerization and RAFT polymerization.

Radical Polymerization			RAFT Polymerization		
Time (h)	Conversion (%)	Mw (kDa)	Time (h)	Conversion (%)	Mw (kDa)
5	7.8	174	5	6.7	27.3
20	23.4	175	10	12.4	41.2
48	46.2	181	20	22.9	66.3
			30	35.1	103

The theoretical molecular weight of RAFT polymerization (Figure 4.3, right) is calculated based on that the efficiency of initiator is 100% and there is no termination during the polymerization (Eq. 4.3). Lower efficiency of initiator and termination during the polymerization can cause higher experimental results of molecular weight. As Figure 4.3 shows, the conversion of monomer increases linearly with time, as well the molecular weights of polymer made by RAFT polymerization grow nearly linearly as the conversion of monomer increases. Nevertheless, this plot of RAFT polymerization has a nonzero initial molecular weight, similar to conventional free radical polymerization, which is indicative of deviation from ideally controlled living radical polymerization at the initial stages of reaction. This might be attributed to a lag in the activation of the RAFT agents and conversion to the polymeric RAFT species. The phenomenon of high initial molecular weight is termed hybrid behavior,⁹⁰ which is caused by a low transfer constant of the initial RAFT agent. The slow rate of addition or fragmentation of intermediate in favor of initiating materials can lead to a low transfer constant. Despite the nonzero initial amount, a linear increase with conversion is still observed for M_n confirming living characteristics of polymerization.

However, in a typical free-radical polymerization, the molecular weight of polymer increases dramatically at low monomer conversion and then increases slowly afterwards (Figure 4.3 right). Compared with free radical polymerization, the control of molecular weight in RAFT polymerization is much better. Therefore, the equal molar ratio between initiator and RAFT agent still maintains the typical character of living polymerization in solution RAFT polymerization. Hence these reaction conditions are acceptable to examine for the corresponding graphene surface “grafting from” RAFT polymerization.

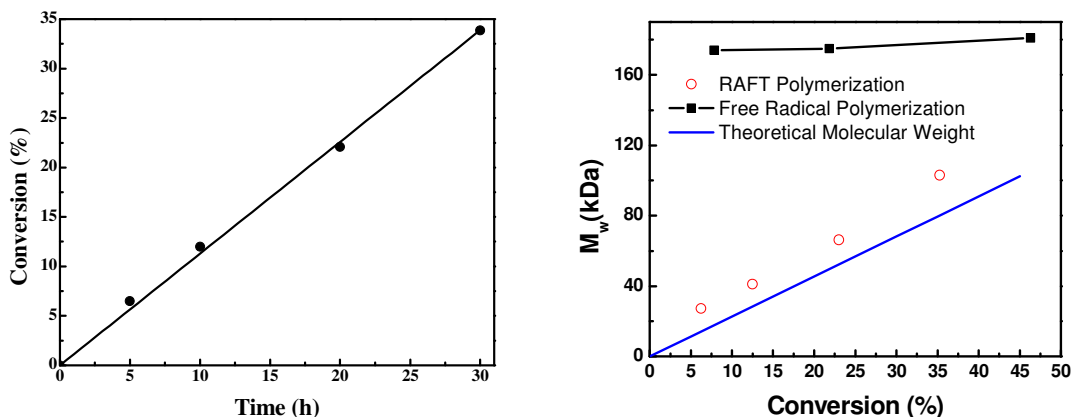


Figure 4.3. Left: Styrene conversion vs. time data for solution RAFT polymerization. Right: Molecular weight vs. styrene conversion data for solution RAFT polymerization (circle), free radical polymerization (square) and theoretical M_w of RAFT polymerization (blue line).

The relative amount of grafted PS on PDA/RGO nanocomposites was determined by TGA. Figure 4.4 shows the TGA traces of PS-PDA/RGO under nitrogen. The relative weight loss increases with an increase of reaction time, providing evidence of the growth of molecular weight of grafted PS.

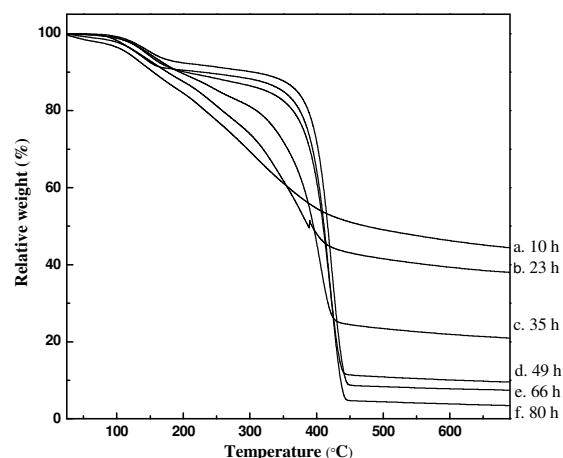


Figure 4.4. TGA thermograms of PDA/RGO-g-PS taken at different time intervals (a-f) under nitrogen. The weight left at 600 °C is (a) 46 %; (b) 39 %; (c) 22 %; (d) 10 %; (e) 8 %, and (f) 4 %.

The EDX image of PS-PDA/RGO nanocomposite after the treatment of concentrated sulfuric acid (Figure 4.5) confirmed the complete cleavage process of grafted polymer. According to Figure 4.5, there is no sulfur detected in the residual solid, which indicates that the dithioester functional group connected with the grafted PS has been removed from the nanocomposite.

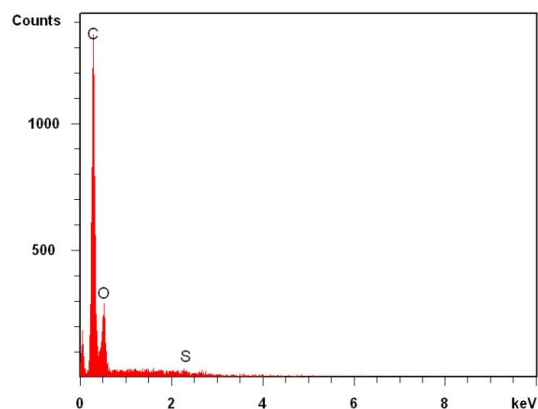


Figure 4.5. EDX analysis of residual solid after acid treatment of PS-PDA/RGO.

4.4.3 Livingness Study of Surface “Grafting from” RAFT Polymerization

After polymerization, the grafted PS was cleaved by acid-catalyzed transesterification in 1-butanol. The GPC analysis of the cleaved PS (Table 4.2) shows that the increase of molecular weight is non-linear with the consumption of monomer (i.e. conversion). The growth slows during the polymerization as shown in Figure 4.6. The molecular weight is near theoretical line at the early stages of polymerization, but diverges later.

Table 4.2. Synthesis of PDA/RGO grafted with PS by RAFT polymerization without free RAFT agent in solution. (g): graft polystyrene, (f): free polystyrene

Time (h)	% C	M _n (g) (g/mol)	M _w (g) (g/mol)	PDI (g)	M _n (f) (g/mol)	M _w (f) (g/mol)	PDI (f)
24	5.7	12430	15020	1.209	34440	54330	1.578
36	14	36600	46690	1.276	61660	95540	1.550
47	24	53370	68930	1.292	80365	116630	1.505
67	34	63070	85120	1.361	80410	121300	1.508

While growing PS from the PDA/RGO surface, free PS would also be produced in solution. This free PS was removed from the grafted PS-PDA/RGO by extensive washing with toluene by filtration. Compared with the grafted PS, the free PS produced at different monomer conversions shows increased non-linear behavior with M_n, indicating weaker living/control of the molecular weights. The M_n value of the free polymer increases with conversion at the early stages of polymerization, but levels off at about 25% conversion. The M_n deviates from the theoretical molecular weight from the beginning of the polymerization. According to the plot of M_n of graft polymer, although the value of M_n does not level off before 35% conversion, the curve tends to even out at higher conversion. The data also suggests that the free polymer has larger M_n.

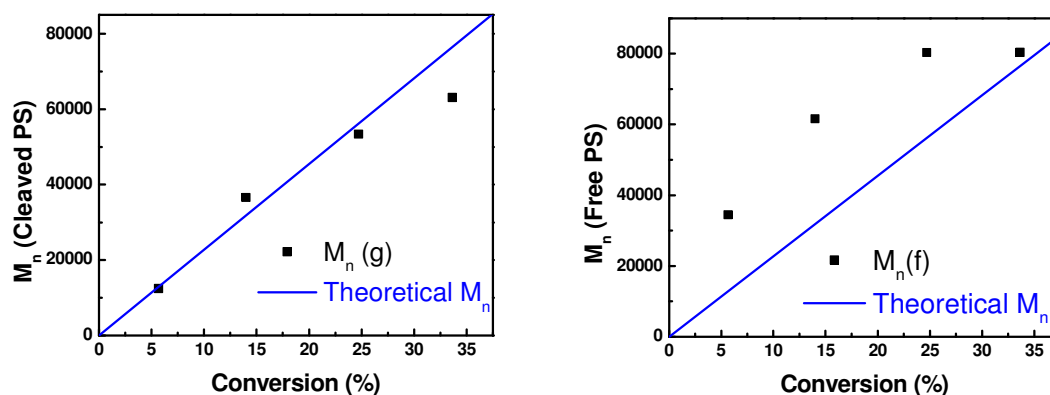


Figure 4.6. Left: Dependence of M_n of grafted polymer on conversion. Right: Dependence of M_n of free polymer on conversion. Condition: without free RAFT agents in solution. Blue line: Theoretical M_n (Eq. 4.2)

In explanation, during the surface-initiated RAFT polymerization, a grafted-polymer radical may undergo the addition-fragmentation equilibrium process with a neighboring grafted polymer, or with a free polymer chain (Figure 4.7)⁹¹. The primary radicals produced via decomposition of AIBN predominantly attacked styrene to generate PS radicals. Some of these polymer radicals could undergo a RAFT process with one of the grafted RAFT agents, converting them to a free PS chain capped with a RAFT moiety (PS-Y)⁹¹. The concentration of free PS-Y would increase with time and conversion. However, it seems that the concentration of free PS-Y is much lower than the concentration of PS radicals. Hence, the free PS-Y would have little influence on controlling the polymerization. In this way, the system will undergo conventional free radical polymerization of styrene with only a slight effect of the free PS-Y chains, yielding a large molecular weight fast⁹¹, as shown in Figure 4.6 (right).

On the other hand, the grafted RAFT agent activated by the free radical would undergo propagation until it undergoes another RAFT process with a neighboring grafted chain or a termination reaction with either grafted or polymer free radicals. In this way, the molecular weight of grafted chains would slowly increase in a controlled manner. Hence, the characteristics of the grafted and free polymer can be different at the early stages of

polymerization.⁹¹ Therefore, the plot of M_n of grafted polymer does not level off as early as the plot of M_n of free polymer. Nevertheless, as the number of dormant grafted chains decreases with conversion, the exchange reaction with neighboring dormant grafted chains would become less likely to occur. Then the control of molecular weight of grafted PS would become weaker as the conversion of styrene increased.

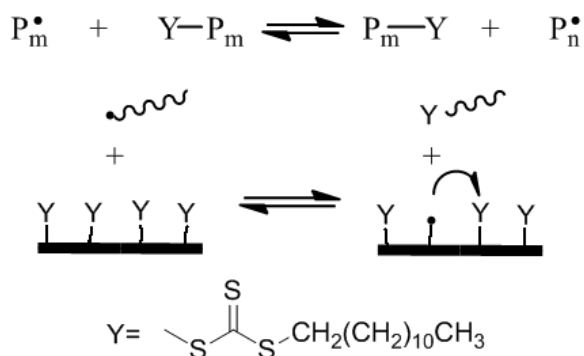


Figure 4.7. Key processes in RAFT-mediated graft polymerizations.

In the “grafting from” living/controlled polymerization research area, it was reported that the use of additional free RAFT agent in solution could help to increase the control over polymerization⁹¹. Free polymers produced in solution have almost the same molecular weight as those prepared on solid substrates with the addition of free RAFT agent to the solution.⁹¹⁻⁹² Some research groups do not measure the molecular weight of the grafted polymer chains directly, but add free RAFT agent to the polymerization system and measure the molecular weight of the polymer produced in solution. They then assume that the molecular weight of grafted polymer and free polymer are the same.^{48, 93} To examine this approach, free RAFT agent (0.015 mmol) was added to the reaction system to investigate the polymerizations under these conditions, with the molecular weight of the free polymer and grafted polymer measured by GPC (Table 4.3). The sample (RAFT-PDA/RGO) of higher density of grafted RAFT agent (447 $\mu\text{mol/g}$, 0.53 RAFT/ nm^2) was used in this reaction system.

Table 4.3. Synthesis of PDA/RGO grafted with PS by RAFT polymerization with free RAFT agent in solution (g: graft, f: free)

Time (h)	% C	M _n (g) (g/mol)	M _w (g) (g/mol)	PDI (g)	M _n (f) (g/mol)	M _w (f) (g/mol)	PDI (f)
35	6.4	12630	15800	1.251	16640	26600	1.599
49.5	15	21890	27470	1.255	28960	43530	1.503
66	25	28240	42220	1.495	40930	56410	1.378
80.5	28.0	33130	49570	1.496	45230	63610	1.406

As shown in Table 4.3, the GPC results of free PS show that the addition of free RAFT agent helps to enhance control of the molecular weight of grafted PS and free PS. Figure 4.8 shows the plot of M_n of grafted (cleaved) and free PS as a function of styrene conversion. Both are directly proportional to conversion, being consistent with living behaviour. The presence of a higher concentration of RAFT species in solution would not only control the polymerization in solution but also effectively maintain the concentration of dormant grafted chains by the exchange reaction of a grafted radical with a dormant free chain with a RAFT moiety. As Figure 4.8 shows, the molecular weight of grafted and free polymer also shows hybrid behavior, the same as solution RAFT polymerization. Therefore, low molecular weight of grafted polymer is not accessible with this grafted RAFT agent. To avoid this hybrid behavior, a more effective RAFT agent needs to be identified or developed and grafted onto the PDA/RGO surface to carry out more effective subsequent surface RAFT polymerization.

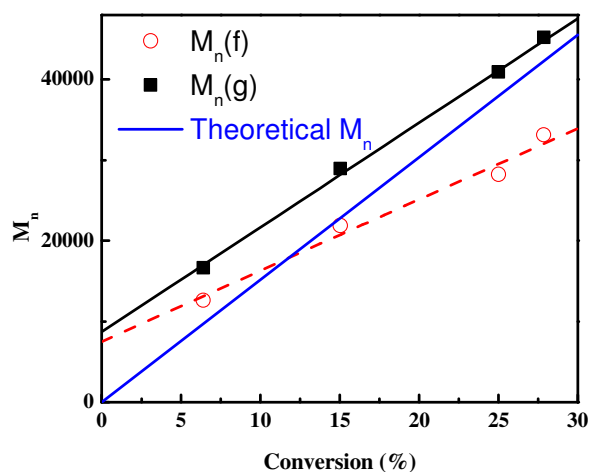


Figure 4.8. Dependence of M_n of grafted polymer (g) and free polymer (f) on conversion. Blue line: Theoretical M_n (Eq. 4.4). Condition: with free RAFT agents in solution.

Compared with the cleaved PS, the molecular weight of free PS is still larger. As a comparison, typical GPC traces of free and grafted PS samples are shown in Figure 4.9. In the GPC traces, the molecular weight of free PS is still higher than that of grafted PS. But the difference is much smaller than the experiments without free RAFT agent in solution. This may be attributed to the localized high RAFT-agent concentration on the PDA/RGO surface. The grafted radical chains and grafted dormant chains (RAFT agent) are chemically bonded to PDA/RGO, while the polymer free radical chains and free dormant chains are dispersed homogeneously throughout the reaction solution, maintaining a constant RAFT concentration throughout the solution. Once a radical in solution is transferred to the PDA/RGO surface via a chain transfer reaction, the surface radical on the surface would experience three reaction modes: initiating surface RAFT grafting polymerization, transfer to neighboring RAFT molecule on the surface, and transfer to free RAFT agent in solution. Since the local concentration of RAFT agent on the PDA/RGO surface was higher due to the immobilization of the RAFT agents, the radical will have a higher probability to transfer to a nearby RAFT agent rather than propagate due to close proximity. This effect will result in a slower growth rate for the grafted polymer chains. Therefore, the molecular weight of grafted polymer will be lower than that of free polymer as was experimentally observed. If the concentration of free

dormant chain (RAFT agent) in solution is the same as the local concentration of grafted dormant chain, the polymer free radical chains will have the same chance to undergo the RAFT process. In this way, the M_n of free polymer should be very close to that of the grafted polymer.

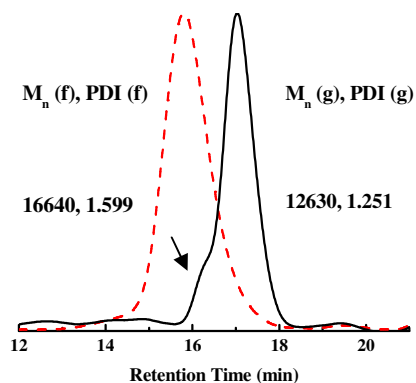


Figure 4.9. GPC elution profiles of free (dashed line) and grafted (solid line) PS samples obtained by surface RAFT polymerization on RAFT-PDA/RGO.

Figure 4.10 shows the GPC elution profiles of the cleaved PS samples obtained using surface RAFT polymerization for 35-80 hours of polymerization time. The molecular weight distribution profiles show a small shoulder peak before the main peak of higher molecular weight, which also appears in Figure 4.10. This shoulder peak may be assignable to dead chains produced by recombination of polymer radicals⁹¹. Also, this peak may be attributed to remaining PDA, as strong acid may not only break the ester bonds between grafted PS and PDA coating, but also cleave the coating from the reduced graphene oxide surface, leaving some of the PDA chains may be mixed with the cleaved PS sample.

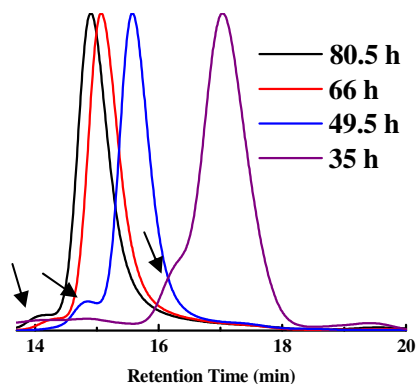


Figure 4.10. GPC elution profiles for surface RAFT polymerization on RAFT-PDA/RGO of styrene with AIBN as initiator at 60 °C, for 35 h ($M_n = 12,630$ g/mol, PDI = 1.251), 49.5 h ($M_n = 21,890$ g/mol, PDI = 1.255), 66 h ($M_n = 28,240$ g/mol, PDI = 1.495), 80.5 ($M_n = 33,130$ g/mol, PDI = 1.496).

4.4.4 Kinetic Study of Surface “Grafting from” RAFT Polymerization

Moreover, the rate of monomer consumption in the “grafting from” reaction system is much slower than conventional RAFT polymerization with the same amount of monomer, CTA, and initiator. At the beginning stage of polymerization, the polymerization rate is much slower (Figure 4.11). The polymerization retardation is ascribed to the localized high RAFT-agent concentration on the PDA/RGO surface ($326 \mu\text{mol/g}$, 0.39 RAFT/nm^2)^{30a}. As discussed before, once a free radical is transferred to the PDA/RGO surface, it will prefer to undergo a RAFT process with a nearby RAFT agent rather than propagate to a long polymer radical chain, hence leading to a pronounced polymerization retardation.

Also, possible impurities may lead to the lower polymerization rate. It was found that nearly none of the grafted polymer was produced with the addition of small amounts of initiator, even after a long reaction time of 168 hours. This may be attributed to a low concentration of initiator, which can be terminated by the small levels of impurities present in the reaction mixture from the PDA/RGO substrate. Therefore a higher concentration of initiator is needed to achieve effective polymerization. Especially at the early stages of polymerization, some free radicals would act as a scavenger for such impurities, resulting in lower polymerization rates.

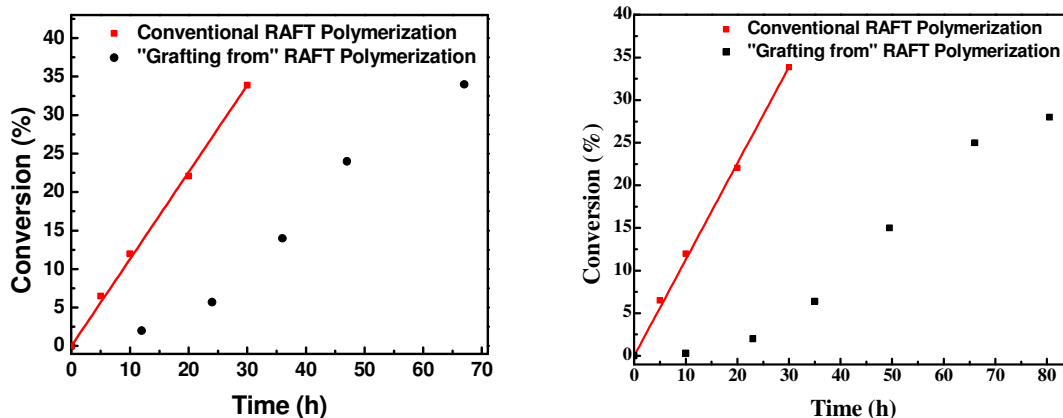


Figure 4.11. Dependence of conversion of monomer on time. Black dots (Left: without free RAFT agent in solution. Right: with free RAFT agent in solution). Red dots (conventional RAFT polymerization).

The results of the kinetic studies for solution RAFT polymerization of styrene and graft RAFT polymerizations of styrene from PDA/RGO are shown in Figure 4.12. If the plot $\ln([M]_0/[M])$ vs. time gives a straight line, the polymerization kinetics is first-order in regards to monomer concentration.

It is clear from this figure that the rates of polymerization from PDA/RGO were considerably lower than those found in solution. In addition, Figure 4.12 shows the induction period for surface RAFT polymerizations (16 h and 20 h). A similar phenomenon has been observed with growing styrene⁹⁴, methyl methacrylate^{94,30b}, and NIPAM⁹⁵ polymer chains from nanomaterials.

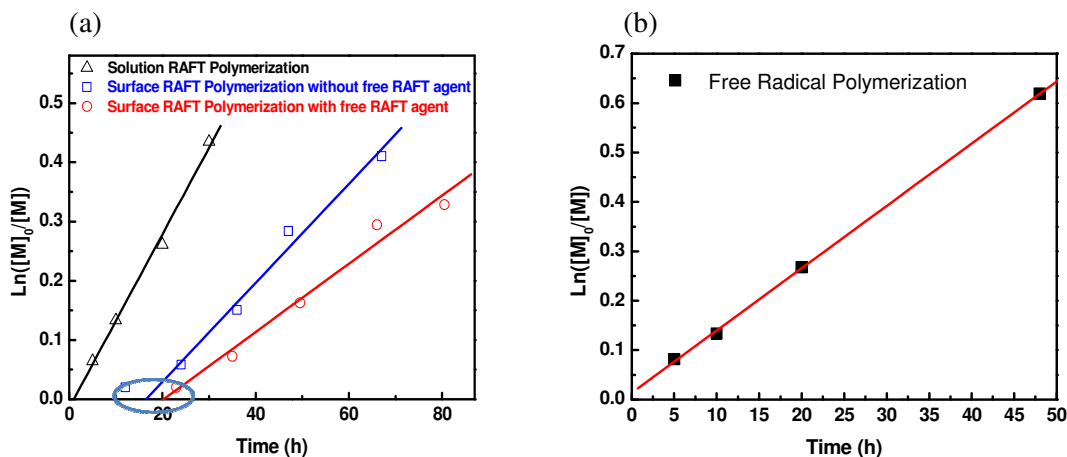


Figure 4.12. (a) First-order kinetic plots for the graft polymerization of styrene with functionalized PDA/RGO; solution RAFT polymerization, surface RAFT polymerization with and without free RAFT agent. (b) First-order kinetic plots for free radical polymerization.

The cause for this inhibition effect in RAFT polymerization has been attributed to two possible factors: slow fragmentation of the intermediate RAFT radicals in the pre-equilibrium and slow re-initiation ability of the leaving group R^{96} . According to a simulation study⁹⁶, slow re-initiation causes a continuous slow increase in the rate of polymerization at an early reaction time and induces rate retardation effects throughout the whole polymerization. The onset of the polymerization activity controlled by slow fragmentation is more sudden. In addition, slow fragmentation does not cause retardation during the polymerization. As Figure 4.13(b) shows, solution RAFT polymerization does not show a strong inhibition and retardation effect. The slight inhibition may be attributed to the slow fragmentation of initial RAFT radicals, which also could cause hybrid behavior of molecular weight. However surface RAFT polymerization shows strong inhibition and retardation. The retardation and slow increase in the rate of polymerization at the early stages of polymerization agrees with the influence of slow re-initiation. As discussed before, the radicals generated in solution could react with surface RAFT agents and subsequently transfer to the surface. Due to the high local concentration of surface RAFT agent, the radicals on the surface tend to transfer to neighboring RAFT molecules on the surface rather than to propagate with monomer, leading to slower re-initiation. The higher the local concentration of RAFT agent on the surface, the slower the re-initiation

process during the polymerization. In addition, surface RAFT polymerization with free RAFT agent shows more intense inhibition and retardation, due to the higher local concentration of grafted RAFT agent on PDA/RGO (447 $\mu\text{mol/g}$, 0.53 RAFT/ nm^2).

Also, since the RAFT concentration on the surface is much higher than that in solution, the rate retardation in the grafting polymerization would be more severe than that in the solution polymerization. The molecular weight of grafted polymer would be lower than that of free polymer as shown in Figure 4.8.

4.4.5 Improvement of dispersibility of PS-PDA/RGO nanocomposites

The dispersibility of graphene in PS matrix can be improved with the help of grafted PS, in which the amount of grafted PS influences the dispersibility significantly.

Figure 4.13 shows three sets of PS/PS-PDA/RGO composites, containing 1.5%, 1.0% and 0.5% graphene. The first set of composites contains the nanocomposite with 10.1% weight of graphene. The second set was prepared with nanocomposite with 39.4% weight of graphene. The last one was made with a mixture of pure PS and synthetic nanocomposite with 46.3% weight of graphene

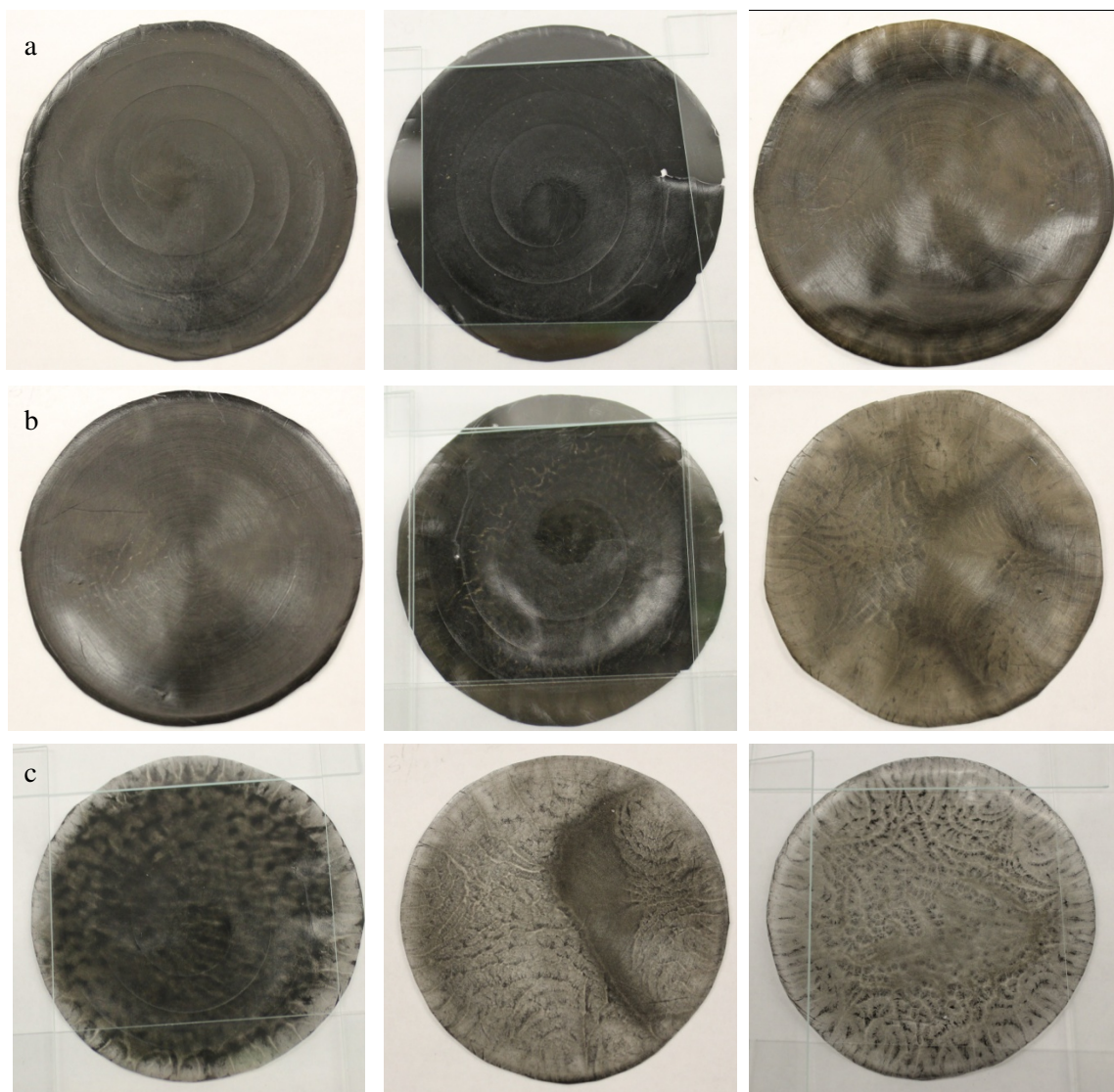


Figure 4.13. PS/PS-PDA/RGO composites (from left to right: 1.5%, 1.0%, and 0.5% RGO); (a) PS-PDA/RGO nanocomposite has 10.1% RGO; (b) PS-PDA/RGO nanocomposite has 39.4% RGO; (c) PS-PDA/RGO nanocomposite has 46.3% RGO.

In the first set of nanocomposites, the graphene was dispersed homogeneously in the matrix in all three composites. In the second set, slight aggregation appears in the low concentrations (1.0% and 0.5%). In the third set, significant black aggregations appear in all of the composites. It is apparent that the more grafted PS (longer length of grafted PS chains) helps improve the dispersibility.

4.4.6 Improvement of thermal stability of PS-PDA/RGO nanocomposites

As shown in Figure 4.14, the thermal stability of PS/PS-PDA/RGO composite is significantly different from pure PS. The majority of weight loss of composite happened later than that of pure PS, indicating better thermal stability. The higher the amount of grafted polymer on PDA/RGO (PS/RGO-1 to PS/RGO-3), the better the thermal stability of the composite. Therefore the good dispersibility of graphene in the polymer composite is significant for enhancing their thermal stability.

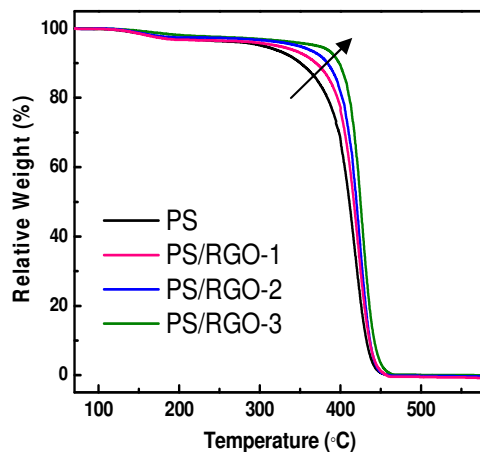


Figure 4.14. Relative weight loss of pure PS and PS/(PS-PDA/RGO) (0.25% RGO) composite under heating. (PS/RGO-1: 46.3% RGO; PS/RGO-2: 39.4% RGO; PS/RGO-3: 21.9% RGO)

When more PS-PDA/RGO nanocomposite was added to the composite, the thermal stability in the low temperature region weakens, while the stability at high temperature strengthens (Figure 4.15). Owing to the higher concentration of RGO in the composite, the stability at high temperature was reinforced. The reason for weakened stability at the early heating stage may be due to the polydopamine content or other impurities playing a significant role, since polydopamine is not stable at low temperature. More PS-PDA/RGO nanocomposite means more PDA component, which leads to the observed higher weight loss at the early heating stage.

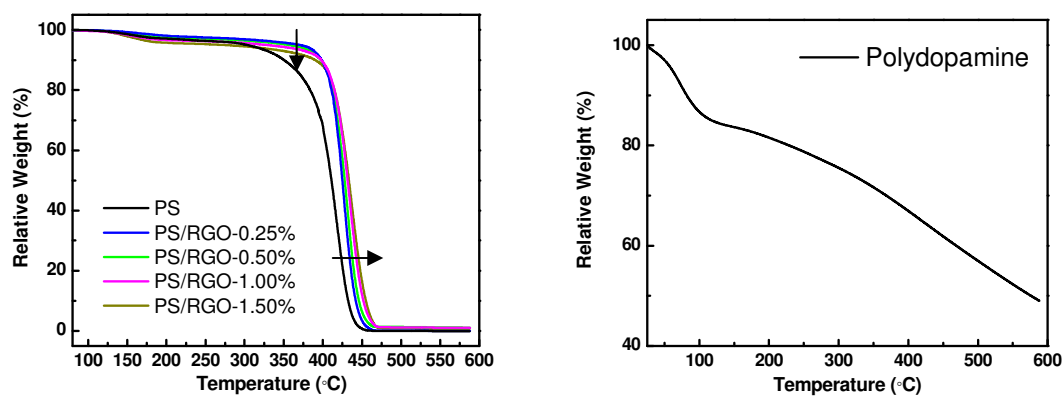


Figure 4.15. Left: Relative weight loss of pure PS and PS/(PS-PDA/RGO) composites with different contents of RGO. (0.25% - 1.5%) PS-PDA/RGO nanocomposite contains 21.9% RGO. Right: Relative weight loss of polydopamine under heating.

4.5 Conclusion

Surface “grafting from” RAFT polymerization was performed on reduced graphene oxide with polydopamine coating, with resultant PS-PDA/RGO nanocomposites being synthesized. The GPC results of cleaved polymer after various reaction times showed that the polymerization, with addition of free RAFT agent, was living after the RAFT agent was attached to PDA/RGO. The use of free RAFT agent in solution can help to increase the control over polymerization. Compared to traditional RAFT polymerization, surface “grafting from” RAFT polymerization shows induction and retardation phenomena during the polymerization. These effects could be attributed to the impurities and the high local concentration of RAFT agent.

The nanocomposites with higher amounts of grafted PS were able to be better separated and distributed in some solvents and the PS matrix. TGA results indicated that all PS/RGO composites had higher thermal stabilities than neat PS. It was also found that an increase in modified RGO content strengthened the thermal stability of the obtained composites at high temperature, but weakened the stability at the early heating stage. This

might be attributed to the relatively higher polydopamine content, which was found thermally unstable.

Chapter 5

Conclusions and Recommendations

Surface functionalization of graphene with polymers, through covalent or noncovalent bonding, is attracting increasing attention since the grafted polymers can modify the surface properties of graphene. According to previous publications, thermal, mechanical and electrical properties of polymers loaded with graphene can be enhanced by improved dispersibility of graphene within the matrix. To prevent aggregation of graphene attributed to π - π stacking, it is necessary to graft molecules from the surface to weaken these van der Waals interactions. Grafting polymers have better properties, since longer chains can result in enhanced steric repulsion to control the graphene aggregation. Another advantage of grafting polymers is that it can improve the compatibility of the polymer matrix with the graphene surface.

In this research, a new approach was investigated to control grafting of polymers from the surface of reduced graphene oxide coated with polydopamine using an emerging living radical polymerization technique, reversible addition fragmentation chain-transfer (RAFT). The study of the utilization of polydopamine coating as a platform for “grafting from” RAFT polymerization and the livingness of polymerization with surface grafted RAFT agents were the most important contributions of this thesis.

Polydopamine is a type of useful coating. The coating on graphene oxide, made by Hummers method from graphite, was prepared via self-polymerization of dopamine in buffer solution. (pH=8.5) Released electrons from the self-polymerization process would help in the graphene oxide reduction process. The simultaneous dopamine-induced reduction and polydopamine coating was clearly demonstrated by XPS, AFM, UV/Vis, and FTIR studies.

RAFT agents having carboxylic groups were chosen to functionalize polydopamine coating via esterification with the hydroxyl groups. TGA and EDX studies provided the evidence of functionalization of PDA/RGO. TGA was also employed to calculate the amount of RAFT agent used on the surface of PDA/RGO. Four kinds of polymers (polystyrene, poly(methyl methacrylate), poly(N-isopropylacrylamide), and poly(tertiary-butyl acrylate)) were grown from the functionalized surfaces.

The GPC results of cleaved polystyrene after various reaction times showed that the surface “grafting from” polymerization, with addition of free RAFT agent, was still living, after the RAFT agent was directly attached to the PDA/RGO surface. Without free RAFT agent in solution, the polymerization shows weak living/control of the molecular weights of grafted and free polystyrene. The addition of free RAFT agent in the reaction system could increase control over polymerization and potentially bridge the distance (molecular weight) between grafted polymer and free polymer in solution. Finally, the nanofillers were found well separated and distributed in the solvents and polymer matrix. As well, the polymer matrix loaded with the nanofiller showed better thermal stability compared with pure polymer.

Recommendations

This new “grafting from” approach of RAFT polymerization from graphene surfaces offers the opportunity to prepare polymer grafted PDA/RGO nanocomposites. However, a significant amount of work still needs to be done in order to fully realize the potential of this method, both in theory and application.

1. In this study, only one RAFT agent was attached to PDA/RGO. Other RAFT agents with carboxylic groups can be developed to be applied to this surface-initiated RAFT polymerization on polydopamine functionalized substrate. Thus, this method can be a versatile one, which can grow any polymer suitable for RAFT polymerization methodology.
2. Several kinds of homopolymer chains were grown from the surface of PDA/RGO. It would be interesting to grow diblock or triblock copolymers based on the homopolymer grafted PDA/RGO to find out whether the macro-RAFT agent can trigger further RAFT polymerization.
3. Besides conducting the polymerization in traditional organic solvents, carrying out this kind of surface RAFT polymerization approach in green solvents, such as

supercritical carbon dioxide (scCO₂), would be interesting to investigate. ScCO₂ can help to exfoliate graphene, providing better separation. The parameters of the polymerization, such as rate of polymerization, can be compared with those in organic solvents. Also synthesis of this nanocomposite using γ -radiation initiated grafting RAFT polymerization would be interesting.

4. Different polymerization conditions, such as reaction temperature and different ratios amongst the monomer, initiator, and RAFT agent grafted PDA/RGO, could be investigated to compare the livingness of the polymerization process. A kinetic study of graft polymerization from the PDA/RGO produced under different reaction conditions would also be valuable, giving better insight into the mechanism of polymerization.
5. More detailed investigations of the electrical, mechanical and thermal properties of polymer matrix loading with different amounts of the nanofiller made via this new approach is also necessary in the future work.
6. This research was to create a “grafting from” method allowing one to grow a wide range of polymers from the nanomaterial surface. To this end, this approach should be performed from substrates other than graphene, since polydopamine can be coated on a variety of material. The successful synthesis of these graphene-based nanocomposites is encouraging to extend this method for preparing other nanostructures, such as titania, carbon nanotube, and metal nanoparticles.
7. Polydopamine itself can also be a platform for more different reactions other than surface polymerization. These reactions can be investigated to functionalize graphene with other materials, such as metal particles, for more potential applications.

Bibliography

1. Balazs, A. C.; Emrick, T.; Russell, T. P., Nanoparticle polymer composites: where two small worlds meet. *Science* **2006**, *314* (5802), 1107-1110.
2. Lin, B.; Gelves, G. A.; Haber, J. A.; Sundararaj, U., Electrical, rheological, and mechanical properties of polystyrene/copper nanowire nanocomposites. *Industrial & engineering chemistry research* **2007**, *46* (8), 2481-2487.
3. Coleman, J. N.; Khan, U.; Blau, W. J.; Gun'ko, Y. K., Small but strong: a review of the mechanical properties of carbon nanotube-polymer composites. *Carbon* **2006**, *44* (9), 1624-1652.
4. Okada, A.; Usuki, A., Twenty Years of Polymer-Clay Nanocomposites. *Macromolecular Materials and Engineering* **2006**, *291* (12), 1449-1476.
5. Liu, Y.; Wang, A.; Claus, R., Molecular self-assembly of TiO₂/polymer nanocomposite films. *The Journal of Physical Chemistry B* **1997**, *101* (8), 1385-1388.
6. Huang, J.; He, C.; Xiao, Y.; Mya, K. Y.; Dai, J.; Siow, Y. P., Polyimide/POSS nanocomposites: interfacial interaction, thermal properties and mechanical properties. *Polymer* **2003**, *44* (16), 4491-4499.
7. Novoselov, K.; Geim, A.; Morozov, S.; Jiang, D.; Zhang, Y.; Dubonos, S.; Grigorieva, I.; Firsov, A., Electric field effect in atomically thin carbon films. *Science* **2004**, *306* (5696), 666-669.
8. Morozov, S.; Novoselov, K.; Katsnelson, M.; Schedin, F.; Elias, D.; Jaszczak, J.; Geim, A., Giant intrinsic carrier mobilities in graphene and its bilayer. *Physical Review Letters* **2008**, *100* (1), 16602.
9. Saito, K.; Nakamura, J.; Natori, A., Ballistic thermal conductance of a graphene sheet. *Physical Review B* **2007**, *76* (11), 115409.
10. Lee, C.; Wei, X.; Kysar, J. W.; Hone, J., Measurement of the elastic properties and intrinsic strength of monolayer graphene. *Science* **2008**, *321* (5887), 385-388.
11. Liu, J.; Tang, J.; Gooding, J. J., Strategies for chemical modification of graphene and applications of chemically modified graphene. *J. Mater. Chem.* **2012**.
12. Cai, D.; Song, M., Recent advance in functionalized graphene/polymer nanocomposites. *J. Mater. Chem.* **2010**, *20* (37), 7906-7915.
13. Wang, J. S.; Matyjaszewski, K., Controlled/" living" radical polymerization. Atom transfer radical polymerization in the presence of transition-metal complexes. *Journal of the American Chemical Society* **1995**, *117* (20), 5614-5615.
14. Hawker, C. J., Molecular weight control by a " living" free-radical polymerization process. *Journal of the American Chemical Society* **1994**, *116* (24), 11185-11186.

15. Chiefari, J.; Chong, Y.; Ercole, F.; Krstina, J.; Jeffery, J.; Le, T. P. T.; Mayadunne, R. T. A.; Meijs, G. F.; Moad, C. L.; Moad, G., Living free-radical polymerization by reversible addition-fragmentation chain transfer: the RAFT process. *Macromolecules* **1998**, *31* (16), 5559.
16. Boyer, C.; Stenzel, M. H.; Davis, T. P., Building nanostructures using RAFT polymerization. *Journal of Polymer Science Part A: Polymer Chemistry* **2011**, *49* (3), 551-595.
17. Vasilieva, Y. A.; Thomas, D. B.; Charles, W.; McCormick, C. L., Direct controlled polymerization of a cationic methacrylamido monomer in aqueous media via the RAFT process. *Macromolecules* **2004**, *37* (8), 2728-2737.
18. Bartels, J. W.; Caue□t, S. I.; Billings, P. L.; Lin, L. Y.; Zhu, J.; Fidge, C.; Pochan, D. J.; Wooley, K. L., Evaluation of isoprene chain extension from PEO macromolecular chain transfer agents for the preparation of dual, invertible block copolymer nanoassemblies. *Macromolecules* **2010**.
19. (a) Moad, G.; Rizzardo, E.; Thang, S. H., Radical addition-fragmentation chemistry in polymer synthesis. *Polymer* **2008**, *49* (5), 1079-1131; (b) Hu, N.; Ji, W. X.; Tong, Y. Y.; Li, Z. C.; Chen, E. Q., Synthesis of diblock copolymers containing poly (N-vinylcarbazole) by reversible addition-fragmentation chain transfer polymerization. *Journal of Polymer Science Part A: Polymer Chemistry* **2010**, *48* (20), 4621-4626.
20. (a) Destarac, M.; Guinaudeau, A.; Geagea, R.; Mazieres, S.; Van Gramberen, E.; Boutin, C.; Chadel, S.; Wilson, J., Aqueous MADIX/RAFT polymerization of diallyldimethylammonium chloride: Extension to the synthesis of poly (DADMAC)-based double hydrophilic block copolymers. *Journal of Polymer Science Part A: Polymer Chemistry* **2010**, *48* (22), 5163-5171; (b) Ali, S. A.; Abu-Thabit, N.; Al-Muallem, H. A., Synthesis and solution properties of a pH-responsive cyclopolymer of zwitterionic ethyl 3-(N, N-diallylammonio) propanephosphonate. *Journal of Polymer Science Part A: Polymer Chemistry* **2010**, *48* (24), 5693-5703.
21. Lowe, A. B.; McCormick, C. L., Reversible addition-fragmentation chain transfer (RAFT) radical polymerization and the synthesis of water-soluble (co) polymers under homogeneous conditions in organic and aqueous media. *Progress in polymer science* **2007**, *32* (3), 283-351.
22. Stenzel, M. H.; Barner-Kowollik, C.; Davis, T. P.; Dalton, H. M., Amphiphilic Block Copolymers Based on Poly (2-acryloyloxyethyl phosphorylcholine) Prepared via RAFT Polymerisation as Biocompatible Nanocontainers. *Macromolecular bioscience* **2004**, *4* (4), 445-453.
23. Mitsukami, Y.; Donovan, M. S.; Lowe, A. B.; McCormick, C. L., Water-soluble polymers. 81. Direct synthesis of hydrophilic styrenic-based homopolymers and block copolymers in aqueous solution via RAFT. *Macromolecules* **2001**, *34* (7), 2248-2256.
24. Boissé, S.; Rieger, J.; Di-Cicco, A.; Albouy, P. A.; Bui, C.; Li, M. H.; Charleux, B., Synthesis via RAFT of amphiphilic block copolymers with liquid-crystalline hydrophobic block and their self-assembly in water. *Macromolecules* **2009**, *42* (22), 8688-8696.
25. Quinn, J. F.; Chaplin, R. P.; Davis, T. P., Facile synthesis of comb, star, and graft polymers via reversible addition-fragmentation chain transfer (RAFT) polymerization. *Journal of Polymer Science Part A: Polymer Chemistry* **2002**, *40* (17), 2956-2966.

26. Hu, Z.; Zhang, Z., "Gradient" Polymer Prepared by Complex-Radical Terpolymerization of Styrene, Maleic Anhydride, and N-Vinyl Pyrrolidone via γ -Ray Irradiation by Use of a RAFT Process: Synthesis, Mechanism, and Characterization. *Macromolecules* **2006**, *39* (4), 1384-1390.
27. Mayadunne, R. T. A.; Jeffery, J.; Moad, G.; Rizzardo, E., Living free radical polymerization with reversible addition-fragmentation chain transfer (RAFT polymerization): approaches to star polymers. *Macromolecules* **2003**, *36* (5), 1505-1513.
28. Bin Zhang, Y. C., Liqun Xu, Longjia Zeng, Ying He, En-Tang Kang, and Jinjuan Zhang, Growing Poly(N-vinylcarbazole) from the Surface of Graphene Oxide via RAFT Polymerization. *Journal of Polymer Science Part A: Polymer Chemistry* **2011**, *49*, 2043-2050.
29. Hong, C. Y.; You, Y. Z.; Pan, C. Y., Synthesis of water-soluble multiwalled carbon nanotubes with grafted temperature-responsive shells by surface RAFT polymerization. *Chemistry of materials* **2005**, *17* (9), 2247-2254.
30. (a) Li, C.; Benicewicz, B. C., Synthesis of well-defined polymer brushes grafted onto silica nanoparticles via surface reversible addition-fragmentation chain transfer polymerization. *Macromolecules* **2005**, *38* (14), 5929-5936; (b) Hojjati, B.; Charpentier, P. A., Synthesis and kinetics of graft polymerization of methyl methacrylate from the RAFT coordinated surface of nano-TiO₂. *Journal of Polymer Science Part A: Polymer Chemistry* **2008**, *46* (12), 3926-3937.
31. Moad, G.; Rizzardo, E.; Thang, S. H., Living radical polymerization by the RAFT process. *Australian Journal of Chemistry* **2005**, *58* (6), 379-410.
32. (a) Geim, A. K.; Novoselov, K. S., The rise of graphene. *Nature Materials* **2007**, *6* (3), 183-191; (b) Gilje, S.; Han, S.; Wang, M.; Wang, K. L.; Kaner, R. B., A chemical route to graphene for device applications. *Nano letters* **2007**, *7* (11), 3394-3398.
33. Schedin, F.; Geim, A.; Morozov, S.; Hill, E.; Blake, P.; Katsnelson, M.; Novoselov, K., Detection of individual gas molecules adsorbed on graphene. *Nature Materials* **2007**, *6* (9), 652-655.
34. Bunch, J. S.; Van Der Zande, A. M.; Verbridge, S. S.; Frank, I. W.; Tanenbaum, D. M.; Parpia, J. M.; Craighead, H. G.; McEuen, P. L., Electromechanical resonators from graphene sheets. *Science* **2007**, *315* (5811), 490-493.
35. (a) Wang, X.; Zhi, L.; Müllen, K., Transparent, conductive graphene electrodes for dye-sensitized solar cells. *Nano letters* **2008**, *8* (1), 323-327; (b) Liu, Z.; Liu, Q.; Huang, Y.; Ma, Y.; Yin, S.; Zhang, X.; Sun, W.; Chen, Y., Organic photovoltaic devices based on a novel acceptor material: graphene. *Advanced Materials* **2008**, *20* (20), 3924-3930.
36. Standley, B.; Bao, W.; Zhang, H.; Bruck, J.; Lau, C. N.; Bockrath, M., Graphene-based atomic-scale switches. *Nano letters* **2008**, *8* (10), 3345-3349.
37. (a) Sofo, J. O.; Chaudhari, A. S.; Barber, G. D., Graphane: A two-dimensional hydrocarbon. *Physical Review B* **2007**, *75* (15), 153401; (b) Dimitrakakis, G. K.; Tyliaakis, E.; Froudakis, G. E., Pillared graphene: a new 3-D network nanostructure for enhanced hydrogen storage. *Nano letters* **2008**, *8* (10), 3166-3170.

38. Stoller, M. D.; Park, S.; Zhu, Y.; An, J.; Ruoff, R. S., Graphene-based ultracapacitors. *Nano letters* **2008**, *8* (10), 3498-3502.
39. Alzari, V.; Nuvoli, D.; Scognamillo, S.; Piccinini, M.; Gioffredi, E.; Malucelli, G.; Marceddu, S.; Sechi, M.; Sanna, V.; Mariani, A., Graphene-containing thermoresponsive nanocomposite hydrogels of poly (N-isopropylacrylamide) prepared by frontal polymerization. *J. Mater. Chem.* **2011**, *21* (24), 8727-8733.
40. Liu, J.; Tao, L.; Yang, W.; Li, D.; Boyer, C.; Wuhler, R.; Braet, F.; Davis, T. P., Synthesis, characterization, and multilayer assembly of pH sensitive graphene– polymer nanocomposites. *Langmuir* **2010**, *26* (12), 10068-10075.
41. Zhuang, X. D.; Chen, Y.; Liu, G.; Li, P. P.; Zhu, C. X.; Kang, E. T.; Noeh, K. G.; Zhang, B.; Zhu, J. H.; Li, Y. X., Conjugated-Polymer-Functionalized Graphene Oxide: Synthesis and Nonvolatile Rewritable Memory Effect. *Advanced Materials* **2010**, *22* (15), 1731-1735.
42. Zhang, B.; Chen, Y.; Zhuang, X.; Liu, G.; Yu, B.; Kang, E. T.; Zhu, J.; Li, Y., Poly (N-vinylcarbazole) chemically modified graphene oxide. *Journal of Polymer Science Part A: Polymer Chemistry* **2010**, *48* (12), 2642-2649.
43. Sun, S.; Cao, Y.; Feng, J.; Wu, P., Click chemistry as a route for the immobilization of well-defined polystyrene onto graphene sheets. *J. Mater. Chem.* **2010**, *20* (27), 5605-5607.
44. Lee, S. H.; Dreyer, D. R.; An, J.; Velamakanni, A.; Piner, R. D.; Park, S.; Zhu, Y.; Kim, S. O.; Bielawski, C. W.; Ruoff, R. S., Polymer Brushes via Controlled, Surface-Initiated Atom Transfer Radical Polymerization (ATRP) from Graphene Oxide. *Macromolecular Rapid Communications* **2010**, *31* (3), 281-288.
45. Fang, M.; Wang, K.; Lu, H.; Yang, Y.; Nutt, S., Covalent polymer functionalization of graphene nanosheets and mechanical properties of composites. *J. Mater. Chem.* **2009**, *19* (38), 7098-7105.
46. Fang, M.; Wang, K.; Lu, H.; Yang, Y.; Nutt, S., Single-layer graphene nanosheets with controlled grafting of polymer chains. *J. Mater. Chem.* **2010**, *20* (10), 1982-1992.
47. Hussein M. Etmimi, M. P. T., and Ronald D. Sanderson, Synthesis and Characterization of Polystyrene-Graphite Nanocomposites via Surface RAFT-Mediated Miniemulsion Polymerization. *Journal of Polymer Science Part A: Polymer Chemistry* **2011**, *49* (7), 1621-1632.
48. Yongfang Yang, X. S., Liang Yuan, Mao Li, Jinchuan Liu, Rongqin Ji, Hanying Zhao, Synthesis of PNIPAM Polymer Brushes on Reduced Graphene Oxide Based on Click Chemistry and RAFT Polymerization. *Journal of Polymer Science Part A: Polymer Chemistry* **2012**, *50* (2), 329-337.
49. Kun Jiang, C. Y., Peipei Zhang, Xiaosong Wang, and Youliang Zhao, One-Pot Controlled Synthesis of Homopolymers and Diblock Copolymers Grafted Graphene Oxide Using Couplable RAFT Agents. *Macromolecules* **2012**, *45*, 1346-1355.
50. (a) Duan, Q.; Miura, Y.; Narumi, A.; Shen, X.; Sato, S. I.; Satoh, T.; Kakuchi, T., Synthesis and thermoresponsive property of end-functionalized poly (N-isopropylacrylamide) with pyrenyl group. *Journal of Polymer Science Part A: Polymer Chemistry* **2006**, *44* (3), 1117-

1124; (b) Charles, W.; Convertine, A. J.; McCormick, C. L., Fluorescent labeling of RAFT-generated poly (N-isopropylacrylamide) via a facile maleimide-thiol coupling reaction. *Biomacromolecules* **2006**, *7* (5), 1389-1392; (c) Zhou, N.; Lu, L.; Zhu, J.; Yang, X.; Wang, X.; Zhu, X.; Zhang, Z., Synthesis of polystyrene end-capped with pyrene via reversible addition-fragmentation chain transfer polymerization. *Polymer* **2007**, *48* (5), 1255-1260; (d) Meuer, S.; Braun, L.; Zentel, R., Solubilisation of multi walled carbon nanotubes by α -pyrene functionalised PMMA and their liquid crystalline self-organisation. *Chemical Communications* **2008**, (27), 3166-3168.

51. Jingquan Liu, W. Y., Lei Tao, Dan Li, Cyrille Boyer, Thomas P. Davis, Thermosensitive graphene nanocomposites formed using pyrene-terminal polymers made by RAFT polymerization. *Journal of Polymer Science Part A: Polymer Chemistry* **2010**, *48* (2), 425-433.

52. Liu, J., Imparting Polymeric Properties to Graphene Nanosheets by Surface Modification via π - π Stacking. *Australian Journal of Chemistry* **2011**.

53. Xu, L. Q.; Huang, C.; Wang, R.; Neoh, K. G.; Kang, E. T.; Fu, G. D., Synthesis and characterization of fluorescent perylene bisimide-containing glycopolymers for Escherichia coli conjugation and cell imaging. *Polymer* **2011**.

54. Hummers Jr, W. S.; Offeman, R. E., Preparation of graphitic oxide. *Journal of the American Chemical Society* **1958**, *80* (6), 1339-1339.

55. Bolotin, K. I.; Sikes, K.; Jiang, Z.; Klima, M.; Fudenberg, G.; Hone, J.; Kim, P.; Stormer, H., Ultrahigh electron mobility in suspended graphene. *Solid State Communications* **2008**, *146* (9), 351-355.

56. Balandin, A. A.; Ghosh, S.; Bao, W.; Calizo, I.; Teweldebrhan, D.; Miao, F.; Lau, C. N., Superior thermal conductivity of single-layer graphene. *Nano letters* **2008**, *8* (3), 902-907.

57. Liang, M.; Luo, B.; Zhi, L., Application of graphene and graphene-based materials in clean energy-related devices. *International Journal of Energy Research* **2009**, *33* (13), 1161-1170.

58. Dikin, D. A.; Stankovich, S.; Zimney, E. J.; Piner, R. D.; Dommett, G. H. B.; Evmenenko, G.; Nguyen, S. B. T.; Ruoff, R. S., Preparation and characterization of graphene oxide paper. *Nature* **2007**, *448* (7152), 457-460.

59. Stankovich, S.; Dikin, D. A.; Dommett, G. H. B.; Kohlhaas, K. M.; Zimney, E. J.; Stach, E. A.; Piner, R. D.; Nguyen, S. B. T.; Ruoff, R. S., Graphene-based composite materials. *Nature* **2006**, *442* (7100), 282-286.

60. Berger, C.; Song, Z.; Li, X.; Wu, X.; Brown, N.; Naud, C.; Mayou, D.; Li, T.; Hass, J.; Marchenkov, A. N., Electronic confinement and coherence in patterned epitaxial graphene. *Science* **2006**, *312* (5777), 1191-1196.

61. (a) Hernandez, Y.; Nicolosi, V.; Lotya, M.; Blighe, F. M.; Sun, Z.; De, S.; McGovern, I.; Holland, B.; Byrne, M.; Gun'Ko, Y. K., High-yield production of graphene by liquid-phase exfoliation of graphite. *Nature nanotechnology* **2008**, *3* (9), 563-568; (b) Viculis, L. M.; Mack, J. J.; Kaner, R. B., A chemical route to carbon nanoscrolls. *Science* **2003**, *299* (5611), 1361-1361; (c) Savoskin, M. V.; Mochalin, V. N.; Yaroshenko, A. P.; Lazareva, N. I.; Konstantinova, T. E.;

Barsukov, I. V.; Prokofiev, I. G., Carbon nanoscrolls produced from acceptor-type graphite intercalation compounds. *Carbon* **2007**, *45* (14), 2797-2800.

62. (a) Reina, A.; Jia, X.; Ho, J.; Nezich, D.; Son, H.; Bulovic, V.; Dresselhaus, M. S.; Kong, J., Large area, few-layer graphene films on arbitrary substrates by chemical vapor deposition. *Nano letters* **2008**, *9* (1), 30-35; (b) Dato, A.; Radmilovic, V.; Lee, Z.; Phillips, J.; Frenklach, M., Substrate-free gas-phase synthesis of graphene sheets. *Nano letters* **2008**, *8* (7), 2012-2016.

63. (a) Stankovich, S.; Piner, R. D.; Chen, X.; Wu, N.; Nguyen, S. B. T.; Ruoff, R. S., Stable aqueous dispersions of graphitic nanoplatelets via the reduction of exfoliated graphite oxide in the presence of poly (sodium 4-styrenesulfonate). *Journal of Materials Chemistry* **2006**, *16* (2), 155-158; (b) Stankovich, S.; Piner, R. D.; Nguyen, S. B. T.; Ruoff, R. S., Synthesis and exfoliation of isocyanate-treated graphene oxide nanoplatelets. *Carbon* **2006**, *44* (15), 3342-3347; (c) Eda, G.; Fanchini, G.; Chhowalla, M., Large-area ultrathin films of reduced graphene oxide as a transparent and flexible electronic material. *Nature nanotechnology* **2008**, *3* (5), 270-274; (d) Park, S.; An, J.; Piner, R. D.; Jung, I.; Yang, D.; Velamakanni, A.; Nguyen, S. B. T.; Ruoff, R. S., Aqueous suspension and characterization of chemically modified graphene sheets. *Chemistry of materials* **2008**, *20* (21), 6592-6594; (e) Fan, X.; Peng, W.; Li, Y.; Li, X.; Wang, S.; Zhang, G.; Zhang, F., Deoxygenation of exfoliated graphite oxide under alkaline conditions: a green route to graphene preparation. *Advanced Materials* **2008**, *20* (23), 4490-4493.

64. Choi, E. Y.; Han, T. H.; Hong, J.; Kim, J. E.; Lee, S. H.; Kim, H. W.; Kim, S. O., Noncovalent functionalization of graphene with end-functional polymers. *J. Mater. Chem.* **2010**, *20* (10), 1907-1912.

65. Brodie, B., Sur le poids atomique du graphite. *Ann Chim Phys* **1860**, *59*, 466-72.

66. Staudenmaier, L., Verfahren zur darstellung der graphitsäure. *Berichte der deutschen chemischen Gesellschaft* **1898**, *31* (2), 1481-1487.

67. (a) McAllister, M. J.; Li, J. L.; Adamson, D. H.; Schniepp, H. C.; Abdala, A. A.; Liu, J.; Herrera-Alonso, M.; Milius, D. L.; Car, R.; Prud'homme, R. K., Single sheet functionalized graphene by oxidation and thermal expansion of graphite. *Chemistry of materials* **2007**, *19* (18), 4396-4404; (b) Wu, Z. S.; Ren, W.; Gao, L.; Zhao, J.; Chen, Z.; Liu, B.; Tang, D.; Yu, B.; Jiang, C.; Cheng, H. M., Synthesis of graphene sheets with high electrical conductivity and good thermal stability by hydrogen arc discharge exfoliation. *Acs nano* **2009**, *3* (2), 411-417.

68. Stankovich, S.; Dikin, D. A.; Piner, R. D.; Kohlhaas, K. A.; Kleinhammes, A.; Jia, Y.; Wu, Y.; Nguyen, S. B. T.; Ruoff, R. S., Synthesis of graphene-based nanosheets via chemical reduction of exfoliated graphite oxide. *Carbon* **2007**, *45* (7), 1558-1565.

69. Wang, G.; Yang, J.; Park, J.; Gou, X.; Wang, B.; Liu, H.; Yao, J., Facile synthesis and characterization of graphene nanosheets. *The Journal of Physical Chemistry C* **2008**, *112* (22), 8192-8195.

70. Shin, H. J.; Kim, K. K.; Benayad, A.; Yoon, S. M.; Park, H. K.; Jung, I. S.; Jin, M. H.; Jeong, H. K.; Kim, J. M.; Choi, J. Y., Efficient reduction of graphite oxide by sodium borohydride and its effect on electrical conductance. *Advanced Functional Materials* **2009**, *19* (12), 1987-1992.

71. Fernandez-Merino, M.; Guardia, L.; Paredes, J.; Villar-Rodil, S.; Solis-Fernandez, P.; Martinez-Alonso, A.; Tascon, J., Vitamin C is an ideal substitute for hydrazine in the reduction of graphene oxide suspensions. *The Journal of Physical Chemistry C* **2010**, *114* (14), 6426-6432.
72. Waite, J. H., Surface chemistry: Mussel power. *Nature Materials* **2008**, *7*, 8-9.
73. Lee, H.; Dellatore, S. M.; Miller, W. M.; Messersmith, P. B., Mussel-inspired surface chemistry for multifunctional coatings. *Science* **2007**, *318* (5849), 426-430.
74. (a) Burzio, L. A.; Waite, J. H., Cross-linking in adhesive quinoproteins: studies with model decapeptides. *Biochemistry* **2000**, *39* (36), 11147-11153; (b) LaVoie, M. J.; Ostaszewski, B. L.; Weihofen, A.; Schlossmacher, M. G.; Selkoe, D. J., Dopamine covalently modifies and functionally inactivates parkin. *Nature medicine* **2005**, *11* (11), 1214-1221.
75. Wen-Cai Wang, J. W., Yuan Liao, Liqun Zhang, Bing Cao, Guojun Song, Xilin She, Surface Initiated ATRP of Acrylic Acid on Dopamine-Functionalized AAO Membranes. *Journal of Applied Polymer Science* **2010**, *117*, 534-541.
76. Herlinger, E.; Jameson, R. F.; Linert, W., Spontaneous autoxidation of dopamine. *J. Chem. Soc., Perkin Trans. 2* **1995**, (2), 259-263.
77. Li Qun Xu, W. J. Y., Koon-Gee Neoh, En-Tang Kang, and Guo Dong Fu, Dopamine-Induced Reduction and Functionalization of Graphene Oxide Nanosheets. *Macromolecules* **2010**, *43*, 8336-8339.
78. Sung Min Kang, S. P., Daewon Kim, Sung Young Park, Rodney S. Ruoff, and Haeshin Lee, Simultaneous Reduction and Surface Functionalization of Graphene Oxide by Mussel-Inspired Chemistry. *Advanced Functional Materials* **2011**, *21*, 108-112.
79. Kovtyukhova, N. I.; Ollivier, P. J.; Martin, B. R.; Mallouk, T. E.; Chizhik, S. A.; Buzaneva, E. V.; Gorchinskiy, A. D., Layer-by-layer assembly of ultrathin composite films from micron-sized graphite oxide sheets and polycations. *Chemistry of materials* **1999**, *11* (3), 771-778.
80. Si, Y.; Samulski, E. T., Synthesis of water soluble graphene. *Nano letters* **2008**, *8* (6), 1679-1682.
81. Grassie, N.; Vance, E., Degradation evidence for the nature of chain termination and transfer with benzene in the polymerization of methyl methacrylate. *Trans. Faraday Soc.* **1953**, *49* (0), 184-189.
82. Hojjati, B.; Sui, R.; Charpentier, P. A., Synthesis of TiO₂/PAA nanocomposite by RAFT polymerization. *Polymer* **2007**, *48* (20), 5850-5858.
83. Matrab, T.; Chancolon, J.; L'hermite, M. M.; Rouzaud, J. N.; Deniau, G.; Boudou, J. P.; Chehimi, M. M.; Delamar, M., Atom transfer radical polymerization (ATRP) initiated by aryl diazonium salts: a new route for surface modification of multiwalled carbon nanotubes by tethered polymer chains. *Colloids and Surfaces A: Physicochemical and Engineering Aspects* **2006**, *287* (1), 217-221.
84. Li, Y.; Li, X.; Dong, C.; Qi, J.; Han, X., A graphene oxide-based molecularly imprinted polymer platform for detecting endocrine disrupting chemicals. *Carbon* **2010**, *48* (12), 3427-3433.

85. Stenzel, M. H.; Davis, T. P., Star polymer synthesis using trithiocarbonate functional β -cyclodextrin cores (reversible addition - fragmentation chain-transfer polymerization). *Journal of Polymer Science Part A: Polymer Chemistry* **2002**, *40* (24), 4498-4512.
86. Stenzel, M. H.; Zhang, L.; Huck, W. T. S., Temperature-Responsive Glycopolymer Brushes Synthesized via RAFT Polymerization Using the Z-group Approach. *Macromolecular Rapid Communications* **2006**, *27* (14), 1121-1126.
87. C. Y. Li, W. C. W., F. J. Xu, L. Q. Zhang, W. T. Yang, Preparation of pH-sensitive membranes via dopamine-initiated atom transfer radical polymerization. *Journal of Membrane Science* **2011**, *367* (1-2), 7-13.
88. Shuhui Qin, D. Q., Warren T. Ford, Daniel E. Resasco, and Jose F. Herrera, Polymer Brushes on Single-Walled Carbon Nanotubes by Atom Transfer Radical Polymerization of n-Butyl Methacrylate. *Journal of the American Chemical Society* **2004**, *126* (1), 170-176.
89. (a) Liu, B.; Kazlauciusas, A.; Guthrie, J. T.; Perrier, S., One-pot hyperbranched polymer synthesis mediated by reversible addition fragmentation chain transfer (RAFT) polymerization. *Macromolecules* **2005**, *38* (6), 2131-2136; (b) Convertine, A. J.; Ayres, N.; Charles, W.; Lowe, A. B.; McCormick, C. L., Facile, controlled, room-temperature RAFT polymerization of N-isopropylacrylamide. *Biomacromolecules* **2004**, *5* (4), 1177-1180.
90. Rahimi-Razin, S.; Haddadi-Asl, V.; Salami-Kalajahi, M.; Behboodi-Sadabad, F.; Roghani-Mamaqani, H., Matrix-grafted multiwalled carbon nanotubes/poly (methyl methacrylate) nanocomposites synthesized by in situ RAFT polymerization: A kinetic study. *International Journal of Chemical Kinetics* **2012**, *44* (8), 555-569.
91. Tsujii, Y.; Ejaz, M.; Sato, K.; Goto, A.; Fukuda, T., Mechanism and kinetics of RAFT-mediated graft polymerization of styrene on a solid surface. 1. Experimental evidence of surface radical migration. *Macromolecules* **2001**, *34* (26), 8872-8878.
92. (a) Yang, Y.; Wang, J.; Zhang, J.; Liu, J.; Yang, X.; Zhao, H., Exfoliated graphite oxide decorated by PDMAEMA chains and polymer particles. *Langmuir* **2009**, *25* (19), 11808-11814; (b) Rowe, M. D.; Hammer, B. A. G.; Boyes, S. G., Synthesis of surface-initiated stimuli-responsive diblock copolymer brushes utilizing a combination of ATRP and RAFT polymerization techniques. *Macromolecules* **2008**, *41* (12), 4147-4157.
93. Grande, C. D.; Tria, M. C.; Jiang, G.; Ponnampati, R.; Advincula, R., Surface-Grafted Polymers from Electropolymerized Polythiophene RAFT Agent. *Macromolecules* **2011**.
94. Li, C.; Han, J.; Ryu, C. Y.; Benicewicz, B. C., A versatile method to prepare RAFT agent anchored substrates and the preparation of PMMA grafted nanoparticles. *Macromolecules* **2006**, *39* (9), 3175-3183.
95. Wang, H.; Luo, W.; Chen, J., Fabrication and characterization of thermoresponsive Fe₃O₄@ PNIPAM hybrid nanomaterials by surface-initiated RAFT polymerization. *Journal of Materials Science* **2012**, 1-8.

96. Vana, P.; Davis, T. P.; Barner-Kowollik, C., Kinetic analysis of reversible addition fragmentation chain transfer (RAFT) polymerizations: conditions for inhibition, retardation, and optimum living polymerization. *Macromolecular theory and simulations* **2002**, *11* (8), 823-835.

Appendices

Appendix 1. Synthesis of PMMA, PNIPAM and PtBA grafted PDA/RGO

A sealed 10 mL dried Schlenk tube was degassed and refilled with nitrogen three times. The mixture of MMA (4.67 mL), RAFT-PDA/RGO (31.5 mg with 2 mL DMF, 0.01 mmol RAFT agent (Appendix 2)), and AIBN (1.7 mg, 0.01 mmol) were injected into the tube via a syringe. Then the solution was bubbled with nitrogen for 30 min. The reaction tube was placed in a thermostated oil bath at 60 °C. After 10 hours, the tube was immersed into an ice bath. The solid was obtained via filtration and the solid was washed with toluene three times to remove free PMMA and the residual products dried under vacuum at 40 °C.

A sealed 10 mL dried Schlenk tube was degassed and refilled with nitrogen three times. The mixture of NIPAM (5 g), RAFT-PDA/RGO (31.5 mg with 2 mL DMF, 0.01 mmol RAFT agent (Appendix 2)), and AIBN (1.7 mg, 0.01 mmol) were injected into the tube via a syringe. Then the solution was bubbled with nitrogen for 30 min. The reaction tube was placed in a thermostated oil bath at 60 °C. After 24 hours, the tube was immersed into an ice bath. The solid was obtained via filtration and the solid was washed with toluene three times to remove free PNIPAM and dried the residual products under vacuum at 40 °C.

A sealed 10 mL dried Schlenk tube was degassed and refilled with nitrogen three times. The mixture of tBA (6 mL), RAFT-PDA/RGO (31.5 mg with 2 mL DMF, 0.01 mmol RAFT agent (Appendix 2)), and AIBN (1.7 mg, 0.01 mmol) were injected into the tube via a syringe. Then the solution was bubbled with nitrogen for 30 min. The reaction tube was placed in a thermostated oil bath at 60 °C. After 24 hours, the tube was immersed into an ice bath. The solid was obtained via filtration and the solid was washed with toluene three times to remove free PtBA and dried the residual products under vacuum at 40 °C.

Appendix 2. Calculation of the amount of RAFT agent attached to PDA/RGO

Basis: 100 g of sample (PDA/RGO + RAFT agent)

Based on TGA results, PDA/RGO has 59 % RGO; RAFT-PDA/RGO (lower RAFT agent density) has 52 % RGO. Therefore, 100 mg RAFT-PDA/RGO has 52 mg RGO.

The weight of PDA/RGO = $52 \text{ mg} / (59 \%) = 88.1 \text{ mg}$.

The weight of RAFT agent = $100 \text{ mg} - 88.1 \text{ mg} = 11.9 \text{ mg}$.

Molecular weight of RAFT agent is 364.63 g/mol, thus:

Mole of RAFT agent/100 g of sample = $11.9 / 364.63 = 0.0326 \text{ mmol} / 100 \text{ g sample} = 326 \text{ } \mu\text{mol} / \text{g sample}$.

RAFT-PDA/RGO (higher RAFT agent density) has 49.4 % RGO. Therefore, 100 mg RAFT-PDA/RGO has 49.4 mg RGO.

The weight of PDA/RGO = $49.4 \text{ mg} / (59 \%) = 83.7 \text{ mg}$.

The weight of RAFT agent = $100 \text{ mg} - 83.7 \text{ mg} = 16.3 \text{ mg}$.

Molecular weight of RAFT agent is 364.63 g / mol, thus:

Mole of RAFT agent/100 g of sample = $16.3 / 364.63 = 0.0447 \text{ mmol} / 100 \text{ g sample} = 447 \text{ } \mu\text{mol} / \text{g sample}$.

Assuming the PDA/RGO sheet is flat square plate, the number of RAFT agent on 1 nm² could be calculate. According to the TEM and AFM image, the length and width of the PDA/RGO sheet was assumed to be 1000 nm. The thickness of the sheet was assumed to be 4 nm.

The volume of one sheet:

$$V = l \times w \times t = 1000 \times 1000 \times 4 \text{ nm}^3 = 4 \times 10^6 \text{ nm}^3$$

The surface area of one sheet:

$$S = 2 \times l \times w + 4 \times l \times t = 2 \times 1000 \times 1000 + 4 \times 1000 \times 4 = 2.016 \times 10^6 \text{ nm}^2$$

The density of PDA/RGO was assumed as 1 g/cm³. Thus $\rho = 1 \text{ g/cm}^3$.

The mass of one PDA/RGO sheet:

$$m = \rho \times V = 4 \times 10^6 \times 10^{-21} \text{ g} = 4 \times 10^{-15} \text{ g}$$

Avogadro number: $N_A = 6.02 \times 10^{23} \text{ mol}^{-1}$

Therefore, the amount of RAFT agent anchored to the PDA/RGO surface is:

$$\text{Low density: } [(326 \times 10^{-6}) \times (4 \times 10^{-15}) \times (6.02 \times 10^{23})] / (2.016 \times 10^6) = 0.39 \text{ RAFT agent / nm}^2.$$

$$\text{High density: } [(447 \times 10^{-6}) \times (4 \times 10^{-15}) \times (6.02 \times 10^{23})] / (2.016 \times 10^6) = 0.53 \text{ RAFT agent / nm}^2.$$

Curriculum Vitae

Name: Renpeng Gu

Post-secondary Education and Degrees: Zhejiang University
Hangzhou, Zhejiang, China
2006-2010 B.E

The University of Western Ontario
London, Ontario, Canada
2010-2012 M.E.Sc

Honours and Awards: Western Engineering Scholarship
2010-2012

Related Work Experience Teaching Assistant
The University of Western Ontario
2011-2012

Research Assistant
The University of Western Ontario
2010-2012